*Ministero dell'Istruzione, dell'Università e della Ricerca*

*Università degli Studi di Palermo*
*Dottorato in Ingegneria Chimica, Gestionale, Informatica e Meccanica*

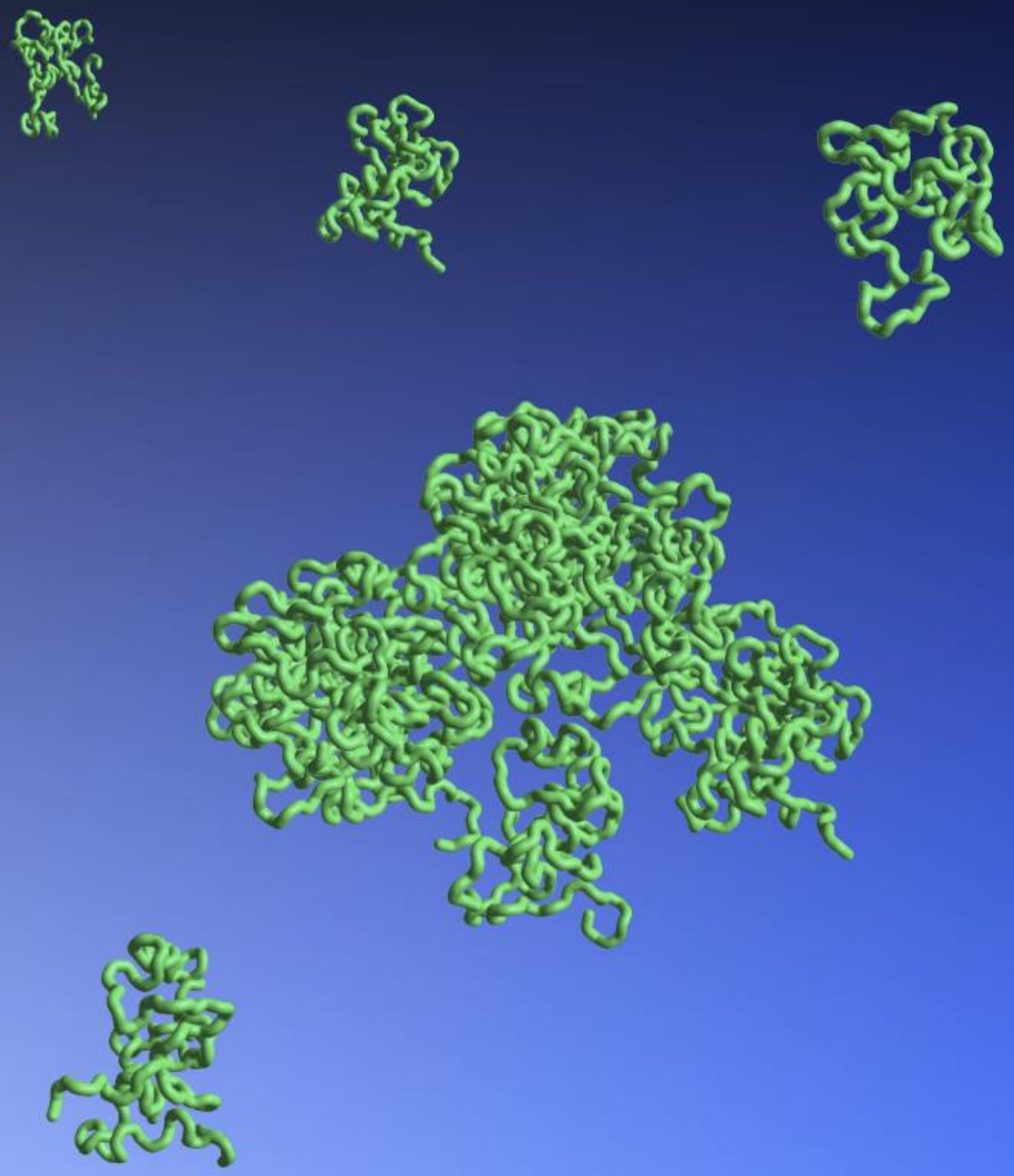

S. Todaro Xyloglucan self-assembled nanostructures and gels for biomedical applications

# XYLOGLUCAN SELF-ASSEMBLED NANOSTRUCTURES AND GELS FOR BIOMEDICAL APPLICATIONS

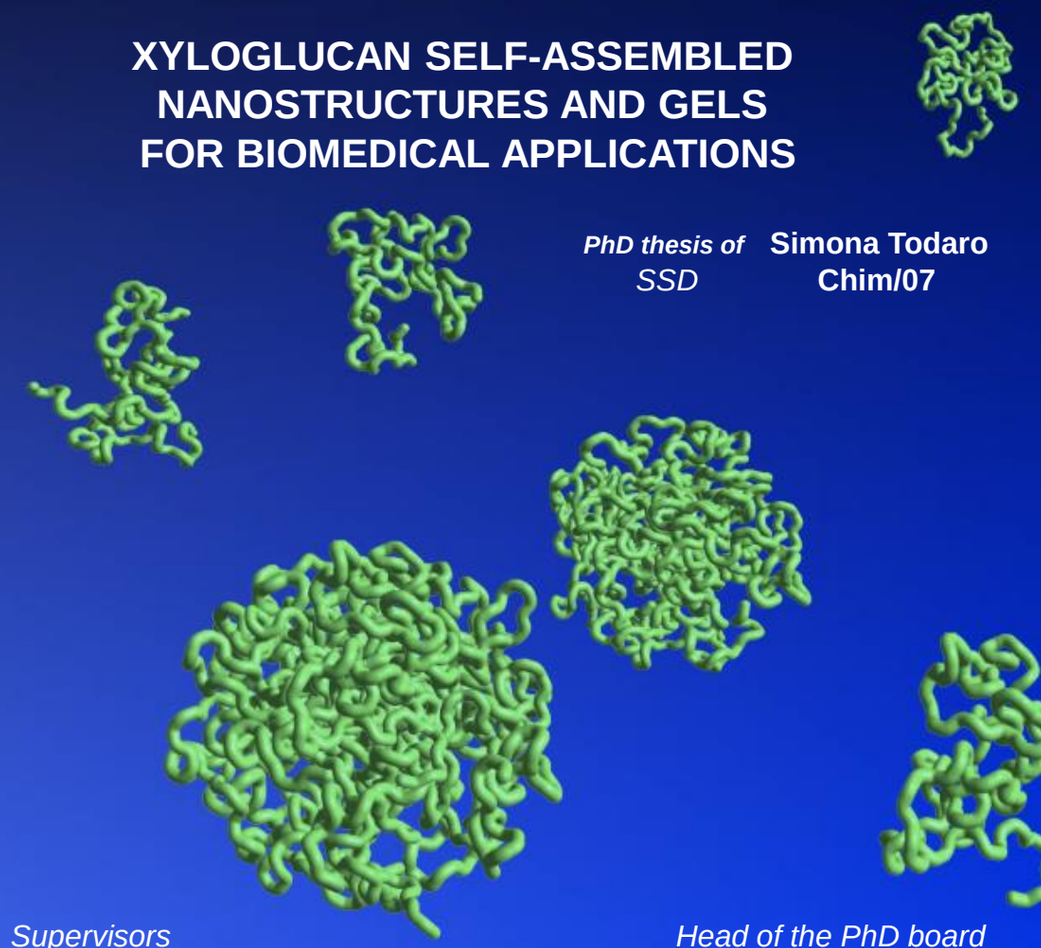

*PhD thesis of* **Simona Todaro**
*SSD* **Chim/07**

*Supervisors*
**Dr. Clelia Dispenza**
**Dr. Donatella Bulone**

*Head of the PhD board*
**Prof. Salvatore Gaglio**

Anno Accademico 2013/2014 Ciclo XXV

UNIVERSITÀ DEGLI STUDI DI PALERMO

Dottorato in Ingegneria Chimica, Gestionale, Informatica e Meccanica
Indirizzo Ingegneria Chimica e dei Materiali
Dipartimento di Ingegneria Chimica, Gestionale, Informatica e Meccanica
Settore Scientifico Disciplinare – SSD Chim/07

# XYLOGLUCAN SELF-ASSEMBLED NANOSTRUCTURES AND GELS FOR BIOMEDICAL APPLICATIONS

IL DOTTORE
**Dr. Simona Todaro**

IL COORDINATORE
**Prof. Salvatore Gaglio**

IL TUTOR
**Dr. Clelia Dispenza**

IL CO-TUTOR
**Dr. Donatella Bulone**

CICLO XXV
ANNO CONSEGUIMENTO TITOLO 2015

## ABSTRACT

Self-assembly of tamarind seed xyloglucan was investigated to exploit its unique properties as drug delivery device or scaffold for tissue reconstruction. The comprehension of the mechanisms at the basis of its supra-molecular organization in aqueous solvent is a fundamental step in the design of polymer architectures with controlled structure, morphology and properties at different length scales.

Xyloglucan was preferred over other polysaccharides for several reasons: it is abundantly present in nature, it should not elicit the response of the human immune system thanks to its vegetal origin, it is already approved by FDA as food additive and a thermo-responsive variant can be obtained with a simple enzymatic reaction by removing part of the galactose content. There are already a few studies concerning the possibility to employ this material for the preparation of biomedical devices, especially its partially degalactosylated variant, although its potential has not yet been fully exploited.

Being naturally occurring polymers, xyloglucans are characterized by very broad molecular weight distributions with high values of average molecular weight. Besides, many factors derived from their natural source, function in the plant and extraction process can influence their structural composition, molecular weight and supra-molecular organization. For this reason it is crucial to find effective methods to extract, purify, characterize and tailor xyloglucans molecular properties and structure and thereby achieve adequate water solubility/dispersibility, as well as to influence the polymer self-assembly behavior.

In my thesis, native xyloglucan (XG) and degalactosylated variants (Deg-XG) derived from tamarind seeds were evaluated. Structural and physical characterizations of their aqueous dispersions were performed on different length scales and concentration regimes, in order to understand macromolecules organization in water and elucidate the self-assembly mechanism triggered by cosolvent addition in the case of native XG or temperature increase in the case of Deg-XG.

The thermo-responsive behavior of Deg-XG in the semi-dilute/dilute regime was exploited for the obtainment of polymer nanoparticles. Radius of gyration, hydrodynamic radius, morphology and biocompatibility of Deg-XG nanoparticles were determined and their ability to incorporate model drugs assessed. [Chapter 6]

High energy irradiation was chosen as a tool to manipulate the polymer molecular weight and functionality and, in turn, tailor its self-assembly behavior. [Chapters 7, 9] The influence of irradiation dose, physical form of the polymer subjected to irradiation (solid vs. dispersed in water) and gaseous atmosphere during irradiation (nitrogen vs. air) were investigated. [Chapter 8]

A study of the macromolecular organization of Deg-XG at concentrations that lead to macroscopic gelation on increasing temperature was carried out in the prospect of using these gels as scaffolds for tissue reconstruction. Changes in the dynamic-mechanical properties and morphology of the gels upon irradiation were investigated. [Chapter 7]

Chemical functionalization protocols were also developed in order to specifically graft carboxyl groups onto XG and Deg-XG as a way to chemically anchor biomolecules with targeting or therapeutic function. [Chapter 10]

Finally, preliminary enzymatic degradation strategies were developed both to tailor xyloglucan properties by modifying its chemical structure and to simulate *in vitro* possible *in vivo* clearance routes. [Chapter 11]

## ACKNOWLEDGEMENTS

These last three years have been very rich of events and professional and personal growth for me. My acknowledgements go to several people.

First of all, I would like to deeply thank my two supervisors during these years, Dr. Clelia Dispenza and Dr. Donatella Bulone: they inspired me with their love for science and I learned a lot from them both.

My gratefulness goes to Dr. Pier Luigi San Biagio and Prof. Giuseppe Spadaro, for their guidance and support.

I also want to acknowledge Dr. Maria Antonietta Sabatino for all her help and advice and I extend my gratitude to Dr. Maria Rosalia Mangione and Dr. Rosa Passantino for their help.

I would like to express my gratitude to Prof. Mats Jonsson and Prof. Minna Hakkarainen from the Royal Institute of Technology (Stockholm, Sweden), for accepting me in their research groups for three months, helping me with my research project with very useful suggestions. I extend my thanks to all the members in their groups.

I gratefully acknowledge DSP Gokyo, Food and Chemical Co., Japan, and particularly K. Yamatoya, M. Shirakawa, A. Tabuchi for supplying the partially degalactosylated xyloglucan sample.

I also acknowledge Dr. G. Przybytniak and Dr. M. Walo for the irradiation experiments performed at the Institute of Nuclear Chemistry and Technology of Warsaw (Poland) and Dr. Radosław Wach and Prof. Piotr Ulanski of the Istitute of Applied Radiation Chemistry of "Lodz University of Technology" for the e-beam irradiation of the native polymer.

I extend my thanks to all of my collegues both at the Biophysics Institute of the National Research Council and at the University of Palermo.

I deeply acknowledge my family for their support.

Then, last but not the least, my deepest gratefulness goes to my boyfriend Rosario Cannici for his invaluable help with all the pictures and sketches in my

dissertation, but most of all I would like to thank him for his support, comprehension, friendship and love.

## TABLE OF CONTENTS

**EXPERIMENTAL**

**DISCUSSION**

## LIST OF TABLES

## LIST OF FIGURES

**7. Gamma-irradiation effects on Deg-XG self-assembly: from nano to macroscale**

**8. Study of the influence of different irradiation conditions on Deg-XG**



**9. Irradiation effects on native XG**

**10. Chemical modifications of xyloglucan functionality**



**11. Preliminary investigation of enzymatic degradation strategies**

**12. Discussion**

# 1 POLYSACCHARIDES IN BIOMEDICINE

## 1.1 Polysaccharide-based devices for biomedical applications

Among biopolymers, such as polypeptides, nucleic acids and biologically synthetised polymers, polysaccharides represent one of the most important renewable resource for the production of advanced polymeric devices, as it is proved by the increasing interest among scientists, research institutes and industrial companies, all of them convinced that polysaccharides will be at the central point of the future world for sustainable fuel, food, materials and medicine production. [1]

Indeed, polysaccharides are abundantly present in nature and readily available from the algal, animal and vegetal kingdoms, so they are often cheaper than synthetic polymers. The broad variety of composition is at the basis of the wide versatility of this class of materials. [2]

Their exceptional properties are far from being fully recognized and render them suitable for completely novel applications. Besides, they are "green", renewable materials.

Nowadays polysaccharide-based materials are used in manufacturing of biomedical and cosmetic products, food and feed production, and for cellulose derived materials (wood products, paper and cellulose derivatives, or textiles). Advances in the use of polysaccharides are strictly related to the ability of the scientific community to unravel their "natural" complexity: it is imperative to fully grasp the knowledge to model and shape the various biological, physical and chemical inter-relations taking place to invent new and improved "smart" materials. [1]

Polysaccharides are particularly attractive for the production of pharmaceutical and biomedical devices thanks to their non-toxicity, biocompatibility, biodegradability and in many cases the good water solubility. [2]

A wide range of polysaccharides has already found applications in human health and wellbeing, namely chitosan, cellulose (both plant and bacterial) and cellulose derivatives, alginates, dextran, starch, hyaluronan, heparin, carrageenan, pectins and guar gums. [2-4]

These applications can be divided into six big categories:

- Drug delivery;
- Wound healing;
- Tissue engineering scaffolds and implants;
- Bioactive compounds as anti-microbial, anti-clotting of blood, drugs and vaccines;
- Skin hydration, anti-aging agents, skin protection;
- Vaccines.

The main goals in the design of polysaccharide-based devices are:

- Development of new spatial architectures. For the application of polysaccharides in tissue engineering, for instance, it is crucial to tailor their mechanical properties, as well as the thermal, chemical and biological stability. Morphology, shape and size, porosity and surface functionality are key properties, too.
- Development of functionalized polysaccharides, such as bioactive hydrogels. Both chemical and enzymatic methods can be used to introduce side chains with the desired bioactive property.
- Design of smarter polymers with specific features, for example for the target delivery of drugs. There is the need to completely characterize the self-assembly behavior to exploit the different mechanisms for different applications. In order to prepare new materials able to target the drugs to a particular place in the body, through selective chemical and enzymatic modification of polysaccharides, there is a need to change the hydrophilic-hydrophobic balance, to increase their hydrophobicity for targeting drug delivery, to add charges or reactive substituents for self-assembly or cross-linking and to crosslink the polysaccharides with other natural or synthetic polymers.
- Control of polysaccharides average molecular weight and molecular weight distribution: being naturally occurring materials, it is difficult to control their molecular weight distribution, that can be influenced by many factors, such

as the extraction process from the natural source. These aspects will be discussed in detail in Section 1.2.

- Control of the rate of degradation and degradation time for each specific application: biodegradability is undoubtedly an advantage for tissue engineering and drug delivery applications, but it could become a problem if a long life-time is required. In some cases chemical modifications are necessary to modify the degradation time of polysaccharides. The understanding of the relationship between the structure of the polysaccharide material used in a specific application and its biodegradability is essential. Degradation will be discussed more in depth in Section 1.3.

The most common polysaccharides employed in the biomedical field (see Fig. 1.1) are:

- Chondroitin sulfate (CS): it is a glycosaminoglycan composed of alternating units of N-acetyl-D-galactosamine and D-glucuronic acid. It possesses excellent bio-characteristics including the binding and modulation of growth factors. Because natural CS is readily water-soluble, chemical crosslinking is required for the obtainment of hydrogels. It has widespread application in the field of tissue engineering, alone or in combination with other polysaccharides or proteins. [5-8]
- Hyaluronic acid: it is a nonsulphated glycosaminoglycan composed of alternating units of D-glucuronic acid and D-N-acetylglucosamine, linked together via alternating β-1,4 and β-1,3 glycosidic bonds. It is one of the major components of the extracellular matrix of skin, cartilage, and the vitreous humor. Some commercial products based on this polysaccharide are already approved by FDA. In the research field, the most common strategy is the chemical crosslinking by polymerization of methacrylate-functionalized hyaluronic acid. It has also been combined with alginate and poly-L-lysine to develop scaffolds for a variety of tissue engineering applications, including nerve regeneration. [9-11]

- Chitosan: it is the partial deacetylated derivative of chitin, which is obtained from the shells of crabs and shrimp. This biocompatible, cationic polymer dissolves in water up to a pH of 6.2. An increased basicity results in a gel-like precipitation of the hydrated polymer by neutralization of the amine groups. The pH-responsiveness can be extended to a pH-dependent, thermoresponsive system by adding polyol salts including β-glycerophosphate. These formulations dissolve at neutral pH and ambient temperature. Upon heating to body temperature, gelation occurs. Chitosan was already studied for the sustained delivery of drugs [12], for the preparation of scaffolds for tendon tissue engineering [13], for neurite outgrowth [14] and nerves [15].
- Cellulose derivatives: a very interesting feature of cellulose derivatives such as methylcellulose and hydroxyl-propyl-methyl-cellulose is that gelation occurs upon heating, in contrast with most other biopolymers [16]. In these cases gelation is mainly due to intermolecular, hydrophobic interactions of the methoxy side groups. While at low temperatures macromolecules are fully hydrated, upon heating, gradual dehydration occurs, resulting in a viscosity increase. Near the transition temperature, polymer-polymer interactions are dominant and result in the formation of a polymer network. These polymers were evaluated for tissue engineering applications by Tate et al. [17] From the results, it was demonstrated that MC is a promising candidate material to be applied as brain cell support.
- Alginate: it is a brown-algae-derived polysaccharide composed of β-D-mannuronic acid and R-L-guluronic acid units. Its aqueous solutions undergo ionotropic gelation upon adding multivalent cations. Alginate is a mucoadhesive, biocompatible and nonimmunogenic polymer. It does not possess cell-interactive properties, but it can be coupled with cell-interactive peptides or growth factors. In addition, alginate-based semi-interpenetrating polymer networks have been prepared possessing stimuli-responsive

behavior. When aiming at bone tissue engineering, alginate is often combined with calcium phosphates. [18-20]

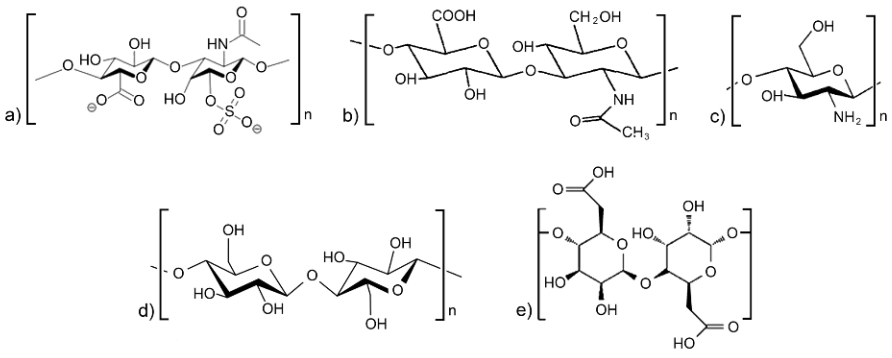


**Fig. 1.1:** Chemical structure of a) chondroitin sulfate; b) hyaluroinc acid; c) chitosan; d) cellulose; e) alginate.

Some of the most important biomedical devices that can be prepared starting from polysaccharides are shown in Fig.1.2.

In the following sections, polysaccharidic nanoparticles and hydrogels are described more in detail, since they are the systems of interest in the present dissertation.

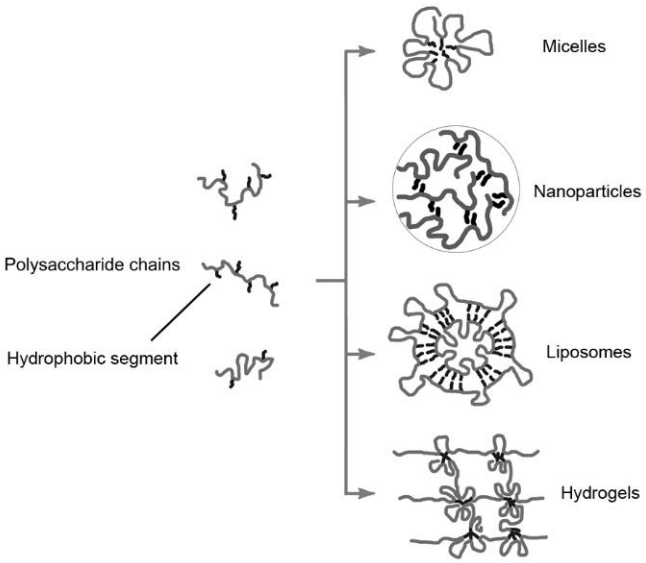


**Fig. 1.2:** Schematic representation of polysaccharide-based biomedical devices.

### 1.1.1 Polysaccharide-based nanocarriers

Polysaccharides are very promising raw materials in the preparation of nanocarriers. In general, nanoparticles have several advantages over other drug delivery devices:

- Ability to pass through the smallest capillary vessels because of their ultra-tiny volume and prolonged duration in blood stream by avoiding rapid clearance by phagocytes;
- Penetration into cells and tissue gap to arrive at target organs such as liver, spleen, lung, spinal cord and lymph;
- When carrying a bio-active molecule, they can show controlled release properties due to the biodegradability, pH, ion and/or temperature sensibility;
- Improving of the utility of drugs and reduction of toxic side effects.

In recent years, polysaccharides are often preferred over other polymeric materials for the production of nanoparticles, due to their abundance in nature and low cost in their processing and the possibility to chemically and biochemically modify their structure. They often possess good bioadhesive properties, thus having a prolonged residence time as nanoparticle carriers and increasing the absorbance of loaded drugs. [2,4]

According to structural characteristics, polysaccharide-based nanoparticles are prepared mainly by four mechanisms, namely covalent crosslinking, ionic crosslinking, polyelectrolyte complexation, and physical self-assembly of amphiphilic polysaccharides. The structure of the self-assembling polysaccharide is chosen depending on the physico-chemical properties of the drug to be loaded and the required route of administration.

### 1.1.2 Polysaccharide-based hydrogels

The most widespread definition for the term "hydrogel" is the one given by Peppas [21]: hydrogels are water-swollen, cross-linked polymeric structures containing either:

- covalent bonds produced by the reaction of one or more comonomers,
- physical crosslinks due to chain entanglements,
- association bonds including hydrogen bonds or strong van der Waals interactions between chains,
- crystallites bringing together two or more macromolecular chains.

A wide variety of natural materials of both plant and animal origin, materials prepared by modifying naturally occurring structures, and crosslinked synthetic polymeric materials are hydrogels. [22] Hydrogels are extremely suitable for a variety of applications in the pharmaceutical and medical industry. Because of their ability to retain large amounts of water and their soft and rubbery consistence, they closely resemble living tissues, thus possessing a high potential for application in regenerative medicine. The wide range of biomedical applications for hydrogels can be attributed to both their satisfactory performance on *in vivo* implantation in either blood-

contacting or tissue-contacting situations and to their ability to be fabricated into a wide range of structural forms. [22]

Bioactive hydrogels incorporating drugs, proteins and/or cell recognizable ligands in their structure are designed and characterized as injectable depots to provide sustained release of therapeutic molecules and/or as supporting matrix for regeneration of tissues (see Fig. 1.3). Injectable hydrogels containing biorecognizable molecules have several merits for drug and cell delivery applications by providing more bio-mimicking environments for sustained release of proteins or for growth and migration of cells. [23] As sustained delivery depots, the hydrogel can be incorporated with bioactive ligands that specifically bind and stabilize the bioactivity of therapeutic drugs or proteins. As a tissue engineering scaffold, the hydrogel can either be injected by itself or with cells of specific type into a tissue defect site, in cases of trauma, tumor excision, or congenital problems, for augmentation or regeneration efficacy by providing mechanical support, promoting tissue in-growth and integration and controlling cell behavior. [23].

Hydrogels can also function as excellent drug delivery vehicles thanks to their characteristics of high water content, functionality, biocompatibility, tunable size, large surface area for multivalent bioconjugation, and interior network for the incorporation of therapeutics. [24]

*In situ* forming polymeric delivery systems are particularly attractive thanks to the ease and reduced frequency of administration, improved patient compliance and comfort.

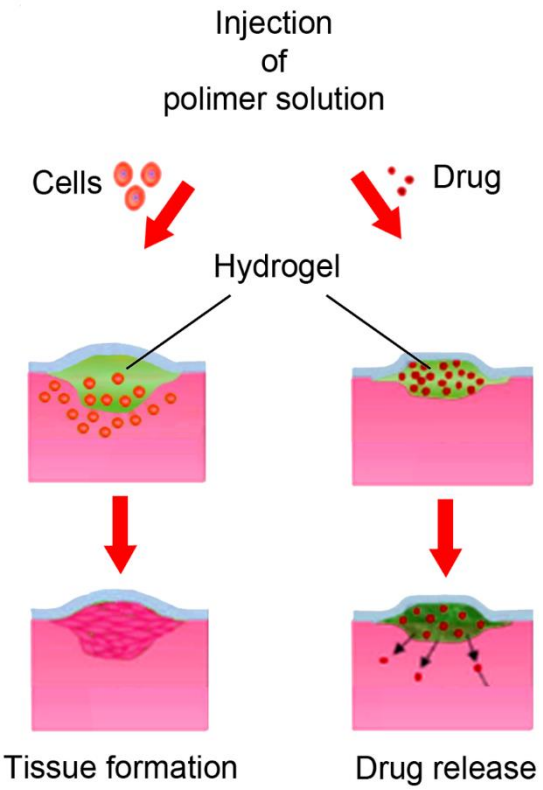


**Fig. 1.3:** Hydrogels application as scaffolds and drug delivery depots.

## 1.2 Tailoring of polysaccharides properties through depolymerization techniques

An important feature in the design of polysaccharide-based biomedical devices is the molecular mass of the employed raw material. Being naturally occurring polymers, polysaccharides are often characterized by very broad molecular weight distributions with relatively high average molecular weight values. Besides, when using vegetal feedstock polysaccharides obtained by a complex extraction process, it

is really difficult to deal with similar molecular weight materials: polysaccharides that are namely the same can broadly vary in their molecular structure as a function of the specific natural source, plant maturity, the part of the plant used and the extraction method.

In the biomedical and pharmaceutical field lower molecular mass polysaccharides have several advantages over the high molecular mass candidates due to the improved diffusion into biological tissues and the possibility to tailor molecular, physico-chemical properties and above all the mechanisms involved in self-assembly by controlling the average polysaccharide molecular weight and its polydispersity.

Shortening of the polysaccharide macromolecular chains (often referred to as "depolymerisation") can be achieved by various methods. In any case, a critical prerequisite is to avoid the alteration of the chemical structure and/or the loss of particular functional properties, such as thermal responsiveness. Partial depolymerisation of polysaccharides can often be achieved by acid hydrolysis of the glycosidic bonds, but this method is applicable only for polysaccharides of a highly regular primary structure, otherwise, the depolymerised products might differ in structure and composition from the parent polymer, because of the different stability of the glycosidic linkages. Another possibility is enzymatic degradation, but in some cases enzymatic digestions could lead to the polymer breakdown into oligosaccharides after very short times, so this method cannot be pursued just for a controlled resizing of the molecular weight distribution. [25, 26] Heating methods can be also employed. Recently, microwave irradiation has received increasing attention over conventional heating procedures due to the low side-products formation. [27, 28] Nevertheless, depolymerisation by physical treatments, such as ultrasonication, is more convenient and frequently used. It has been already applied on a huge variety of polysaccharides, such as dextran, [29, 30] schizophyllan, [31, 32] pullulan, [33] heteroxylans, [34, 35] chitosan, [36] hyaluronic acid [37, 38] and carboxymethylcellulose. [39] The sonomechanical effect resulting from cavitation and combined with the formation of radicals seems to be at the basis of this process but reaction mechanisms have not been fully elucidated yet.

An interesting alternative is the recourse to gamma irradiation. It is widely recognized that radiation treatments reduce the molecular mass of polysaccharides, both in solution and in the solid state. [40, 41] In general, high energy irradiation has several advantages: it is a simple and environmentally friendly technology, it is a non-thermal process and can be performed at ambient or low temperature, it does not require any additional reagent and can guarantee the simultaneous sterilization of the irradiated materials, provided that the imparted doses are within the sterilization dose range.

Gamma irradiation has been already widely employed for the depolymerisation of cellulose [42], starch [43], chitosan [44], and heteroxylans [34, 35]. This process is based on the cleavage of the molecular chain promoted by radicals, the dominant event being the scission of the glycosidic bond. Free radicals are generated in the primary stages of irradiation, then macroradicals are formed by propagation and their reaction can be accompanied by modifications in chemical composition and primary structures of the polysaccharides. The main effects are fragmentation, hydrolysis and rearrangement leading to low molecular weight products. However, if the polysaccharide molecular weight distribution is initially of random character, the breakdown of polymer chains is expected to be random, too. [45] The depolymerization mechanism is complex: it seems to involve a "random explosion" of molecules and a great number of compounds are formed, probably because multiple ionizations occur in radiation action, causing damage in their vicinity. [46] On the other hand, impurities or other components in the material prior to irradiation may act as electron traps (for example, aromatic compounds may stabilize the radicals), thus impairing the irradiation efficacy in reducing the polysaccharide molecular weight or helping to control its effects. [47]

Polysaccharide degradation promoted by gamma irradiation can be described by the following reaction: [48]

$$R_1 - O - R_2 \xrightarrow{irradiation} \dot{R}_1 + \dot{O} - R_2 \rightarrow degraded\ product \quad \textbf{Eq. 1.1}$$

Radiation chemistry of cellulose can be considered as an example to describe irradiation effects on many polysaccharides and their derivatives. [49] In this case, the leading degradation reaction is the random cleavage of glycosidic bonds in the main chain promoted by radicals. Several mechanisms of these radical processes have been proposed. [42, 50]

The most important effect of irradiation on cellulose is the breaking-down of the ordered system of intermolecular and intramolecular hydrogen bonds. As a result, hydroxyl groups form less stable hydrogen bonds, causing the decrease of chain rigidity and crystallinity. [51] After initial ionization, most of kicked out electrons thermalize and eventually recombine with their parent ions. This causes the formation of excited polymer fragments that decompose, generating free radicals.

## 1.3 Biodegradation

A critical point in the design of polymer-based devices to be employed as scaffolds and/or drug delivery systems is represented by clearance mechanisms. In principle, the use of naturally occurring polymers like polysaccharides is a valid solution, thanks to the biodegradability of these materials. Indeed, biodegradable polymers have the ability to function for a temporary period and subsequently degrade, converting into lower molecular weight products easily eliminated in the body's metabolic pathways. However, degradation behavior must be completely understood and extensively evaluated in order to determine if a certain material is suitable for a particular application. The optimization of the design and the applications of these materials require, then, the comprehension of the degradation mechanisms.

The term "biodegradation" is referred to as "a degradation process occurring in a biological environment". More specifically, in the biomedical field, biodegradation can be defined as the "gradual breakdown of a material mediated by a specific biological activity." [52]

Biodegradability is also strictly related to biocompatibility: the possibility to remove the biomaterial in this simple, spontaneous way eliminates the risks of

complications due to the prolonged presence of a foreign material inside the body, but the changes that occur in the biomaterial physico-chemical properties during the degradation process can alter the associated biological response. This is caused not only by the modified biomaterial functionality, but also by the appearance of the degradation products that are the real responsible of the ultimate biocompatibility of the materials.

### 1.3.1 Degradation mechanisms

In general, the degradation process can be divided in two main steps: [53]

- Increase of water uptake of the biomaterial, due to the gradual diffusion of the aging medium into the polymer matrix, accompanied by negligible changes in molar mass and mechanical properties. Indeed, during this first stage the degradation products are not small enough to diffuse into the solution and no significant weight loss occurs. The main changes occur on the polymer surface and eventually some hydrolysis-induced chemical modifications are observed.
- Significant decrease of the polymer molecular weight and weight loss caused by chain scission and diffusion of large polymer fragments into the solution. During this stage significant changes affect the biomaterial, especially its porosity and mechanical properties. The molecular weight of the degradation products is further reduced by hydrolysis, so that they can diffuse from the material to the surface and then to the solution.

Polymers can be degraded by bulk degradation [54-57] or surface erosion mechanisms. [54, 58-61]

Bulk degradation takes place at the “center” of the material, where hydrolysis of chemical bonds in the polymer chain occurs. The system becomes an “empty shell”, but it maintains its size for a considerable time. [62]

Surface erosion mechanisms imply loss of material only from the surface, resulting in predictable mass loss profiles. As time goes by materials become smaller and smaller but they maintain their original geometric shape. This feature may be

beneficial for delivering molecules at constant rate and maintaining the mechanical and structural integrity of the material during degradation.
Among the degradation mechanisms it is possible to distinguish:

- hydrolytic degradation;
- enzymatic hydrolysis;
- chemical and enzymatic oxidation.

*Hydrolytic degradation*

All biodegradable polymers contain hydrolysable bonds. Polymer hydrolytic degradation may be defined as the scission of chemical bonds in the polymer backbone caused by water, that leads to oligomers and then monomers formation. These reactions can be catalyzed by acids, bases, salts, or enzymes. [52]

Initially, contact between water and the water-labile bonds in the polymer chains occurs due to either direct access to the polymer surface or to imbibitions into the polymer matrix.

For a biodegradable polymer matrix, degradation usually progresses from the exterior of the material toward its interior. Degradation rate is strongly influenced by the balance between the hydrophilic and the hydrophobic nature of the material: for instance, hydrophilic materials with hydrolysable bonds will degrade faster than hydrophobic materials with hydrolysable bonds.

*Enzymatic hydrolysis*

Hydrolysis reactions may be catalyzed by enzymes present in the human body, like cell-derived proteins that are responsible for the catalysis of several reactions.

This is a possible explanation of the higher *in vivo* degradation rates of some biomaterials when compared with *in vitro* experiments.

The enzymatic hydrolysis of polymeric biomaterials is a heterogeneous process that is affected by the mode of interaction between the enzymes and the polymeric chains and involves typically four steps: (1) diffusion of the enzyme from the bulk

solution to the solid surface, (2) adsorption of the enzyme on the substrate, resulting in the formation of the enzyme–substrate complex, (3) catalysis of the hydrolysis reaction, and (4) diffusion of the soluble degradation products from the solid substrate to the solution. [63] The rate of the global reaction is controlled by the slowest step. The physico-chemical properties of the biomaterial, such as its molecular weight and chemical composition, and the features of the enzyme (activity, stability, local concentration, amino acid composition, and 3D conformation) are determining parameters in the degradation process.

Biomaterial and enzyme properties may also be affected by the nature of the aging medium, pH and temperature and by the presence of stabilizers, activators, or inhibitory products resulting from material degradation or leaching out of processing additives.

Generally, the enzyme-mediated degradation process stops when the enzyme concentration reaches a saturation point on the biomaterial surface. Eventual chemical modification of the polymer affects the degradation kinetics because it may compromise the ability of the enzyme to recognize the substrate.

In the case of implanted biomaterials the situation is further complicated by the presence of inflamed tissues around the implant, the variability associated with biological systems and the complexity of body fluids: for example, blood plasma contains over 150 proteins, and most of them can interact with the biomaterial, [64] thus promoting the adherence of cells.

Surface-erosion degradation mechanism prevails when enzymes cannot penetrate the tightly packed structures of polymers: in this case enzymatic catalysis occurs at the polymer-enzyme interface. Surface area may increase as the degradation process progresses, enhancing the enzymatic action.

*Chemical and enzymatic oxidation*

During inflammatory response to foreign materials, inflammatory cells such as leukocytes and macrophages produce highly reactive oxygen species like superoxide $O^{2-}$, hydrogen peroxide $H_2O_2$, nitric oxide NO and hypochlorous acid HOCl. [52]

The oxidative effect of these species may cause polymer chain scission and contribute to their degradation.

# 2 SELF-ASSEMBLING POLYSACCHARIDES

The central property for the use of polysaccharides in the biomedical field is their ability to self-assemble in complex structures with size ranging from a few nanometers (i.e. nanocarriers and nanoparticles for prolonged and sustained delivery of drugs) [3] to the macro-scale (i.e. stimuli-responsive hydrogels). [4]

The control and modulation of the self-assembly properties are therefore of large interest for the development of biomedical devices based on polysaccharide systems. In the following sections, the definition of self-assembly is given together with a brief description of the main interactions involved in self-assembly mechanisms.

## 2.1 Self-assembly

Self-assembly is the spontaneous association of an ensemble of molecules into one or more supramolecular structures, driven by multiple non-covalent interactions. These interactions include hydrogen bonding, electrostatic association, van der Waals forces, hydrophilic-hydrophobic associations. Usually, the assembling subunits used in biomaterials form thermodynamically stable structures that reflect the balance between the enthalpic and entropic contributions of the molecular species and the solvent. [65]

The simplest self-assembly systems are nano-sized materials composed of small molecules aggregated through short range interactions into supramolecular objects such as clusters of molecules, [66] ribbons, [67] tubes, [68] helices. [69]

More complex systems, as observed in biology, achieve higher levels of self-organization and form hierarchical structures.

Biopolymers such as polypeptides, nucleic acids and polysaccharides are all capable to self-associate in structures of different levels of complexity. [70]

Self-assembly can be either “static” or “dynamic”. Static self-assembly involves systems that are at global or local equilibrium, like molecular crystals or folded globular proteins, and do not dissipate energy. In this case, the formation of the ordered structure may require energy at the beginning, but once the structure is

formed, it remains stable. In dynamic self-assembly, the interactions responsible for the formation of structures or patterns between components only occur if the system is dissipating energy. [71]

The exploitation of self-assembly mechanisms for the construction of functional biomaterials is a highly promising and exciting area of research, with great potential for the biomedical and pharmaceutical field. The molecular design of materials based on the control of non-covalent interactions among the constituent units is a powerful tool for the production of complex and adaptable biomaterials with highly tunable properties and significant biological effects. [65]

In general, most biological macromolecular assemblies are predominantly made from mixtures of stiff biopolymers, and our cells, muscles, and connective tissue owe their remarkable mechanical properties to these complex biopolymer networks. The understanding of their incessant assembly, disassembly, restructuring, active and passive mechanical deformation needs a lot of theoretical modeling efforts because if flexible polymer behavior is well depicted in literature, the stiffness of these biopolymers and the resulting anisotropic networks that lead to smart mechanical and dynamical properties are far from being understood. The competition between processes of aggregation, gelation, and phase separation plays a major role in the self-assembly of most complex systems.

### 2.1.1 Non-covalent interactions

As stated before, non-covalent interactions are at the basis of self-assembly: coulombic, hydrophobic, van der Waals, ionic, metal-ligand interactions, hydrogen bonds, and the entropy contribution. [72] All these are considered as "long-range" interactions. It is worth noting that one kind of non-covalent interaction is not independent from others and the properties of these systems are the result of the combination of all the different interactions, among which one dominates, depending on the actual thermodynamic conditions. Self-assembly can be induced by adjusting the solvent quality, too.

Self-assembling polymeric systems serve as stimuli-responsive materials. Indeed, specific properties can be tuned by an appropriate stimulus, like temperature, pH, electric and magnetic fields, ions, reactants, visible and UV radiation and mechanical stress. Among these stimuli, temperature is the most frequently used. It is worth noting that thermal responsiveness is a common phenomenon for polymers in solution: the solubility of all polymers in any solvent depends on temperature. For this reason, intelligent stimuli-responsive polymers are conventionally defined as polymers that respond to a small physical or chemical stimulus with large property changes. [73]

***Hydrophobic interactions***

Hydrophobic interactions are actively involved in the self-assembly processes of thermo-responsive systems. Nevertheless, not only stimuli-responsive polysaccharides can self-assemble in aqueous solutions. Some amphiphilic polysaccharides, for instance, do not experience changes in the solubility of their hydrophobic parts upon temperature variations, but still they undergo self-association due to the hydrophobic interaction.

Water-soluble neutral polysaccharides are often composed of hydrophilic groups, strongly interacting with water and promoting the polymer dissolution, and hydrophobic groups (sometimes chemically grafted to the polysaccharide backbone), that tend to organize the surrounding water molecules, leading to the formation of an ordered hydration layer. The hydrophobic interaction is a strong solvent-mediated "attraction" among hydrophobic molecules in order to minimize the contact surface between hydrophobes and water. [73]

Upon contact with an aqueous environment, polymeric amphiphiles spontaneously form micelles or micelle-like aggregates via intra- or intermolecular associations between hydrophobic moieties, primarily to minimize interfacial free energy. Aggregation of amphiphilic polymers is analogous to micelle formation of small surfactants or lipids: this phenomenon is controlled by the balance between the interactions of the hydrophobic groups and the hydrophilic chains. The concentration

at which the polymer aggregation starts is usually called the "critical aggregation concentration" (CAC).

Amphiphilic polysaccharides provide a positive outlook for the preparation of nanoparticle drug delivery systems without the need to add solvents or surfactants. The hydrophobic core of these structures can be used to solubilize and encapsulate active ingredients with low solubility in aqueous media, whereas the hydrophilic shell would adsorb hydrophilic molecules through non-covalent interactions. [74]

The shape and the size of these self-assembled structures are governed by the balance between three major forces acting on the system, reflecting the constraints between the core-forming blocks, the interaction between the chains in the corona, and the surface energy between the solvent and the core. [75] The most commonly observed morphologies are spheres, cylinders and vesicles. [75-79]

Micelles serve as the cross-links that can dissociate and associate by temperature, external forces, added agents, etc. Indeed, micellization is the basis of the macroscopic gelation of amphiphilic polysaccharides.

***Ionic interactions***

Charged polysaccharides in aqueous solutions are affected by electrostatic interactions that involve all the ionic species. There are two types of electrostatic interactions: attraction between polyions and oppositely charged ions such as counter-ions, and repulsion between species with the same charge. If no external salts are present, the interaction between a charged polymer and counter-ions is governed by the electrostatic potential around the polyelectrolyte as exposed in the Katchalsky or Manning theories. [80, 81]

For charged polysaccharides, the self-assembly process is ruled by the balance among hydrophobic interactions and electrostatic repulsion within the same polymer chain and/or between different polymer chains.

Polyelectrolyte polymers with a few hydrophobic groups show a strong tendency for interpolymer associations even at very low polymer concentrations, resulting in the hydrophobic cross-linking of the polymer chains, that in turn causes a large

increase in solution viscosity. Gelation can occur upon further increasing polymer concentration. When all polymer-bound hydrophobes undergo completely intra-chain associations the formation of single molecular self-assemblies ("unimolecular micelles" or "unimer micelles") is observed. When the content of hydrophobes in a polymer is sufficiently low, a "flower-like" unimolecular micelle forms, which consists of hydrophobic core surrounded by hydrophilic loops. At the increase of hydrophobes, this flower-like structure becomes instable because a large portion of the surface of the hydrophobic core is exposed to water. This can lead to a further collapse into a more compact micelle with a third-order structure due to secondary association of hydrophobic cores of the flower-like micelles. A more realistic situation is a compromise between these two extreme cases, where intra-chain associations mainly occur but a portion of hydrophobes undergoes inter-chain associations, forming intermolecularly bridged flower-like structures. The extent of such micelle bridging may strongly depend on the content of hydrophobes in the polymer as well as the polymer concentration. [82]

***Hydrogen-bond and dipolar interactions***

Hydrogen bonds are loose dipolar interactions that involve hydrogen atoms interacting with highly electronegative atoms such as oxygen or nitrogen. Polysaccharides are very rich in hydroxyl groups. Hydrogen bonds can promote the formation of intra-chain or inter-chains networks. Hydrogen bonds play an important role in the local conformation of polysaccharides; indeed, the intra-chain hydrogen bonds control the local stiffness of the polymer. Hydrogen bonds are also involved in the hydration and dissolution of polysaccharides. Inter-chain hydrogen bonds allow the formation of original cooperative polymer A/polymer B complexes, against the usual rule of polymer incompatibility. [72]

If polymers carry dipole moments that are sparsely dispersed along the chains, they can be crosslinked by aggregation of these dipole moments, too.

### 2.1.2 Stimuli-responsive gelling systems

Gelation of many polysaccharides can be induced by one or a combination of different external stimuli like temperature variation, pH change, swelling, solvent exchange, photo-crosslinking, stereocomplexation, ionic crosslinking and synergistic interactions among different polysaccharides. [89]

Among these stimuli, temperature is the most widely used in environmentally responsive polymer systems. The thermodynamic principle at the basis of this response is the insolubilization–solubilization equilibrium, which is affected by the change in the solubility of the polymer chain or by the formation of a complex among polymer chains, that may accompany temperature variations. Generally, the solubility of solute molecules changes drastically with the change in temperature. Besides, the behavior of a polymer in a given medium reflects the balance of interactions among its own segments and the surrounding solvent molecules. [22]

The change of temperature is not only relatively easy to control, but also easily applicable both *in vitro* and *in vivo*. [83] Typical phenomena regarding thermosensitive polymers are the "coil to globule transition" and thermo-reversible gelation, that will be discussed in Section 2.1.2.1 and 2.1.2.2, respectively.

Biopolymers with pendant acidic or basic groups that can accept or release protons in response to pH changes are **pH-sensitive**. This feature can be exploited for the design of smart hydrogels, a protonation-deprotonation mechanism being at the basis of their sol-gel transition. Hydrogels prepared with polymers containing weakly acidic (anionic) groups swell on increasing the external pH, whereas a shrinking occurs if polymers contain weakly basic (cationic) groups. The most of anionic pH-sensitive polymers are based on PAA (Carbopol®, carbomer) or its derivatives. [89]

The pH-responsiveness can be artificially induced by the chemical conjugation to the end or side chain of the polymer structure of charged moieties that cause the occurrence of a pH-dependent sol-gel transition due to their reversible change between the ionized and non-ionized state. [23] A schematic representation of a pH-responsive hydrogel is reported in Fig. 2.1.

In some cases “hybrid” smart hydrogels, both temperature and pH-responsive, have been produced by grafting pH-sensitive moieties to a thermosensitive polymer. For example, Pluronic was grafted with oligo (lactic acid) chains and terminal hydroxyl groups were converted in carboxyl groups. In this way, the copolymer solutions showed both temperature and pH-dependent sol-gel phase transition depending on the protonation/deprotonation state of the end-capped carboxylate groups. The sol-gel transition was based on temperature-induced micellar packing of the Pluronic copolymers, while critical gelation temperatures were largely influenced by pH with a maximum at neutral pH. [23]

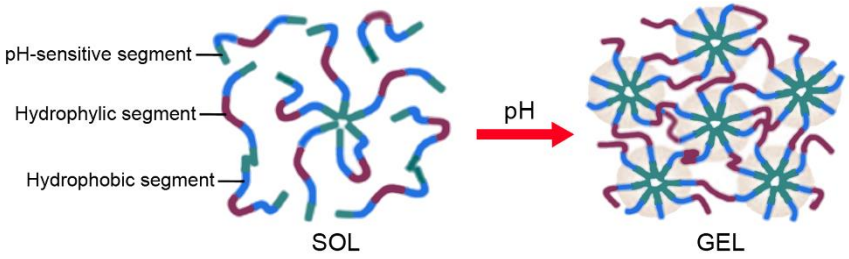


**Fig. 2.1:** Pictorial representation of a pH-sensitive hydrogel.

Gelation can be based on a **swelling** mechanism: in this case, polymers absorb water from the surrounding environment and consequently they expand their volume. An example is myverol (glycerol mono-oleate), a polar lipid that swells in water to form lyotropic liquid crystalline phase structures. [89]

The **solvent exchange** approach consists of dissolving a water-insoluble polymer in a water-miscible, biocompatible solvent. Upon contact with body fluids, the solvent diffuses out of the polymer while water permeates the liquid polymer matrix. Due to its insolubility in water, the polymer precipitates, resulting in the formation of a solid polymeric implant.

Photo-crosslinkable hydrogels are obtained by **photo-polymerization** of macromolecular monomers. [23] Radicals are generated after exposure of an aqueous

solution of the polysaccharide containing a water-soluble photo-initiator, and hydrogels with tunable mechanical and degradation properties can be obtained.
The advantage of this gelation mechanism is that the macromer solution containing cells, protein, or DNA can be injected into the body and subsequently crosslinked *in situ* by exposure to the light source. However, an important drawback in the recourse to these systems is that photopolymerization requires the presence of a photo-initiator that could be toxic. Furthermore, the penetration capacity of the radiation source limits the number of application sites, and the reaction can develop enough heat to damage surrounding tissues.

This approach has been applied to produce depot formulations, biological adhesives for soft tissues, and orthopedic biomaterials. [23 and references within]

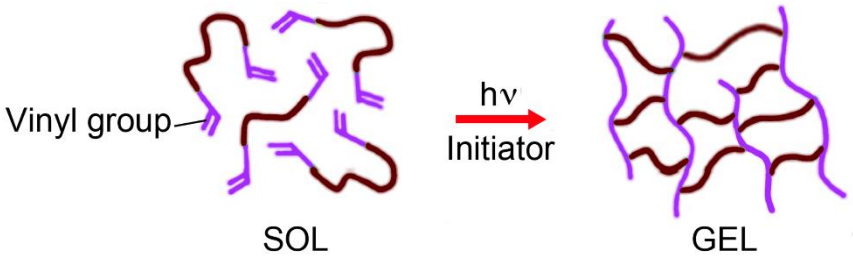


**Fig. 2.2:** Pictorial representation of a photo-crosslinked hydrogel.

**Stereocomplexation** has been a useful strategy in forming robust, in situ hydrogels. Gelation is based on the self-assembly of an enantiomeric pair of water-soluble polymers into stereocomplex crystalline structures in aqueous solutions. An example is the preparation of a dual component system, where a pair of water soluble polymers with corresponding enantiomeric D- or L-lactic acid oligomers turn into a gel structure upon mixing, resulting from stereocomplexation. [23 and references within]

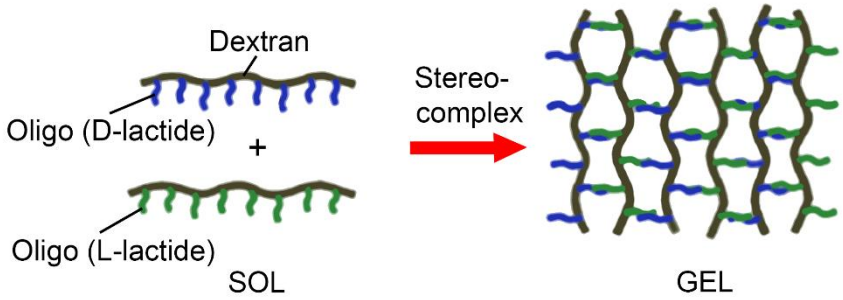


**Fig. 2.3:** Pictorial representation of a stereocomplexed hydrogel.

In some materials, a change in the concentration of specific ions in solution can trigger sol-gel transition because of **ionic crosslinking**, since the ion exchange weakens the interactions between polymer and solvent. For example, alginate undergoes gelation in the presence of $Ca^{2+}$ and other divalent ions. [90]

Some polysaccharides cannot undergo gelation alone, but they can form gels in presence of other polysaccharides. The gel formation is due to the **synergistic interaction between the involved polysaccharides**. In particular, if the addition of the other polysaccharide induces phase separation, the thermodynamic incompatibility will promote gelation. This is what happens upon adding galactomannan in an aqueous solution of carrageenan: phase separation occurs, and when the carrageenan concentration in the carrageenan rich phase becomes high enough, a gel forms because of the aggregation among polymer helices. It is possible to distinguish between two classes of binary systems (formed by the mixing of two polysaccharides) that undergo gelation through this mechanism:

- Class I: one of the two polysaccharides can form a gel by itself (at the experimental conditions considered).
- Class II: neither of the two polysaccharides can form a gel by itself (at the experimental conditions considered). [91]

#### 2.1.2.1 Coil to globule transition

The conformation in dilute solution of an ideal polymeric chain of non-interacting monomers can be modeled as a self-avoiding random walk of the subunits since only the excluded volume effect must be taken into account. The mean square dimension of this ideal chain will also depend on the interaction with the solvent. In a "good" solvent the interactions are favorable and the polymer chain will expand to maximize the contact whereas in a "bad" solvent the polymer chain will contract. If the solvent is poor enough to cancel the excluded volume effect the *theta condition* is realized. For a given polymer-solvent pair, the theta condition is generally obtained at a certain temperature, called theta temperature. When $T = T\Theta$, the polymer adopts an ideal Gaussian coil conformation and its repeating units can be described simply as non-interacting molecules of an ideal gas connected in a chain. In the Θ-state, the second osmotic virial coefficient, $A_2$, that is the first coefficient in the power series expansion of the internal energy of the segmental interactions, is zero and the molar mass of the polymer is infinitely high. [84]

The behavior of real polymers in solution is more conveniently explained in the frame of the *thermal blob model*. In this frame, the polymer chain is viewed as a sequence of blobs whose size is temperature-dependent and corresponds to the cutoff distance within which the chain is ideal. Beyond this distance, the blobs repel each other due to the excluded-volume effect. The thermal blob model describes the conformational changes of a polymer chain with temperature in the following way: in the high-temperature region (i.e. over the theta temperature) the chain expands not uniformly but forms temperature blobs, groups of correlated monomers. These blobs repel each other due to the excluded-volume effect. At temperature lower than the crossover temperature between the theta region and the high-temperature swollen region, the polymer chain forms blobs that are attracted to each other and are packed into a compact form by the negative excluded-volume interaction. The close packed blobs form a polymer globule. The change from Gaussian chain to globule is generally a gradual crossover, but discontinuous change (collapse transition) is also reported in

the literature. Such a discontinuous collapse is considered to be thermally reversible and it is called coil-globule transition (see Fig. 2.4).

For some thermosensitive polymers the coil-globule transition occurs upon heating. It corresponds to a true phase separation that can be described by a phase diagram with a Low Critical Solution Temperature (LCST). The phase transition involves a local structural transition of water molecules surrounding specific segments of the polymer in solution. Indeed, at low temperature the polymer is hydrated and dissolves in water. On heating, bound water molecules dissociate (dehydration occurs) and the hydrophobic segments aggregate into globules to repel water. The polymer chain can be thus depicted as a pearl-necklace made of compact spherical globules formed by close-packed hydrophobic aggregates of the dehydrated chain segments and connected by the hydrated swollen random coils.

LCST depends upon pressure and the polymer polydispersity. The coil-globule transition is a reversible process, but the rate of polymer re-dissolution is often slower and the chain expansion takes place at a lower T, which results in a thermal hysteresis. [85]

Some water-soluble polymers exhibit a peculiar conformational change in water by addition of a second water-miscible good solvent such as an alcohol. Such a transition from coil to globule, followed by an expansion from globule to coil, is called *reentrant coil–globule–coil transition* and it is related to the competition between the formation of polymer-water H-bonds and the polymer-alcohol H-bonds.

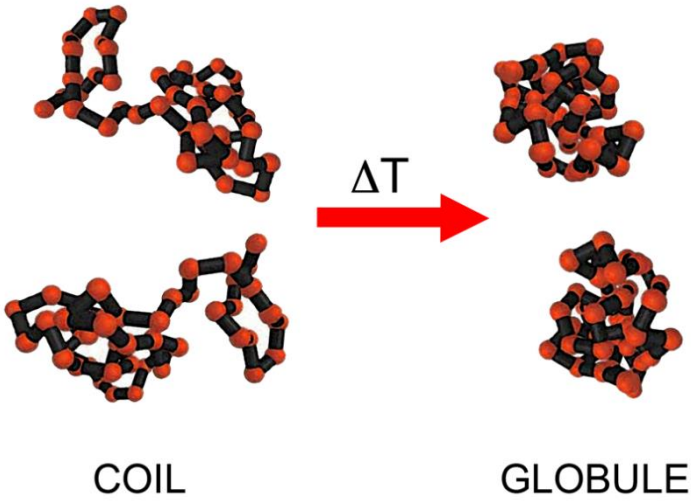


**Fig. 2.4:** Coil to globule transition.

#### 2.1.2.2 Thermo-responsive gelation

A large number of biopolymers possess the property to self-assemble upon temperature variation, forming macroscopic hydrogels when dispersed in water at highly enough concentration. There are two main types of temperature-sensitive polymers: the first present an upper critical solution temperature (UCST) while the second present a lower critical solution temperature (LCST). Some thermo-responsive polymers possess both these transitions: when dispersed in aqueous solvent, they form solutions at temperature below the LCST and above the HCST, while they undergo gelation for intermediate temperatures. Indeed, upon heating, aggregation of the hydrophobic groups occurs, inducing phase separation and hydrogel formation. The endothermal gelation is driven by an entropy change. In contrast with the increase in order during the aggregation of the hydrophobic segments, the entropy increases during the hydrogel formation. This is due to the large amount of water molecules released by the hydrophobic part of the polymer. Gelation thus occurs spontaneously upon heating because the entropy ($T\Delta S$) compensates for the unfavorable enthalpy ($\Delta H$) and the free Gibbs energy, expressed by Eq. 2.1, is favorable:

$$\Delta G = \Delta H - T\Delta S \qquad \textbf{Eq. 2.1}$$

More in detail, the self-assembly mechanism induced by temperature variations can be described as follows: some biopolymers are constituted by hydrophobic segments in the main chain coupled with hydrophilic ones as branches. These macromolecules are generally water-soluble at low temperature, but at the increase of temperature hydrophobic domains tend to aggregate to minimize the hydrophobic surface area exposed to bulk water, thus reducing the amount of structured water surrounding the hydrophobic domains and maximizing the solvent entropy. The gelation temperature is related to polymer concentration and chemical structure and to the length of the hydrophobic segment: the entropic cost of water structuring increases as the segment hydrophobicity increases, thus increasing the driving force for hydrophobic aggregation and reducing the gelation temperature. [86]

A thermo-reversible gelation of a polymer exhibiting both LCST and HCST transitions can present thermal hysteresis. This is often caused by the aggregation of rigid polymer chains and the existence of some associated aggregates or weak connections that have not been completely dissociated. [87] Differences in the critical gelation temperature between the heating and cooling processes are due to the different association and dissociation kinetics. [88]

Many derivatives of cellulose, such as methylcellulose, hydroxypropylcellulose and carboxymethylcellulose belong to this category and are studied for drug release applications.

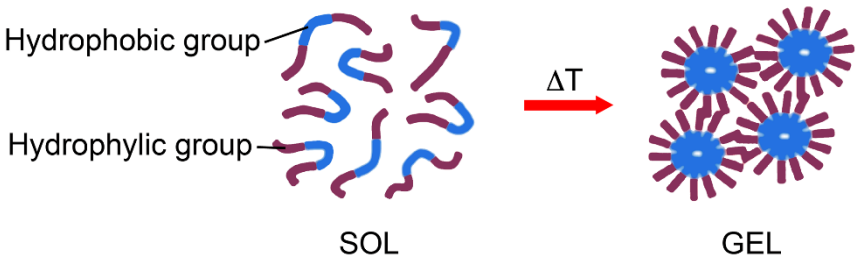


**Fig. 2.5:** Pictorial representation of a thermosensitive hydrogel.

# 3 XYLOGLUCAN

Among the other polysaccharides, the hemicellulosic xyloglucan was preferred for the research activities described in this dissertation for several reasons:

- It is abundantly present in nature. Indeed, cellulosic materials are the most abundant renewable resource in the world.
- Due to its vegetal origin, it should not elicit the response of the human immune system.
- It is characterized by a very interesting self-assembly behavior.
- It is approved by FDA as food additive.
- A thermo-responsive variant of xyloglucan can be prepared with a simple enzymatic reaction.
- There are a few studies concerning the possibility to employ this material for the preparation of biomedical devices, especially its degalactosylated variant, but its potential has not been fully exploited yet.

In the following sections, xyloglucan chemical, solubility and gelation properties are discussed. Please, note that there is a significant difference between the two polymer variants (the native and the degalactosylated one), especially in terms of solubility in water and gelation behavior. Then, a brief description of the irradiation effects on xyloglucan and of its biodegradability is presented, too.

## 3.1 Origin and chemical structure

Xyloglucan is a structural polysaccharide found in the primary cell walls of higher plants. It is a hemicellulosic polysaccharide: its backbone is formed by β-(1,4) D-glucan, partially substituted by α-(1->6)-linked xylose units (Fig. 3.1). Some of the xylose residues can be β-D-galactosylated at the O-2. Its role is of primary importance in plant growth: the xyloglucan transglucosylhydrolases cut xyloglucan backbone, inducing the reformation of the network structure made of cellulose and xyloglucan that is at the basis of plants expansion and growth processes. [92, 93]

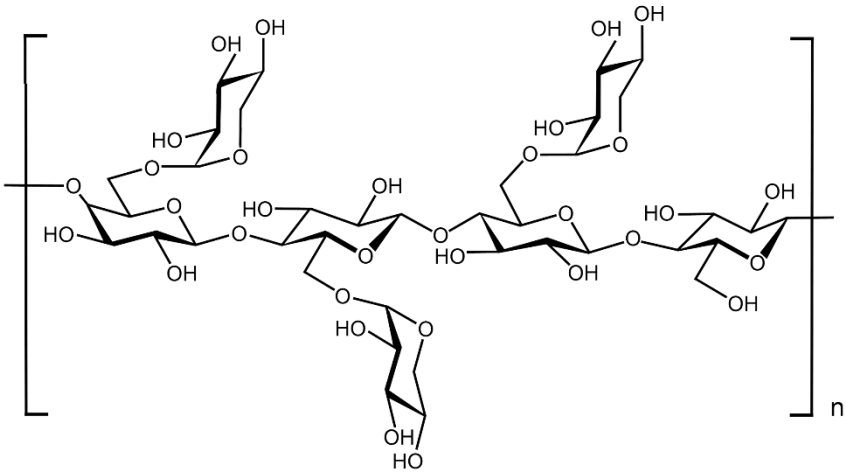


**Fig. 3.1:** A possible xyloglucan repeating unit.

As for all natural biopolymers, the reported chemical structure is only an idealized one, because the real distribution of the repeating units is not homogenous and varies according to many external conditioning factors, such as the polysaccharide origin, the extraction process from seeds and so on. In particular, the branching pattern is strongly dependent on species. [94]

Xyloglucans can be found as a storage polysaccharide in different seeds, such as *Tamarindus*, *Impatiens*, *Annona*, *Tropaeolum*, *Hymenaea*, and *Detarium*. In these seeds it represents 50% (w/w) of the storing energetic resources. [95]

The most studied xyloglucan is that extracted from *Tamarindus Indica*, thanks to its commercial availability. This polymer is already approved by FDA for use as food additive, stabilizing and thickening agent or gelling agent in presence of other additives. [96, 97]

Xyloglucan from Tamarind seeds has a high molecular weight, with reported average molecular weight ($M_w$) values in the range 650,000 to 2,500,000 Da. This is a marked difference compared with wood-derived hemicelluloses, which have

lower molecular weights, in the order of 10,000 – 50,000 Da after the extraction process.

Four different monomers have been observed in xyloglucan from Tamarind seeds, that differ for the number and the distribution of galactose residues (Fig. 3.2). These different structural units are $Glc_4Xyl_3$ heptasaccharide (XXXG), two types of $Glc_4Xyl_3Gal$ octasaccharide (XLXG, XXLG), and $Glc_4Xyl_3Gal_2$ nonasaccharide (XLLG). The molar ratio is typically 1:0.42:2.08:6.20. In this abbreviation, X represents a Xylp(α1→6)-Glcp unit, L represents a Galp(β1→2) Xylp(α1→6)Glcp unit, and G represents a Glcp residue. [98]

Xyloglucans extracted from different seeds have different features, for example in terms of chain flexibility, that are at the basis of the different physiological activities or physicochemical properties.

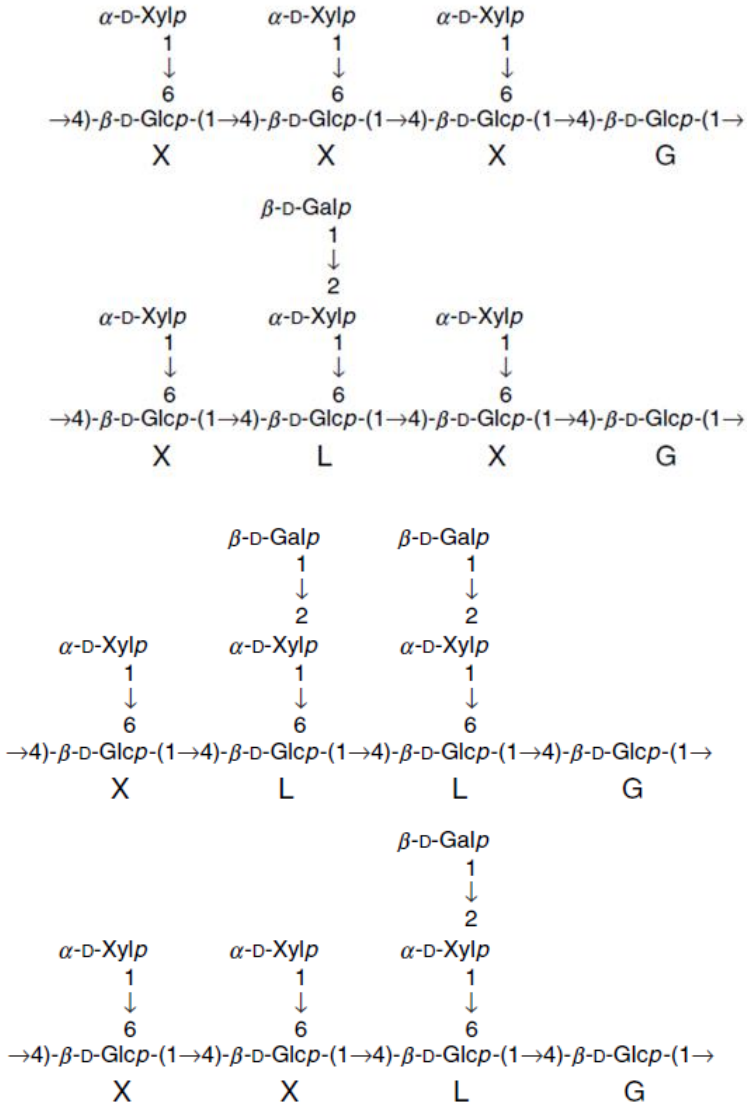


**Fig. 3.2:** Chemical structure of four monomers of xyloglucan.

## 3.2 Solubility and aggregation

Differently from cellulose, that is insoluble in water because of its crystal structure that involves inter- and intra-molecular hydrogen bonding, xyloglucan is water-soluble thanks to the presence of xylose and galactose residues. Indeed, their presence prevents the cellulose-like crystallization of xyloglucan chains via steric hindrance. However, as for other biopolymers, the complete dissolution is limited by xyloglucan tendency to self-association in aqueous solutions. The cellulose-like backbone promotes inter-chain interactions and so the polymer shows a balance between hydrophobic and hydrophilic character: macromolecules do not fully hydrate and supramolecular aggregates form even in very dilute solutions.

In particular, xyloglucan forms multistranded, flat, ribbon-like aggregates with hindered rotation and elliptic cross sections. The statistical Kuhn length and the cross-sectional radius of gyration were calculated as 150 nm and 148 ± 5 nm, respectively.

Radius of gyration values were estimated as 0,86 nm for heptamer, 0,62 nm for octamer and 0,77 nm for nonamer, while width of cross-sections were calculated as 0.62 for heptamer, 0.71 for octamer and 0.75 for nonamer. The higher radius of gyration value for heptamer indicates that the lack of galactose side chains leads to a strong tendency to aggregation, because of the lesser steric hindrance. Hindered rotation and this specific aggregation in solution are responsible for the stiffness of the polymer and its so-called "hyper-entanglement" behavior. [99]

The presence of "hyper-entanglements" interactions between polymer chains makes the analysis of solution properties quite difficult. Besides, the degree of association is influenced by many factors, such as molar mass, concentration, temperature and so on. [98] The "hyper-entangled" polysaccharides show stiffness of the chains in non-ionised environment, differently from the other polysaccharides coils with classical entanglement behavior. This is probably due to a tenuous alignment of neutral and stiff segments in solution. [100]

The question of XG conformation and organization in aqueous solvent is very delicate, but nevertheless it is really important for the understanding of XG self-assembly mechanism and the exploitation of this mechanism in the design of complex

supramolecular structures. To enhance xyloglucan solubility a "pressure cell" heating method was used and the effect of appropriately varying pressure, time and temperature was studied. [101] In this way, a better dissolution of xyloglucan in water was achieved and the macromolecular properties were investigated by capillary viscosimetry and light scattering techniques. This method was applied both on tamarind and detarium xyloglucan and no significant differences were evidenced. Parameters regarding chain structure and flexibility in water allowed to conclude that xyloglucan chains behave like semi-flexible random coils.

A drawback of this solubilisation method is that it can cause thermal decomposition of the polymer. [102]

More recently, the complete dissolution of xyloglucan was attempted by using a solvent with a chaotropic character, i.e. a 0.01 M NaOH solution. The absence of compact aggregates in solution was suggested by SANS measurements and the conformational characteristics of the individual polymer chains were evaluated. Results indicated that xyloglucan chains behave like semiflexible worm-like chains with excluded volume statistics. [103, 104] However, further studies showed the existence of swollen aggregates that contain a few chains and persist upon dilution (even in the dilute regime), due to weak attractive interactions among polymer chains. These large structures were investigated as a function of dilution by static light scattering and low-shear viscosity experiments. The overlap concentration c* was estimated to be 3.4 $g*L^{-1}$, with an association degree dependent on xyloglucan concentration and independent on the dilution regime, unlike other biopolymers such as xanthan and hyaluronan. [105]

The solubility issue is even worse for the degalactosylated polymer, because water is a solvent of lower quality for xylose groups than for the galactose side residues, which are partially removed by the degalactosylation process.

## 3.3 Gelation

In its native form, xyloglucan is a thermally stable biopolymer capable to form films. [106] Its aqueous solutions, although very viscous, cannot form a gel unless

appropriate substances are added to promote xyloglucan self-aggregation. Procedures to obtain a gel are listed below:

- Addition of sucrose;
- Addition of polyphenols;
- Mixing with other polysaccharides;
- Addition of iodide solutions;
- Addition of Congo Red;
- Mixing with alcohols;

Moreover, the polymer is capable of forming gel if an appropriate amount of the galactosyl residues are removed via enzymatic hydrolysis.

***Addition of sucrose***

Similarly to other polysaccharides such as pectin, xyloglucan may undergo gelation in presence of 40-65% sucrose, over a wide pH range. Xyloglucan backbone has a cellulose-like conformation and the gelation mechanism in high concentrated sucrose systems involves the aggregation of chains that have a regular, ribbon-like conformation. [107] Sugar substituents along polymer chains limit the degree of aggregation, thus preventing polymer precipitation and promoting gelation, instead. The gels are highly elastic, show low water release, and are thermoreversible, that is they form upon cooling and dissolve at higher temperatures. Freeze-thaw cycles render them mechanically stronger and more elastic.

***Addition of polyphenols***

Xyloglucan may form thermoreversible gels at relatively low concentrations in water in the presence of polyphenols such as epigallo-chatechin gallate. Again, gelation occurs on cooling, while heating causes melting. Small angle X-ray scattering measurements showed that gelation is due to random aggregation promoted by the synergistic interaction between xyloglucan and polyphenol. [108]

***Mixing with other polysaccharides***

A similar phenomenon is observed when xyloglucan is mixed with other polysaccharides, such as gellan gum and xanthan. When subjected to experimental conditions at which neither of these polysaccharides can reach gelation alone, binary systems of the two different polysaccharides at appropriate concentrations form gels by the synergistic interactions between the polysaccharides chains. Xyloglucan-xanthan and xyloglucan-gellan gum interactions are quite different, as it is demonstrated by the thermal hysteresis observed for the latter but not for the former system. Essentially, thermal hysteresis in the gelation of a solution containing two different polysaccharides is observed only when aggregation among helices occurs, promoting structure stabilization. This means that, although xanthan and xyloglucan backbones are very similar, their interaction and the formation of the heterotypic junction zones is somewhat hindered, in partly because of steric hindrance of the bulky side chains of both polymers. [91]

***Addition of iodide solutions***

The addition of iodine to xyloglucan solutions makes them develop a blue color, due to the formation of a complex between xyloglucan and iodine. These complexes act as crosslinking domains for gelation and polymer precipitation is avoided thanks to the combined effect of hydrophilic and bulky side chains and electrostatic repulsion of the iodine/iodide ions. [109]

***Addition of Congo Red***

Gels formed by addition of Congo Red have a peculiar structure, as evidenced by SAXS analysis: rod-like xyloglucan chains associate in a side-by-side way to build up a plate structure with Congo Red molecules inserted between the polymer chains. Congo Red amino or azo groups form hydrogen bonds with xyloglucan hydroxyl groups, and van der Waals forces between Congo Red aromatic groups and the hydrophobic cellulose surface can contribute to stabilize the structure. Consequently, xyloglucan chains stack through Congo red intercalation. The saccharide side chains

also play an important role for the formation of aggregates, providing many hydrogen bonding sites and inclusion space for Congo red molecules between cellulose backbones. [110]

***Gelation of xyloglucan in water-alcohol systems***

The collapse of the transient network formed by a water soluble polymer in aqueous solution by the addition of a polyhydric alcohol is a well-known mechanism of gelation of certain biopolymers, such as gelatin or pectin. [111, 112]

In the presence of ethanol, xyloglucan can undergo thermo-reversible gelation: the resulting, slightly opaque gels form at low temperature. Gelation mechanism was elucidated by time-resolved small angle X-rays scattering measurements as function of temperature. Results showed that the crosslinking domains are composed of random aggregates and no ordered structure is present. The complete dissolution of the aggregates causes the gel-sol transition. [113]

Xyloglucan gels structure in various kinds of mono or polyhydric alcohols was further studied by small angle X-ray scattering. Gelation behavior is strongly dependent on the type of alcohol. In particular, gelation of xyloglucan in the presence of monohydric alcohols seems to be due to random aggregation while the gelation in the presence of polyhydric alcohols is promoted by side-by-side association of alcohols with a few xyloglucan chains. [114] In the case of monohydric alcohols, the gel structure depends on the number of carbon atoms with a melting temperature decreasing with their increase.

One of the possible causes of xyloglucan gelation in water/alcohol solution is the destruction of the tetrahedral-like structure of water by addition of alcohol at concentrations above 20 wt%. [115] Water molecules in liquid form a connected, random network of hydrogen bonds having tetrahedral-like structure within the second neighbor and undergoing continuous topological reformation. [116] Addition of alcohol disrupts this structure with hydrophobic and hydrophilic interactions and yields less-restricted water molecules with higher mobility and less hydrogen bonds. [117] Such water molecules can be reformed and retained within the network of

xyloglucan more easily and contribute to the gelation more than those in the tetrahedral-like structure.

A somewhat different picture of gelation mechanism of xyloglucan in water-alcohol systems was proposed by using a molecular dynamics simulation of a xyloglucan oligomer in water, water/methanol and water/ethanol solution. The study showed that xyloglucan and alcohol molecules interact hydrophobically and not via hydrogen bond. Alcohol molecules are proposed to interact with xyloglucan mainly by hydrophobic interactions, filling the void of the hydrating water. The gelation is prompted by the adhesion of alcohol to xyloglucan with consequent slowing down of the swelling-shrink motion of the polymer chains that aggregate each other. Alcohol destroys and reforms the hydrogen bond network structure of water, which can be easily retained in the xyloglucan network. Therefore, xyloglucan in water/alcohol solution can form a gel containing rich water among the xyloglucan network. [118]

***Gelation promoted by partial degalactosylation***

When xyloglucan is enzymatically degraded by reaction with *β-Galactosidase* to remove more than 35% of galactose residues, it develops the almost unique property to gel on heating and dissolve on cooling, exactly the opposite of the previously described mechanisms. This gelation is a thermo-reversible process and, depending on the galactose removal ratio (GRR), a Low Critical Solution Temperature (LCST), at which sol-to-gel transition occurs, and a High Critical Solution Temperature (HCST), at which gel-to-sol transition occurs, can be encountered. These transitions are completely reversible and occur without adding any different substance. This phenomenon is not recognized with other gelling polysaccharides, such as pectin and carrageenan. With increasing GRR, the gel strength and the amount of water syneresis increase. With increasing temperature (but at temperature lower than the HCST) both the elastic modulus *G'* and the gel strength increase. Rheological studies at the variance of temperature and GRR showed that, at low GRR value, steric hindrance renders difficult the interaction of the main chains and so hindering gel formation,

while at high GRR value interactions among polymer chains are strong enough to build up a network. [119]

The sol-gel transition of Deg-XG at the variance of GRR was further investigated by rheological measurements and static and dynamic light scattering experiments. In particular, a correlation among GRR, molar mass, polymer-polymer interactions and molecular conformation was attempted. [88]

Although Deg-XG gelation has been often compared with that of Pluronic, that undergoes phase transition by heating and dissolve on cooling, nevertheless the gelation mechanism is rather different. In the case of Pluronic, the gelation is due to the packing of micelles, while for xyloglucan, a lateral stacking of the rodlike chains is responsible for the network formation. [120]

From a thermodynamic point of view, the thermoreversible gelation can be justified as follows: xyloglucan is characterized by a balance of hydrophobic (main chain) and hydrophilic character (galactose residues). The polymer is water soluble at low temperature, but upon temperature increase the hydrophobic domains start to aggregate in order to minimize the hydrophobic surface area exposed to bulk water and reducing the amount of structured water surrounding the hydrophobic domains. In this way the solvent entropy is maximized. The temperature at which gelation occurs depends on the polymer concentration, the length of the hydrophobic segment and the chemical structure of the polymer: the more hydrophobic the segment, the larger the entropic cost of water structuring, the larger the driving force for hydrophobic aggregation, and the lower the gelation temperature. [85, 88]

A thermal hysteresis of Deg-XG gelation was observed. The thermal hysteresis in a thermoreversible gel is often caused by the aggregation of rigid polymer chains and the existence of some associated aggregates or weak connections that have not been completely dissociated. [87] The difference in the critical gelation temperature between the heating and cooling processes is due to the kinetics of association and dissociation.

Besides, the sol–gel transition temperature decreases with increasing polymer concentration. The reason for this could be that at higher concentration polymer-

polymer interactions overwhelm polymer-solvent interactions, thus promoting the gel network formation. At lower concentration, a higher temperature value is required to establish the interactions necessary for the stabilization of the gel network. [121, 122]

Light scattering measurements were performed to investigate the polymer behavior in the high and low concentration regime. Results showed that the increase in the hydrophobic content by galactose removal induced a reduction on the value of the second virial coefficient $A_2$ and of the ratio between gyration and hydrodynamic radius $\rho$, indicating an increase in polymer–polymer interactions and a change in the molecule conformation to a more compact structure. [88] Degalactosylation of xyloglucan was monitored in real time by static light scattering, viscosimetry and HPSEC-MALLS. An increase in aggregation during the degalactosylation process was observed, thus confirming that the major tendency to aggregate is the main responsible of Deg-XG gelation, while polymer conformation is not affected by the enzymatic degradation. The aggregates formed after degalactosylation are rigid and rod-like, as previously observed by Brun-Graeppi et al. (2010), and are responsible for the increase of the solid-like behavior observed in the rheological experiments. [123]

SAXS measurements on degalactosylated xyloglucan gels revealed that the gel has an ordered structure, with crosslinking domains composed of aligned polymer chains in the shape of flat plates. [124]

The possibility offered by degalactosylated xyloglucan to be injected as a liquid and to form strong gels at physiological temperature makes the use of its hydrogels as drug carriers or matrixes for tissue engineering highly interesting. A detailed description of its potential applications is reported in Chapter 4.

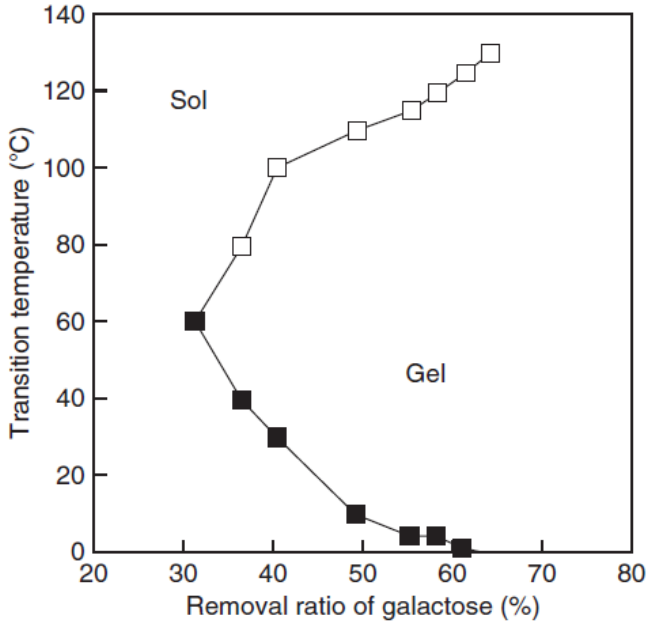


**Fig. 3.3:** Sol-gel transition as function of galactose removal ratio.

## 3.4 Chemical modifications

The possibility of functionalizing xyloglucan is currently under evaluation. As the hydroxyl-groups of this polymer cannot be directly connected with drugs, it has been thought of substituting them with active moieties. Studies of this type mainly regarded the native polymer that is better soluble in water. Carboxyl and alkylamino-groups were introduced to provide site-specific interactions, while sulphate-groups provided non-specific interactions.

Carboxylated and alkylaminated xyloglucans were prepared by oxidation of terminal side-chain galactose with galactose oxidase to form formyl residues followed either by further oxidation to carboxylate groups by addition of alkaline $I_2/I^-$, or reductive amination reaction with different alkylamines. Sulphated xyloglucan was prepared by swelling the polymer in dimethylformamide and treating it with sulphur trioxide-pyridine complex. [125] The architecture of carboxylated xyloglucan in aqueous solution was investigated by dynamic and static light scattering. [126]

Carboxymethylated xyloglucan was prepared by reaction with sodium salt of monochloro acetic acid in the presence of sodium hydroxide. Functionalization was confirmed through various techniques and the material was evaluated as a matrix for controlled drug release, with promising results. [127]

Carboxylation was also conducted on xyloglucan extracted from *Hymenaea Courbaril* seeds. In this case, oxidation of the polysaccharide was mediated by 2,3,6,6-tetramethylpiperidine-1-oxyl (TEMPO) and NaBr, followed by reaction with sodium hypochlorite. $NaBH_4$ was used to stop the reaction. This procedure converted each 0.1 mmol of primary alcohol in acid group. Physico-chemical properties of carboxylated xyloglucan were evaluated. Derivatives adopted spherical form, which can be useful for drug encapsulation. [128]

Amination of xyloglucan was conducted by reaction with ethylene diamine. The hydroxyl group of XG in the $2^{nd}$, $3^{rd}$ and $6^{th}$ position was substituted by

$-NHCH_2CH_2NH_2$ which was further reduced to $-NH_2$ using $NaBH_4$ as reducing agent. At low concentration in water, aminated xyloglucan forms self-assembled spherical nanoparticles, while at higher concentrations it forms irreversible hydrogels with blue fluorescence characteristics. Besides, anti-microbial activity was evaluated and it was found to be better than that of chitosan. [129]

All of the described functionalization reactions have been performed on the native xyloglucan. So far, only a functionalization reaction conducted on the degalactosylated variant of the polymer is described in the literature. Deg-XG hydroxyl-groups have been replaced by modifiable carboxylic derivatives for the grafting of doxorubicin. It can also be covalently attached to a targeting unit, in this case galactosamine. [130] The application of this drug delivery device will be described in Chapter 4.

## 3.5 Tailoring of xyloglucan properties through depolymerization techniques

Xyloglucan properties are dependent on the average molecular weight, as often observed with other polysaccharides. Owing to their natural source, xyloglucans show high average molecular weight and broad molecular weight distribution.

Xyloglucan degradation was chemically attempted with a free-radical reaction promoted by 4,4'-azobis-(4-cyanopentanoic acid), potassium persulfate (KPS), hydrogen peroxide ($H_2O_2$) and $H_2O_2$ with ascorbic acid at 75-80°C in aqueous solution. Xyloglucan degradation was similar to that of hydroxyethylcellulose. The predominant mode of degradation is believed to be random chain scission of sterically unhindered glycosidic main-chain linkages, with an increasing contribution from side-group scission as the degree of polymerization reduces and the relative concentration of side-group linkages increases. [131]

Differently from other natural biopolymers, such as cellulose, [45] starch [43] and chitosan, [44] there are only a few studies concerning the application of irradiative methods on xyloglucans to tailor its molecular weight distribution and/or for sterilization purposes, [132-134] but they have proven that γ-irradiation in air is an effective method of reducing the polymer molecular weight without altering the chemical structure. A comparative investigation on the effects of different radiation sources, namely ultrasound, γ-irradiation and microwave heating, on xyloglucan structural and molecular properties had shown that ultrasonication and relatively low dose γ-irradiation in air are the most convenient methods of reducing the molecular weight without altering the chemical structure and thermal responsiveness. When γ-irradiation was performed at doses higher than 40 kGy, unsaturated structures of higher molecular mass were observed. [132]

More recently, xyloglucans were subjected to γ-irradiation in the 10-70 kGy dose range. It was observed that doses up to 50 kGy caused no significant change in the degree of branching of the residual polymer chains, while a small increase of branching was detected at doses above 50 kGy. [133]

Different sterilization methods, including gamma-irradiation performed on the polymer dispersed in water, were tested for a partially degalactosylated xyloglucan variant and the effects on the thermally-induced gelation were investigated. In this case, the polymer was gamma-irradiated both at room temperature and in dry ice with an absorbed dose of 10 kGy. Results showed that gamma-irradiation of the polymer dispersion at room temperature markedly modified the polymer structure and impaired gelation, while after gamma-irradiation in dry ice Deg-XG was still able to form gels when conditioned at higher temperatures. [134]

### 3.6 Xyloglucan biodegradation

Xyloglucan is a neutral and non-toxic polysaccharide and its degradation products are assumed non-toxic because they should be consisting of naturally occurring saccharides, although the experimental evidence for this conclusion is limited. [135]

In a biological environment xyloglucan could be subjected to both hydrolytic and enzymatic degradation. Xyloglucan-active enzymes belong to the glycoside hydrolases (GH) family: they all split glycosidic bonds and can degrade xyloglucan to monosaccharides. Several *β-Galactosidases* are known. [136, 137] Also, *Xylosidases* have been studied. [138, 139] The glucose backbone can be broken down by endoglucanases in the same way as for cellulose. [140]

The partial enzymatic degradation of xyloglucan was already studied by its digestion with pure endo-β-(1,4)-glucanase of fungal origin, which cuts the backbone at unsubstituted D-glucose positions. With this enzyme, xyloglucan degradation is almost complete and leads to a mixture of the four xyloglucan oligosaccharides. Xyloglucan degradation has also been attempted with a xyloglucan-specific endo-(1->4)-beta-D-glucanase from nasturtium (Tropaeolum majus L.) cotyledons: in this case the same four oligosaccharides were obtained but together with large amounts of higher oligosaccharides and higher polymeric material. [141]

More recently, native xyloglucan nanoparticles were prepared in an aqueous $NaNO_2$ solution with an average diameter of about 60 nm and their enzymatic

hydrolysis with the enzymatic complex *Cellulase* of *Trichoderma reesei* was investigated using dynamic light scattering, atomic force microscopy and gel permeation chromatography. The apparent molar mass of the polymer was drastically reduced, proving that the polymer was fully hydrolyzed by the complex, that had to uncoil the nanoparticles before cutting the β-(1→4) bonds. [142]

# 4 BIOMEDICAL APPLICATIONS OF XYLOGLUCAN

While a relevant number of publications and patents are reported for the use of xyloglucan as a food additive, much less has been published about its use in the pharmaceutical and biomedical fields. However, the already published works indicate its potential for a wide variety of applications with numerous advantages compared with other macromolecular systems. [2]

XG applications will be classified as follows:

- Films for drug delivery;
- Nanocarriers for drug delivery;
- Hydrogels for drug delivery;
- Hydrogels for scaffolds preparation.

## 4.1 Films

The native polymer, alone or in combination with other polysaccharides such as starch and chitosan, can form transparent and thermostable films that have been tested for the dermal delivery of streptomycin as a model drug. Films mechanical properties in terms of tensile strength and flexibility were tailored by varying xyloglucan concentration. *In vitro* release studies showed that, after an initial small burst, a slow constant release of the model drug occurred. [143]

More recently, xyloglucan was evaluated for the preparation of buccal mucoadhesive films for the systemic delivery of rizatriptan benzoate. [144]

## 4.2 Nanocarriers

In comparison with the application of xyloglucan macroscopic hydrogels for drug delivery, there are very few studies regarding the preparation of nanocarriers with this polymer. However, xyloglucan and its degalactosylated variant possess both a great potential for the preparation and employment of nanocarriers, thanks to their self-assembly properties and their biocompatibility and biodegradability. Besides, the

possibility to introduce functional moieties by chemical reactions should not be underestimated.

Native xyloglucan was tested for its ability to form aggregates of about 60-140 nm, with an ordered and compact spherical conformation. The aggregates were then employed for the encapsulation of camptothecin, an anti-cancer drug. In this study, the encapsulation efficiency of camptothecin in xyloglucan nano-aggregates was found to be about 40% and sustained camptothecin release was demonstrated by *in vitro* studies. [145]

A partially degalactosylated variant of xyloglucan was grafted with doxorubicin (its content was over than 5 wt% in the conjugate), an anti-cancer drug, and galctosamine, a terminal moiety that can be used to target polymeric conjugates to liver hepatocytes. A self-assembly mechanism promoted by the presence of doxorubicin was exploited to induce the formation of nanoparticles with average size of about 140 nm. In a human tumor xenograft nude mouse model, the drug-grafted and targeted nanoparticles generated a greater therapeutic effect with respect to non-targeted doxorubicin nanoparticles or free doxorubicin. These results suggest that this system, which has improved transfection efficiency and hepatocyte specificity, may be useful for tumor therapy. [130]

### 4.3 Hydrogels for drug delivery

Deg-XG hydrogels at 1-2 wt% polymer concentration, which have the almost unique property to be liquid at room temperature and to gel within the human body, have been tested for drug delivery after different administration ways.

The optimal mucoadhesive properties of xyloglucan make it particularly attractive for these applications: indeed, it is expected to reside in the target area for relatively prolonged periods, so the clearance from the site of application is slowed down with consequent reduction of the hepatic first pass metabolism and local degradation of the drug. [146]

Studies showed that xyloglucan hydrogels can be used for controlled release of both water-soluble and water-insoluble drugs. [147] A more detailed description follows.

Deg-XG with a GRR of 44% was used for the preparation of hydrogels to be employed as carriers for rectal drug delivery: *in vitro* release of indomethacin (pKA = 4.5) and diltiazem (pKA = 7.7) were significantly more sustained from Deg-XG gels than from commercial suppositories. These formulations were rectal-administrated to rabbits and Deg-XG gels showed a longer residence time and a broader absorption peak of the drug, when compared to commercially available formulations loaded with the same drug concentration. The difference in hydrophilic and hydrophobic character of the two drugs entailed different cumulative release profiles: diffusion of diltiazem (the more hydrophilic drug) was more rapid, probably because it has a great tendency to reside in the water channels of the gels rather than interact with the polymer chains. This demonstrated that the interaction of Deg-XG gels with more hydrophobic drugs is more favorable. [148]

As well as for rectal drug delivery, Deg-XG gels loaded with indomethacin were tested for oral delivery by administration to rats and a suspension of indomethacin was administered as a comparison. Bioavailability of indomethacin from xyloglucan gels formed *in situ* was approximately threefold increased compared with that from the suspension. Deg-XG gelation at 1 wt% polymer concentration is not instantaneous, so it is probably possible to orally administer chilled polymer solutions that will undergo gelation inside the stomach. [149]

Deg-XG hydrogels were also formulated for the incorporation of indomethacin in the form of beads coated with Eudragit, to improve stability in the gastrointestinal track and obtain efficient gastro-resistant release of irritant drugs in the stomach. [150]

Deg-XG hydrogels and solutions prepared at the same polymer concentration were tested for oral release of paracetamol in rats. *In vitro* studies were conducted in mock gastric fluid (pH 1.2) and mock intestinal fluid (pH 6.8) and *in vivo* tests were performed by oral administration of Deg-XG hydrogels comprising paracetamol at rats. The cumulative amount of released drug from Deg-XG solutions and hydrogels

was significantly different: after 15 hours, about 50% of paracetamol was released from the hydrogels, while solutions released about 97% of the initial loaded drug. The hydrogels erosion during the experimental time was evaluated by gravimetric measurements, and the corrosion rate was found to be slower than the drug release rate. All of these results show that Deg-XG hydrogels are very promising candidates for oral delivery of drugs. [151]

The potential use of Deg-XG gels for intraperitoneal administration was explored as well. *In vitro* and *in vivo* release of mitomycin C, an antineoplastic antibiotic, was evaluated: the drug diffusion coefficient decreased at the increase of polymer concentration and the intraperitoneal administration to rats resulted in a broad concentration-time profile in both the ascites and the plasma, compared with a narrow peak and rapid disappearance when the drug was administered alone as a solution. [152]

More recently, xyloglucan-mitomycin conjugates were synthesized through a lysosomally degradable peptide spacer and galactosamine for the active targeting to hepatoma. This system presents many advantages over the classical chemotherapy methods: intracellular drug delivery, long circulation and high affinity to the target.

Xyloglucan very promising muco-adhesive properties render this polysaccharide a suitable candidate as vehicle for the opthalmic delivery. In particular, it was tested for the delivery of pilocarpine [153] and timolol. [154] In this case, the rapid gelation is an essential feature to avoid loss of the drug caused by drainage from the eye.

Percutaneous administration of Deg-XG gels was also tested for the topical delivery of anti-inflammatory drugs like ibuprofen and ketoprofen. In this case, results were compared with that obtained using Pluronic F127 gels as synthetic carriers. Some of the advantages of xyloglucan in comparison with the other temperature responsive systems have been already reported, as well as the differences in gels structure. The difference in release rates was here attributed to differences in the gel structure. The bioavailabilities of ibuprofen and ketoprofen were significantly higher when released from xyloglucan gels compared to Pluronic F127 gels. [155]

### 4.4 Hydrogels as scaffolds for tissue engineering applications

Thermoresponsive hydrogels, both natural and synthetic, are particularly attractive for application in the field of regenerative medicine, thanks to the solution-gelation transition occurring at physiological temperature and hence the possibility to be delivered by minimally invasive injection. [156]

In most cases, a strict requirement for cell survival is their anchorage to biocompatible, non cytotoxic surfaces, that also play a critical role in many cellular functions including migration, proliferation, differentiation and apoptosis. [157]

Galactose-containing polymers, such as xyloglucan, have been studied to induce the selective adhesion of primary hepatocytes, because galactose is recognized by cell receptors. [158-160] For this reason, xyloglucan can be proposed as an extra-cellular matrix for hepatocyte attachment. Seog-Jin Seo et al. (2004) exploited this xyloglucan property for the coating of Ca-alginate capsules. Cell adhesion results confirmed that xyloglucan is a good material for hepatocyte attachment due to its multivalent galactose ligands. Indeed, similar cellular adhesion rates between the xyloglucan- and collagen type I-coated surface were found, because galactose residues in the side chain of xyloglucan were recognized by asialoglycoprotein receptors on hepatocytes. [161]

Thermoresponsive xyloglucan hydrogels were already tested as candidates for neural tissue engineering of the spinal cord, after functionalization with poly-D-lysine to promote neurone adhesion and neurite outgrowth. The aim of this study was to provide neural stem cells with a scaffold that acted as a proliferative niche to support differentiation and to reduce glial scarring, thus facilitating repair by direct cell replacement. Xyloglucan was not toxic and supported neuronal differentiation.

Functionalization of xyloglucan yielded biological scaffolds that had superior capacity to support *in vitro* neuronal survival, differentiation, and neurite extension. [156]

More recently, these xyloglucan-based scaffolds were directly implanted within the brain, in particular in the caudate putamen of adult rats. The inflammatory response after the implantation, as well as scaffolds' capability to promote the controlled infiltration of axons, were investigated. [162]

# 5 EXPERIMENTAL

## 5.1 Materials

Xyloglucan (XG) was purchased from Megazyme International (Ireland). The partially degalactosylated variant with a galactose removal ratio of 44% (Deg-XG) was kindly provided by DSP Gokyo, Food and Chemical Company (Japan).

Camptothecin, 2,2,6,6-Tetramethyl-1-piperidinyloxy (TEMPO), sodium bromide (NaBr), sodium hypochlorite solution, sodium borohydride ($NaBH_4$), ethanol, *Cellulase* from *Trichoderma reesei*, *β-Glucosidase* from almonds and *β-Galactosidase* from *Aspergillus oryzae* were purchased from Sigma Aldrich and used without further purification.

## 5.2 Purification protocol

Deg-XG was dispersed in MilliQ water at 0.1 wt% polymer concentration by homogenization for 5 hours at 13500 rpm and 5°C, then it was autoclaved for 20 minutes at 121°C and 1 bar. After autoclaving, the polymer dispersion was centrifuged for 15 minutes at 8000g and 5°C and then the supernatant was recovered and dialyzed against a great excess of MilliQ water at 5°C for 2-3 days. The solid product was recovered after 3 days of freeze-drying. For this process, polymer recovery is about 75%.

## 5.3 Degalactosylation protocol

XG purchased from Megazyme International was partially degalactosylated according to an estabilished protocol. [88] Briefly, 2 wt% XG aqueous solution was mixed with *β-Galactosidase* solution (7.4 U/ml) and reaction was performed at 50°C and pH 5. After that, samples were heated at 100°C for 20 minutes to inactivate the enzyme. The degalactosylated polymer was recovered by precipitation in ethanol and the galactose content was evaluated by an enzymatic kit (Lactose/D-Galactose UV method).

## 5.4 Preparation of dilute/semi-dilute systems

### 5.4.1 XG dispersions

0.1 - 0.5 wt% XG aqueous dispersions were prepared by prolonged magnetic stirring at room temperature (20 - 24 hours), followed by autoclaving at 121°C and 1 bar for 20 min.

### 5.4.2 Deg-XG dispersions

0.1 - 0.5 wt% Deg-XG aqueous dispersions were prepared by homogenization at 5°C for 5 h at 13500 rpm and 5°C, followed either by centrifugation at 8000 rpm for 45 minutes to remove insoluble parts (nonpurified polymer) and/or autoclaving at 121°C and 1 bar for 20 min (purified polymer). These procedures are described in detail in the Appendix.

## 5.5 Preparation of Deg-XG nanoparticles

0.1 wt% Deg-XG aqueous dispersions prepared as described in Section 5.4.2 were incubated at 37°C for 20 h.

## 5.6 Incorporation of drugs in Deg-XG nanoparticles

Deg-XG aqueous dispersions (polymer concentration: 0.1 wt%) were loaded with camptothecin (to a final nominal concentration of $2*10^{-5}$ M) previously solubilized in DMSO ($10^{-3}$ M). The maximum DMSO concentration in the final formulation was 5%. Sample was prepared by magnetic stirring for 24 hours in the dark. An aliquot was incubated at 37°C for 24 hours. Then, liquid-liquid extraction with diethyl-ether was performed to remove the drug that was not interacting with the polymer. The extracted CPT was re-dispersed in DMSO and CPT concentration was evaluated by UV-Vis absorption measurements.

The drug load content and the entrapment efficiency were expressed as:

$$Drug\ load\ content\ (\%) = {}^{W_{drug}}/_{W_{polymer}} \times 100 \qquad \textbf{Eq. 5.1}$$

$$Entrapment\ efficiency\ (\%) = {}^{W_{entrapped\ drug}}\Big/_{W_{initial\ drug}} \times 100$$

**Eq. 5.2**

## 5.7 Preparation of Deg-XG concentrated dispersions and gels

2 - 6 wt% Deg-XG aqueous dispersions were prepared by homogenization at 5°C for 5 hours at 13500 rpm and 5°C, followed by autoclaving at 121°C and 1 bar for 20 minutes.

Deg-XG gels were prepared by conditioning concentrated Deg-XG aqueous dispersions at 37°C for at least 5 minutes.

## 5.8 High-energy irradiation treatments

### 5.8.1 $^{60}$Co irradiation

Gamma-irradiation of nonpurified Deg-XG dry powder was carried out in air at room temperature using a $^{60}$Co source (Gamma Chamber 5000 (see Fig. 5.1), Institute of Nuclear Chemistry and Technology, Warsaw, Poland) at 8 kGy/h and irradiation doses of 10, 20, 40 and 60 kGy. Samples codes are reported in Tab. 5.1.

**Fig. 5.1:** Gamma chamber of the Institute of Nuclear Chemistry and Technology (Warsaw).

### 5.8.2 $^{137}$Cs irradiation

Nonpurified and purified Deg-XG powders were gamma-irradiated both in air and in $N_2$ atmosphere using a Gammacell 1000 Elite $^{137}$Cs-source (see Fig. 5.2) (School of Chemical Science and Engineering, Royal Institute of Technology, Stockholm, Sweden) in the dose-rates range 0.36-1.07 kGy/h and at doses of 10, 20, 40 and 60 kGy. Samples codes are reported in Chapter 8, Tab 8.1.

Dilute Deg-XG aqueous dispersions (polymer concentration: 0.1 wt%) prepared as described in Section 5.4.2 were gamma-irradiated in air, in the same dose-rate range and with doses of 0.01, 0.05, 0.1, 0.5, 2, 20 and 60 kGy. After irradiation, Deg-XG aqueous dispersions were freeze-dried to recover the solid products.

All the irradiated samples were then dispersed in aqueous NaOH 10 mM at 0.2 wt% polymer concentration for SEC analysis. Samples codes are shown in Tab. 8.2.

**Fig. 5.2:** Gammacell of the Royal Institute of Technology (Stockholm)

### 5.8.3 Electron-beam irradiation

XG powder was irradiated in air at room temperature with the linear electron accelerator (see Fig. 5.3) of *"Lodz University of Technology"* (Lodz, Poland), with

doses of 10, 20, 40 and 60 kGy and a dose rate of 300 kGy/h. Samples codes are reported in Tab. 5.1.

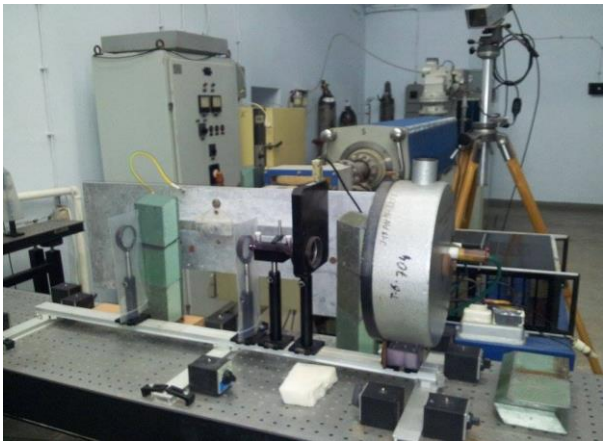

**Fig. 5.3:** Linear electron accelerator of Lodz University of Technology.

**Tab. 5.1:** Samples codes for $^{60}$Co gamma and electron-beam irradiated polymers.

| Polymer | Irradiation conditions | Atmosphere | Sample code |
|---|---|---|---|
| Deg-XG | Nonirradiated | // | γ 0 |
| Deg-XG | 10 kGy, gamma | air | γ 10 |
| Deg-XG | 20 kGy, gamma | air | γ 20 |
| Deg-XG | 40 kGy, gamma | air | γ 40 |
| Deg-XG | 60 kGy, gamma | air | γ 60 |
| XG | Nonirradiated | // | E 0 |
| XG | 10 kGy, e-beam | air | E 10 |
| XG | 20 kGy, e-beam | air | E 20 |
| XG | 40 kGy, e-beam | air | E 40 |
| XG | 60 kGy, e-beam | air | E 60 |

## 5.9 Chemical modifications

Carboxylation reactions were conducted both on XG and Deg-XG dispersed in water at 0.2 wt% and then autoclaved at 121°C and 1 bar for 20 minutes. Polymer dispersions were previously deoxigenated with $N_2$ for 30 minutes, then the carboxylation reaction was conducted in inert atmosphere and providing continuous magnetic stirring, at 5°C. Carboxylation reactions were performed on 150 ml of each polymer dispersion, by adding 3 mg (or 0.128 mM) TEMPO, 12.5 mg (or 0.81 mM) NaBr and 720 µl of 15% sodium hypochlorite solution. During the oxidation process small volumes of NaOH 0.1 M were added to maintain the pH around 9. The first reaction was stopped after 2 hours and the second one after 4 hours, by adding 22.8 mg (or 4 mM) $NaBH_4$. Functionalized polymers were recovered by precipitation in ethanol followed by freeze drying.

## 5.10 Enzymatic degradation

Enzymatic degradation studies were performed on 0.1 wt% purified Deg-XG dispersions with the enzymatic complex *Cellulase* and the enzyme *β-Glucosidase*.

Degradation of xyloglucan with *Cellulase* is already described in the literature. [142] In particular, 0.1 wt% Deg-XG aqueous dispersions were incubated at 37°C with the complex (0.084 U/ml). The enzymatic degradation was stopped after 1 and 2 hours by freeze drying the samples to recover the solid degraded polymer.

To perform degradation with *β-Glucosidase*, 0.1 wt% Deg-XG aqueous dispersions were incubated at 37°C with the enzyme (0.084 U/ml and 0.168 U/ml). The enzymatic degradation was stopped after 1, 2, 24 and 48 hours by freeze drying the samples to recover the solid degraded polymer.

## 5.11 Characterizations

### 5.11.1 Infrared spectroscopy

FT-IR analysis of gamma-irradiated Deg-XGs (Section 5.8.1), e-beam-irradiated XGs (Section 5.8.3) and functionalized XGs and Deg-XGs (Section 5.9) was carried out with a Perkin Elmer-Spectrum 400 apparatus at the University of

Palermo. Samples were prepared by dispersing the dry products in potassium bromide and compressing into pellets. Spectra were recorded at 30 scans per spectrum and 1 $cm^{-1}$ resolution in the 4000-450 $cm^{-1}$ range. All spectra have been normalized with respect to the peak correspondent to the stretching of methylene groups (2956 $cm^{-1}$).

### 5.11.2 Chromatography

The chromatographic profiles of gamma-irradiated Deg-XGs (Section 5.8.1), e-beam-irradiated XGs (Section 5.8.3) and functionalized XGs and Deg-XGs (Section 5.9) were obtained by using two Shodex SB HQ columns in series (806 and 804) thermostated at 15 °C with a Knauer oven and connected to a HPLC device (LC-2010 AT Prominence, Shimadzu, Kyoto, Japan) equipped with a 50 µl sample loop. This equipment belongs to the Biophysics Institute (Palermo Unit) of the National Research Council. All samples were eluted with 0.02% sodium azide solution at 0.5 ml/min and the refractive index was recorded with a Smartline RI detector 2300 Knauer.

SEC measurements of gamma-irradiated Deg-XGs (Section 5.8.2) and enzymatically degraded Deg-XG (Section 5.10) were performed with a Dionex Ultimate-3000 HPLC system (Dionex, Sunnyvale, CA, USA) at the Royal Institute of Technology, Stockholm, Sweden. Measurements were performed at 40°C with 10 mM NaOH as mobile phase flowing at a rate of 1 ml/min. The system consisted of three PSS suprema columns in series (300 × 8 mm, 10 µm particle size) together with a guard column (50 × 8 mm, 10 µm particle size). The system was equipped with a LPG-3400SD gradient pump, a WPS-3000SL autosampler and a Waters-410 refractive index (RI) detector (Waters, Milford, MA, USA). Pullulan standards ranging from 342 to 708,000 Da (PSS, Germany) were used for calibration. Samples were dissolved in 10mM NaOH at a concentration of 2 mg/mL and 20 µL were injected in the system.

### 5.11.3 Small angle X-ray scattering (SAXS)

Small Angle X-Ray scattering (SAXS) experiments were performed at the 5.2 beamline of Elettra Synchrotron in Trieste, Italy, on purified and gamma-irradiated Deg-XG dispersions (Section 5.8.1). Measurements were carried out at 20 °C, using a sealed 1 mm diameter glass capillary enclosed within a thermostated compartment connected to an external circulation bath and a thermal probe for temperature control. The sample-detector distance was set to 2.72 m and the X-ray wavelength λ was 0.154 nm. Because the scattering vector is $Q = 4\pi \sin\theta/\lambda$ (where $2\theta$ is the scattering angle), the investigated Q-range was $0.06 < Q < 3.0$ nm$^{-1}$. SAXS profiles were recorded on an image plate detector and for each SAXS measurement the acquisition time was 2 min.

### 5.11.4 Static and Dynamic Light scattering (SLS, DLS)

Both for static and dynamic light scattering measurements, samples were placed into a thermostated cell compartment of a Brookhaven Instrument BI200-SM goniometer (Biophysics Institute, Palermo Unit, National Research Council). Temperature was controlled to within 0.1°C using a thermostated recirculating bath. The light scattered intensity and time autocorrelation function (TCF) were measured by using a Brookhaven BI-9000 correlator and a 100mW solid-state laser (Quantum-Ventus MPC 6000) tuned at $\lambda$ = 532 nm or a 50mW He–Ne tuned at $\lambda$ = 632.8 nm. Measurements were taken at different scattering vectors $q=4\pi n \lambda_0^{-1}/\sin(\theta/2)$, where $n$ is the refractive index of the solution, $\lambda_0$ is the wavelength of the incident light, and $\theta$ is the scattering angle. In dynamic light scattering (DLS) experiments the correlator operated in the multi-$\tau$ mode and the experimental duration was set to have at least 2000 counts on the last channel of the correlation function. Static light scattering data were corrected for the background scattering of the solvent and normalized by using toluene as calibration liquid. All samples were filtered through 5 or 1.2 μm cellulose acetate (Millipore) syringe filters to remove gross contaminants.

Scattering measurements results reported in Tab. 9.1 have been obtained through the Zetasizer Nano ZS (MALVERN), of the Institute of Applied Radiation Chemistry at the University of Lodz (Poland). The instrument was tuned at 670 nm and measurements were performed at 173° scattering angle ("back scattering").

### 5.11.5 Rotational viscosimetry and dynamic-mechanical stress rheometry

A stress-controlled Rheometer Ar G2, TA Instruments (Bipohysics Institute, Palermo Unit, National Research Council) was used in rotational mode for shear viscosity measurements and in oscillatory mode for strain and frequency sweep tests. Low concentrated samples were analyzed with an acrylic plate-cone geometry (diam. 4 cm) and a gap of 30 μm, while concentrated samples and gels were analyzed with an acrylic plate-plate geometry (diam. 4 cm) and a gap of 500 μm.

Shear viscosity measurements were performed at 15 and 20°C and the duration of measurements was chosen according to the explored shear rate range.

Dynamic-mechanical properties of gels were evaluated in terms of the shear elastic modulus, *G'*, and the shear loss modulus, *G''*. Measurements were performed at 37°C. Temperature control was provided by a Peltier plate and samples were cast between the lower Peltier plate and the upper parallel plate. The exposed edges of the samples were coated with silicone oil to prevent water evaporation and the plates were enclosed in a chamber to ensure temperature control during measurements. Preliminary experiments showed that mechanical properties of the gels were unaffected by the silicone oil, whereas the absence of silicone oil led to progressive increments of both elastic and loss modulus while the gel was drying out on the rheometer plates.

Preliminary strain sweep tests at 1 Hz frequency in the shear strain range 0.001-10 were performed, then frequency sweep tests in the frequency range 0.01-100 Hz were performed at 0.004 strain, i.e. within the linear viscoelastic region of the gels. Frequency sweep tests were both carried out after 5 and 30 minutes of incubation at 37°C.

Shear viscosity measurements described in Fig. 9.6 were performed at 25°C with a Haake Rheometer RT 20 (University of Lodz, Poland). Rotational tests were carried out in the shear rate range 0.3-2900 1/sec. Due to the different features of the analyzed samples, two sensors were used: 0.1 wt% polymer concentration systems were analyzed with a cone-plate sensor (double cone), while 0.5 wt% polymer concentration systems were evaluated with a coaxial cylindrical sensor. Indeed, the 0.5 wt% systems are less homogeneous and the cylindrical sensor allows a better containment of them.

### 5.11.6 Scanning Electron Microscopy (SEM)

Surface morphology was imaged by a field emission scanning electron microscopy (FESEM) system (JEOL) at an accelerating voltage of 10 kV. Samples for FESEM were coated with a gold layer by JFC-1300 gold coater (JEOL) for 50 s at 30 mA before scanning. Freeze-dried samples were mounted on SEM aluminium stubs by means of a graphite adhesive layer.

For the analysis of Deg-XG nanoparticles morphology, samples were diluted 100 times before deposition on aluminium stubs to avoid collapse of Deg-XG aggregates during water evaporation, and then coated with a gold layer by JFC-1300 gold coater (JEOL) for 50 s at 30 mA.

### 5.11.7 Biological evaluation of Deg-XG nanoparticles

***Cell Cultures:*** The mouse embryonic fibroblast (NIH/3T3) cell lines from the American Type Culture Collection (ATCC), USA, were grown in Dulbecco's modified Eagle's medium (DMEM) supplemented with 10% fetal bovine serum, penicillin (100 units/mL), and streptomycin (100 µg/mL). Cells were maintained in a humidified atmosphere of 5% $CO_2$ at 37°C. Confluent cells were detached using 0.25% (w/v) trypsin-EDTA.

***Cell Viability:*** NIH/3T3 cells were seeded in 96-well plates at a density of $1.0x10^4$ cells per well and incubated for 24 h at 37°C in a humidified atmosphere of 5% $CO_2$. The aggregation products of Deg-XG were added into the wells at different

concentrations. Negative control cells were also included (untreated with Deg-XG). After 48 h of incubation the cell viability was determined by CellTiter 96 Aqueous One Solution Assay (Promega) that contains tetrazolium compound [3-(4,5-dimethylthiazol-2-yl)-5-(3-carboxymethoxyphenyl)-2-(4-sulfophenyl)-2H-tetrazolium, inner salt] (MTS). 20 µL of MTS solution was added into the well, and the plate was incubated for 1 - 4 h at 37°C in 5% $CO_2$ atmosphere. Viable cells colonies would produce formazan whose amount could be determined by measuring its absorbance at 490 nm with a 96-well plate reader (BioRad). Cell viability, expressed in percentage of control cells, was calculated as:

$$Viability\ (\%) = \frac{Abs\ (sample) - Abs\ (blank)}{Abs\ (control) - Abs\ (blank)}\ x\ 100 \qquad \textbf{Eq. 5.3}$$

Treatments were tested in triplicates.

# 6 TEMPERATURE-TRIGGERED SELF-ASSEMBLY OF DEG-XG AT LOW CONCENTRATION

## 6.1 Aim and introduction

The partially degalactosylated xyloglucan variant is able to self-assemble in response to a temperature variation. [119] In particular, at appropriate galactose removal ratios (when more than 35% of the galactose residues are removed) and polymer concentration (around 1-2 wt%), this transition is triggered by physiological temperature and leads to the formation of gels that can be employed as drug delivery systems [146-155] or as scaffolds for tissue engineering. [156] The understanding of the self-assembly mechanism that is at the basis of the gelation process is mandatory for the tailoring of gel properties to satisfy specific requirements of the desired applications. This task is particularly arduous in the case of natural polysaccharides such as xyloglucan: many factors derived from their natural source, function in the plant and extraction process can influence their structural composition, molecular weight and supramolecular organization. For this reason, it is crucial to find effective methods to extract, purify, characterize and tailor Deg-XG molecular properties and structure and thereby achieve adequate water solubility/dispersibility, as well as to influence the polymer self-assembly behavior. Dispersibility and purification protocols are described in the experimental section of this dissertation (Sections 5.2 and 5.4) and in the Appendix.

In this chapter, the temperature-triggered self-assembly of Deg-XG dispersed in water at concentration low enough not to run in macroscopic gelation (0.1 wt%) is investigated to elucidate the mechanism by which a modification of the interactions landscape leads to self-assembly. To this purpose, the effect of temperature changes are studied over a length scale ranging from molecular to supramolecular, by recurring to different and complementary experimental techniques. The effects of temperature variations are studied both upon temperature jumps or during temperature scans, in the range 15-50°C, by static and dynamic light scattering (SLS and DLS). Then, the aggregation products obtained after prolonged conditioning of Deg-XG

aqueous dispersions at 37°C are analyzed by small angle X-ray scattering (SAXS), shear viscosity and scanning electron microscopy.

Finally, the suitability of these nanoparticles for the incorporation and delivery of hydrophobic drugs is evaluated. Indeed, there are very few studies concerning the use of semi-dilute/dilute xyloglucan systems for the preparation of nanoparticles to be employed in drug delivery [128, 130] and this is probably due to the intrinsic difficulties related to the obtainment of collodailly-stable polymer dispersions. Here, Deg-XG nanoparticles cytotoxicity against mouse embryonic fibroblast (NIH/3T3) cell line was tested by a MTS assay. Then camptothecin, an anti-tumoral drug, [164] was physically incorporated in the nanoparticles.

## 6.2 Materials and methods

Xyloglucan with a galactose removal ratio of 44% (Deg-XG) was kindly provided by DSP Gokyo, Food and Chemical Co, Japan. Suitable dispersion and purification protocols were developed to obtain colloidally stable polymer dispersions in water: these protocols are described in Sections 5.2 and 5.4 and in the Appendix.

***Light Scattering measurements***

Dynamic and static light scattering (DLS and SLS) measurements were performed as described in Section 5.11.4. All samples were filtered through 1.2 µm cellulose acetate (Millipore) syringe filters to remove gross contaminants.

For single measurements performed at 90° scattering angle and at 15°C the method of cumulant [164] and the exponential stretched method were compared to obtain information on the apparent hydrodynamic size and width of the size distribution. According to the cumulant method, the logarithm of the electric field autocorrelation function can be expanded in terms of the cumulants of the distribution:

$$\ln[g(\tau)] \equiv K(-\tau, \Gamma) = -\Gamma\tau + \frac{k_2}{2!}\tau^2 - \frac{k_3}{3!}\tau^3 + \frac{k_4}{4!}\tau^4 \ldots \qquad \textbf{Eq. 6.1}$$

The fitting of the auto-correlation function to a stretched exponential is given by the equation:

$$g(\tau) = A\, exp(-(t/\tau)^{-\beta}) \qquad \textbf{Eq. 6.2}$$

where $\tau$ is the relaxation time and $\beta$ is the stretched exponential and it is related to the width of the relaxation time distribution. $\beta$ values are in the range 0-1, with smaller values corresponding to wider distributions.

The average relaxation time $\tau_c$ can be calculated by:

$$\tau_c = \frac{\tau}{\beta}\, \Gamma\left(\frac{1}{\beta}\right) \qquad \textbf{Eq. 6.3}$$

where $\Gamma$ is the gamma function.

In Fig. 6.1 the comparison between these two fitting methods is shown for a decay curve obtained at 15°C and at the scattering angle of 90° by a DLS measurement performed on a 0.1 wt% purified Deg-XG aqueous dispersion.

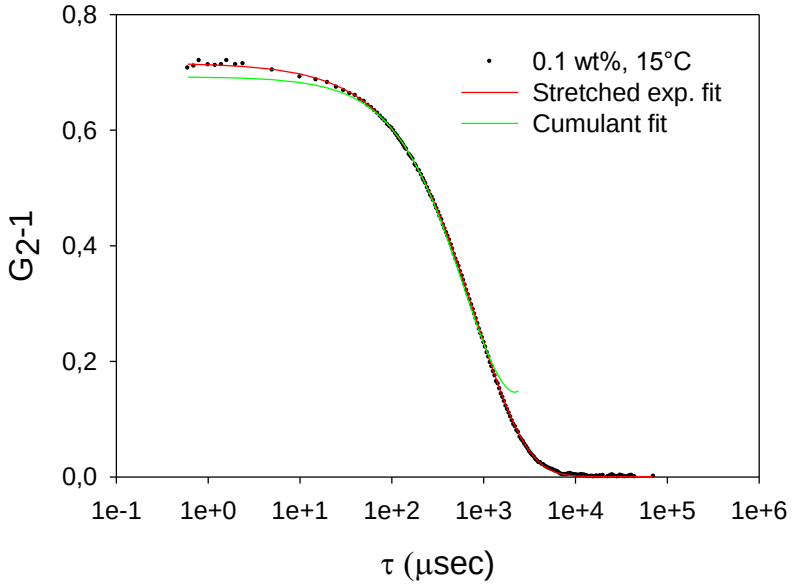


**Fig. 6.1:** Comparison between the cumulant method and the stretched exponential method for the fitting of decay curves obtained by DLS measurements.

Quite evidently, the better fitting is the stretched exponential one. Indeed, with the cumulant method the contribution of the large objects is excluded from the analysis by truncating the fitting at $\tau$ of about 1000 μs. Besides, the stretched exponential method better fits the initial part of the decay curve.

The normalized scattered intensity obtained by static light scattering measurements at the variance of the scattering angle can be fitted according to the typical expression for fractal aggregates shown in Eq. 6.4.

$$P(q) = \left(1 + a\left(qR_g\right)^2\right)^{-d_f/2} \quad with\ a = \frac{2}{3d_f} \qquad \textbf{Eq. 6.4}$$

where $R_g$ is the gyration radius and $d_f$ is the fractal dimension.

Aggregation kinetics at 0.1 wt% polymer concentration were studied by collecting the scattered light intensity from a set of DLS runs performed in isothermal conditions and as function of time, at the following temperatures: 20, 25, 30, 34, 37, 45, 50°C. Then, aggregation was also studied by the imposition of a temperature ramp of 10 °C/h, from 15 to 60°C.

***Shear viscosity measurements***

Shear viscosity measurements were performed according to Section 5.11.5. Besides, Deg-XG aqueous dispersion prepared at 0.1 wt% polymer concentration was analyzed imposing a temperature ramp of 10°C/h from 15 to 60°C and then of -10°C/h from 60 to 15°C.

***SAXS experiments***

Small Angle X-Ray scattering (SAXS) experiments were performed at the 5.2 beamline of Elettra Synchrotron in Trieste, Italy, as described in Section 5.11.3.

***Scanning Electron Microscopy***

SEM images were acquired according to Section 5.11.6. Samples were diluted 100 times before deposition on aluminium stubs to avoid collapse of Deg-XG aggregates during water evaporation, and then coated with a gold layer by a JFC-1300 gold coater (JEOL) for 50 s at 30 mA.

***Cell Cultures and Cell Viability***

Cell cultures and cell viability protocols are described in Section 5.11.7. Cell viability was computed according to Eq. 5.3.

***Physical incorporation of camptothecin***

Deg-XG aqueous dispersions were loaded with camptothecin as described in Section 5.6. After liquid-liquid extraction and re-dispersion in DMSO of the drug that

was not interacting with the polymer, the drug load content and the entrapment efficiency were evaluated according to Eq. 5.1 and Eq. 5.2, respectively.

## 6.3 Results

### 6.3.1 Characterization of low concentrated Deg-XG aqueous dispersions at 15°C

In applying light scattering techniques to the study of natural polysaccharides such as Deg-XG, the major difficulty is caused by the presence of large aggregates even in dilute solutions. [103, 104, 165] This, along with the heterogeneity of polymer molecular structure and its dependence on the extraction techniques, can make very arduous to obtain accurate determination of molecular weight and mean-square gyration radius. [166]

Different techniques of solution clarification based on the use of chaotropic solvent [103, 104] or "pressure-cell" heating method [101] had proved that it is quite impossible to obtain a solution of monodisperse chains. Rather than pursuing impervious strategies, we have chosen to work on mildly clarified, semidilute solutions prepared following a well-established protocol, [167] as the aim is to gather information that can be reasonably compared with that obtained on the same system at gelling concentration.

Multi-angle SLS and DLS measurements were performed at 15°C on 0.1 wt% Deg-XG aqueous dispersions: results shown in Fig 6.2-a (form factor obtained by SLS measurements) and 6.2-b (average relaxation time obtained by fitting DLS measurements with the stretched exponential method) indicate the presence of more complex structures than isolated polymer chains. Indeed, the form factor reported in Fig 6.2-a can be fitted by Eq. 6.4: $R_g$= 230 nm and $d_f$ = 2.7 are obtained. The $d_f$ value indicates the presence of quite compact structures (the fractal dimension of an hard sphere being 3 [168]).

Electric field autocorrelation functions at any scattering angle were fitted to the stretched exponential method expressed by Eq. 6.2.

This expression is often used to describe the complex dynamics of disordered materials such as polymeric melts or supercooled liquids close to the glass transition. [169] The microscopic origin of this dynamical behavior has been ascribed to the existence of structural heterogeneities at microscopic level. Different regions of the sample all relax exponentially, but with different structural relaxation times. The width of relaxation time distribution is characterized by the value of $\beta$ ($0 < \beta < 1$), with a smaller value corresponding to a wider distribution. Fig 6.2-b shows the q-dependence of the average relaxation time calculated by Eq. 6.3.

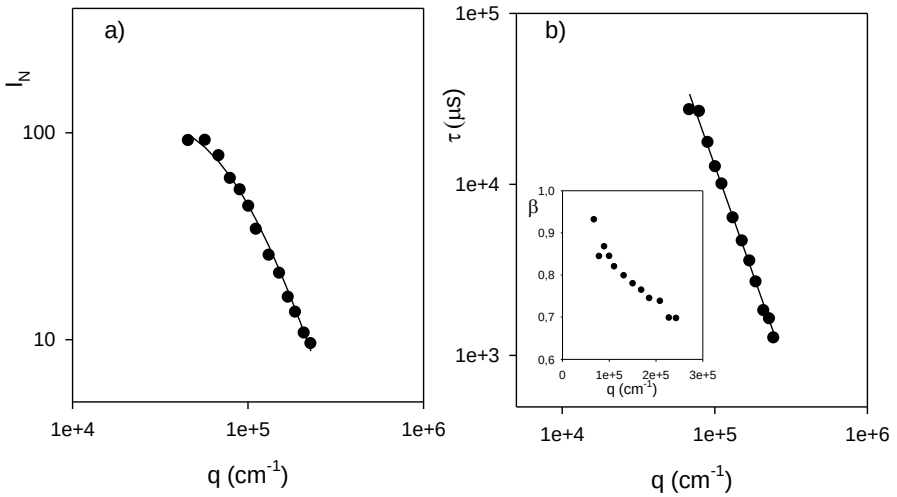


**Fig. 6.2:** Characterization by static and dynamic light scattering of Deg-XG in aqueous dispersion at 0.1 wt% and T=15 °C. Panel A: form factor; the continuous line through data points was fitted to Eq. 6.4. Panel B: average relaxation time obtained by fitting a stretched exponential to the correlation function. The inset shows the q-dependence of the exponent $\beta$.

The exponent of the *q*-dependence of the average relaxation time is 2.5, thus indicating that the detected dynamics could contain vibrational motions contribution. [170] Interestingly, $\beta$ exponent is closer to 1 at smaller q-values, thus signifying that

the dynamical behavior appears more homogeneous when probed on longer length scale. The q-dependence of $\beta$ is curiously similar to that determined by Molecular Dynamics simulations for the self-dynamics of supercooled water on approaching the glass transition. [171] Authors discussed this dependence in terms of confined motions inside molecular cages that become less relevant when the solute movement is probed over lengths larger than the confinement dimension. It is not so simple to extend this perspective to the case of a polydisperse polymer solution. One could figure that the largest polymeric clusters, which give a major contribution to the correlation function at low q-values, move more freely than smaller clusters and individual polymer chains, which instead experiment a hindered motion due to mutual interaction. [172]. An alternative interpretation can be provided by the Coupling model, that attributes the non-exponential behavior to the existence of motional constraints imposed by inter-particle interactions. [172] In this frame, all sample regions relax with the same stretched exponential behavior with a $\beta$ value as lower as stronger are the interactions. The model also predicts a q-dependence of the characteristic relaxation time expressed by Eq. 6.5: [172]

$$\tau(q) \propto q^{-2/\beta} \qquad \textbf{Eq. 6.5}$$

with $\beta$ independent on $q$. It is noteworthy that in our case the exponent that describes the q-dependence of the average relaxation time should correspond to a constant $\beta$ value of 0.8. We observed instead that $\beta$ monotonically decreases from 0.85 to 0.75 while $q$ increases, suggesting that the interactions are progressively weaker at the increase of the length interval probed by DLS measurements.

### 6.3.2 Self-assembly of Deg-XG upon temperature jump

The response of Deg-XG aqueous dispersions to temperature changes were investigated by static and dynamic light scattering measurements at 90° angle.

Fig. 6.3 shows the time dependence of the light scattered intensity by samples conditioned at different constant temperatures.

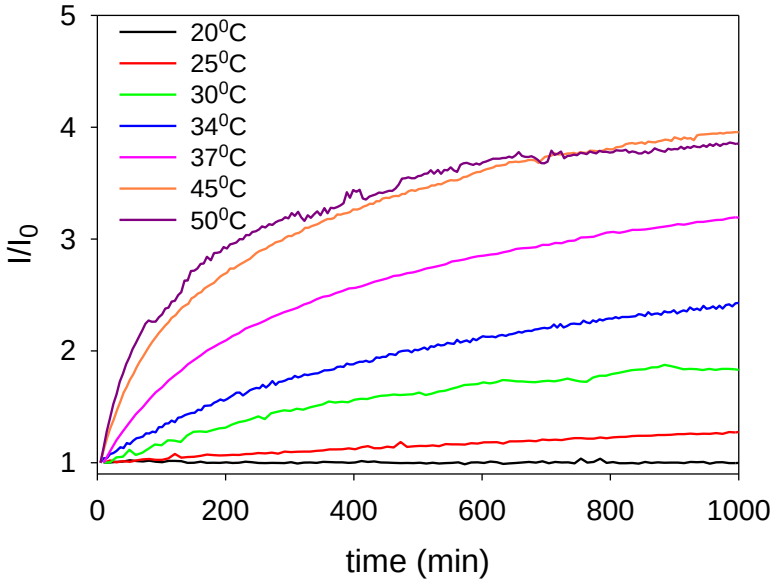


**Fig. 6.3:** Time-course of the normalized scattered intensity from Deg-XG aqueous dispersions conditioned at different temperatures.

At temperatures above 20°C, the signal was observed to increase with larger rate at higher temperature. No changes were observed at 20°C and below, even after some days.

The fitting parameters derived from the stretched exponential method, i.e. the characteristic relaxation time $\tau_c$ and the exponent $\beta$, are shown in Fig. 6.4-a and Fig. 6.4-b, respectively, for some selected temperatures. Both $\tau_c$ and $\beta$ grow with time, indicating that the system dynamics become progressively slower but, at the same time, more homogeneous, at least on the length scale of a few tens of nanometers. The temperature effect on both parameters gradually reduces as no large differences are noted between 37 and 50°C.

The increase of scattered intensity and average relaxation time upon a temperature jump above the threshold value of 20°C indicates the occurrence of an aggregation process at mesoscopic scale, similarly to the one leading to macroscopic gelation at higher concentration. Interestingly, the aggregation of single polymer chains and pre-existing clusters is accompanied by a decrease of dynamical inhomogeneity. In principle, this could be ascribed to a reduction of structural inhomogeneity of microscopic regions in the scale of a few hundreds of nanometers, as discussed above, or interpreted in the frame of the Coupling model as a sign of the weakening of mutual interactions.

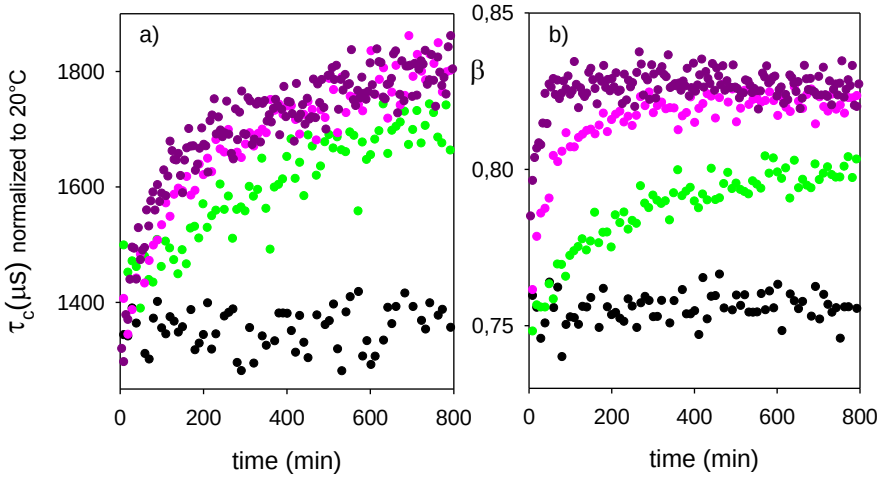


**Fig. 6.4:** Fitting parameters of the autocorrelation function as function of time for Deg-XG aqueous dispersions conditioned at different temperatures: 20°C (black), 30°C (green), 37°C (pink), 50°C (purple). Panel a: average relaxation time $\tau_c$. Panel b: stretching exponent $\beta$.

To verify if the changes induced by prolonged incubation at physiological temperature are reversible, DLS measurements at 90°C were performed. In particular, the decay curve of the "freshly prepared" sample (black plot), of the sample after

prolonged incubation at 37°C (red plot) and of the sample that was incubated again at 5°C for 48 hours after prolonged conditioning at 37°C (green plot) are shown in Fig. 6.5 and fitting parameters are reported in Tab. 6.1.

It is possible to notice that these changes are not reversible. Indeed, when the incubated sample was re-conditioned at lower temperature, neither the scattered intensity nor the dynamics parameters regain their initial values.

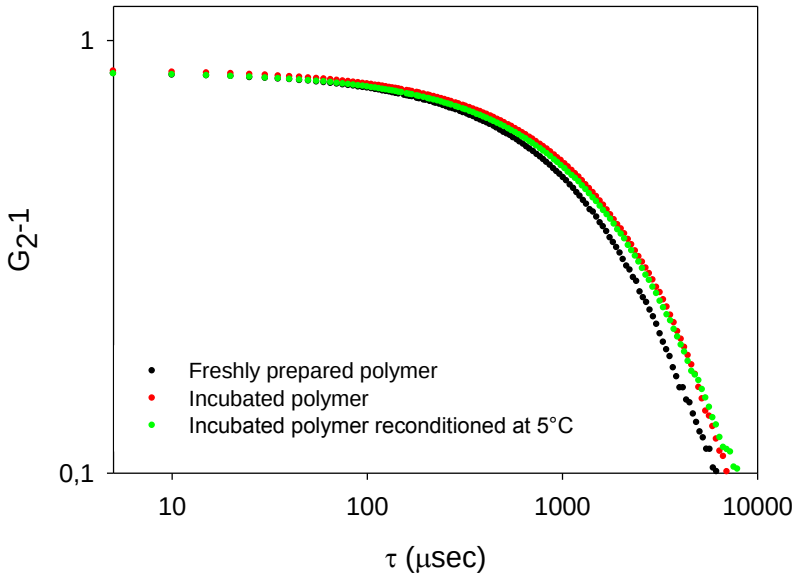


**Fig. 6.5:** DLS measurements performed to test the reversibility of the aggregation process.

**Tab. 6.1:** Fitting parameters of the decay curves reported in Fig. 6.5.

| **Sample** | **$\tau_c$** | **β** |
|---|---|---|
| Freshly prepared | 2155.7 | 0.81 |
| Incubated | 2504.7 | 0.81 |
| Incubated and reconditioned | 2414.8 | 0.81 |

### 6.3.3 Deg-XG self-assembly over a temperature scan

As xyloglucan deprived of a certain amount of hydrophilic groups becomes capable of undergoing gelation upon a temperature increase, it could be argued that the change of solute-solvent interaction landscape has made accessible the phase transition region. We attempted to detect LCST of Deg-XG aqueous dispersions by light scattering measurements in the course of a temperature scan. Results are shown in Fig. 6.6, Panels a and b. Starting from 30°C, the scattered intensity steadily increases by following a diverging behavior up to about 45°C, then the growth rate progressively decreases. The characteristic relaxation time $\tau_c$ and the stretched exponent $\beta$ remain constant up to 30°C, then they both start to increase indicating that the system dynamics become progressively slower but less inhomogeneous, similarly to the behavior observed for the isothermal kinetics carried out at different temperatures.

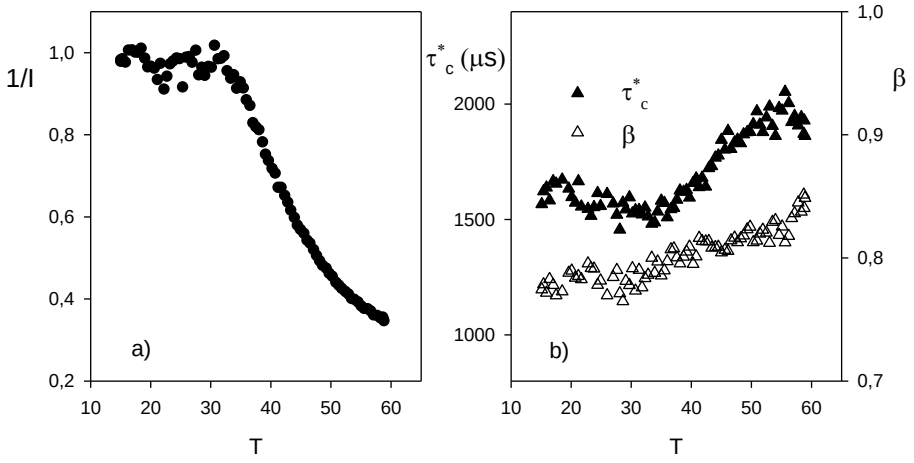


**Fig. 6.6:** Results from light scattering measurements during a temperature scan (at 10°C/hr) on Deg-XG aqueous dispersion. Panel a reports the inverse of static scattered light as a function of temperature. The red line is drawn to indicate the divergence temperature value predicted by 1/I linear trait. Panel b shows the characteristic relaxation time $\tau^*_c$ and stretched exponent $\beta$ obtained by fitting the intensity autocorrelation functions with Eq. 6.2. Values of $\tau^*_c$ at different

temperature are scaled for the quantity [T $\eta_{15°C}$ / 288.15 $\eta_T$] to take into account the normal dependence on temperature and viscosity.

It is noteworthy that final values for $\tau_c$ and $\beta$ obtained after isothermal treatments at different temperatures are about the same of those measured during the temperature scan. This result is not so obvious since it could be expected that the aggregation process is influenced by non-equilibrium conditions. Moreover, the final aggregation state of LCST thermosensitive polymer should strongly depend on the rate of temperature change due to the competition between phase separation and coil-globule transition. [165] Another temperature scan was performed using a lower scan rate, but no difference was found (data not shown). However, the presence of a temperature threshold below which the system remains in equilibrium state supports the hypothesis of a phase separation whose detection could be obscured by non-reversible aggregation and intrinsic polydispersity of the system.

### 6.3.4 Change of structural and dynamical properties upon prolonged incubation at 37°C.

Since Deg-XG aggregates formed upon a temperature increase were stable over time and did not revert to their initial state when conditioned again at lower temperature, it was possible to perform a detailed characterization of their structural and dynamical properties. Results from light scattering measurements performed at different scattering angles before and after prolonged incubation at 37°C are shown in Fig 6.7.

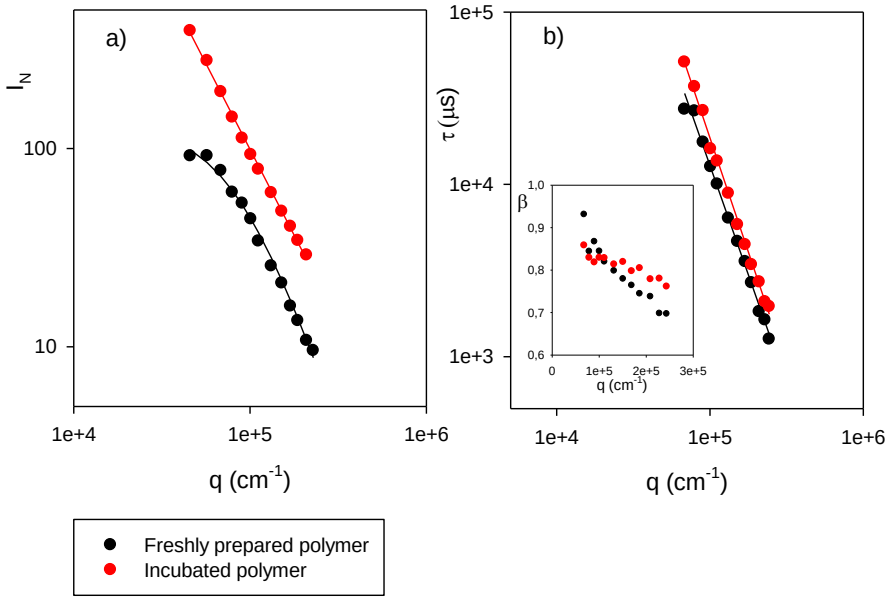


**Fig. 6.7:** Light scattering characterization of Deg-XG aqueous dispersions before and after incubation at 37°C for 24 hr (measurements performed at 15°C). Panel a: form factor; Panel b: average relaxation time obtained by fitting the correlation function to a stretched exponential. The inset shows the q-dependence of the stretched exponential $\beta$. Results obtained for nonincubated samples have been already shown in Fig. 6.2 but they are again reported here for comparison.

The static light scattered intensity was much higher for the incubated sample, and displayed a power law q-dependence over the entire q-interval explored, thus indicating a large increase of the average size of objects in solution. Larger average relaxation times were observed at any scattering angle following a $q^n$ dependence with a $n$-value about equal to that found for the non-incubated polymer. The exponent $\beta$ exhibited, instead, a weaker q-dependence, since higher values were found at large $q$. This indicates that on the length scale of some tens of nanometers the dynamics of the

incubated systems are more homogeneous, or, in the frame of the Coupling model, the strength of interactions is lower.

An increase of the average size was also indicated by the comparison of the flow curves measured at 15°C on a freshly prepared sample and a dispersion re-conditioned at low temperature after the temperature scan. Indeed, the heated polymer shows a shear thinning behavior and a higher value of the high shear rate viscosity, thus suggesting the presence of larger and stiffer aggregates formed upon heating up to 60°C.

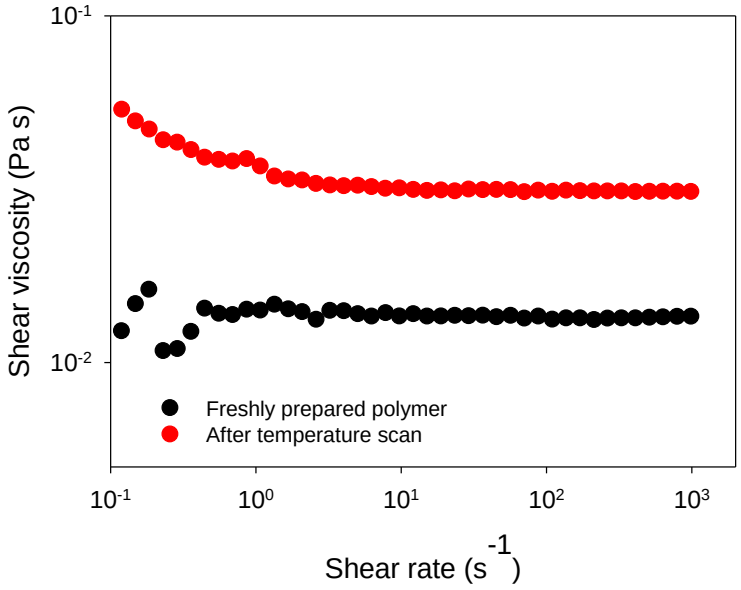


**Fig.6.8:** Flow curves for a freshly prepared Deg-XG aqueous dispersion and after a temperature scan up to 60°C. Measurements were performed at 15°C.

The difference between the structural properties of freshly prepared and incubated polymer, on a few nanometers length scale, was investigated by SAXS measurements. Results reported in Fig. 6.9 are presented in the form of Kratky plots.

A large difference can be noted between the two plots. The Kratky plot for the freshly prepared polymer is that typical of a random chain, with the characteristic plateau at large q-values, whereas the one for the sample incubated at 37°C exhibits a bell-shaped profile indicating the presence of globular structures. [173]

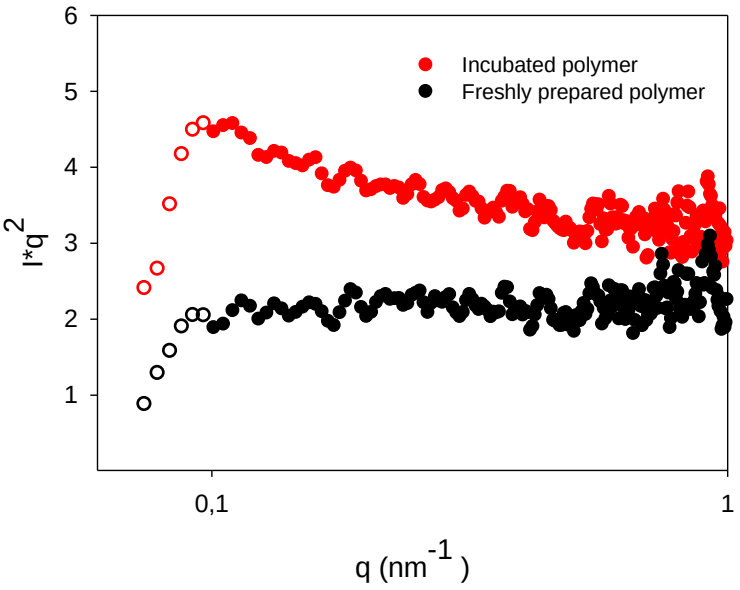


**Fig. 6.9:** Kratky plot for the freshly prepared polymer and the polymer that was incubated at 37°C for 20 hours (measurements performed at 20°C).

SEM technique was also employed to get a picture of polymeric arrangement over the microscopic scale. Images of samples casted from the freshly prepared and incubated systems are shown in Fig. 6.10-a and Fig. 6.10-b, respectively.

A solid residue composed by bigger, compact and roundly shaped nanoparticles forms upon drying from the incubated sample (Panel b), while the one obtained from the freshly prepared system forms a more compact layer where smaller nanoparticles and filamentous structures can be observed (Panel a). Such structural difference at

microscopic scale provides a clue on the origin of the dynamical properties change. Indeed, it is reasonable that compact, yet larger, aggregates can move more freely than entangled clusters.

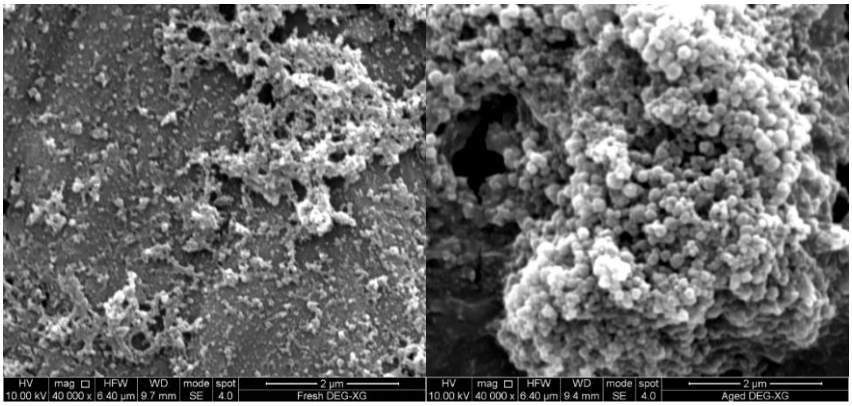


**a)** **b)**

**Fig. 6.10:** SEM images for a) freshly prepared Deg-XG and b) after prolonged incubation at 37°C.

### 6.3.5 Potential use of Deg-XG as thermo-responsive drug delivery system

*Cell viability*

Before testing the ability of Deg-XG aggregates to serve as drug delivery systems, their effect on cell viability was investigated. Preliminary DLS measurements showed that Deg-XG aggregates were not affected by dilution in water (data not shown). The tetrazolium salts MTS test was chosen to investigate the activity of reducing enzymes in the cells. As shown in Fig. 6.11, the presence of Deg-XG nanoparticles in a wide concentration range did not affect the metabolic activity of NIH/3T3 cells after 48 h of treatments, thus proving the absence of cytotoxicity effects.

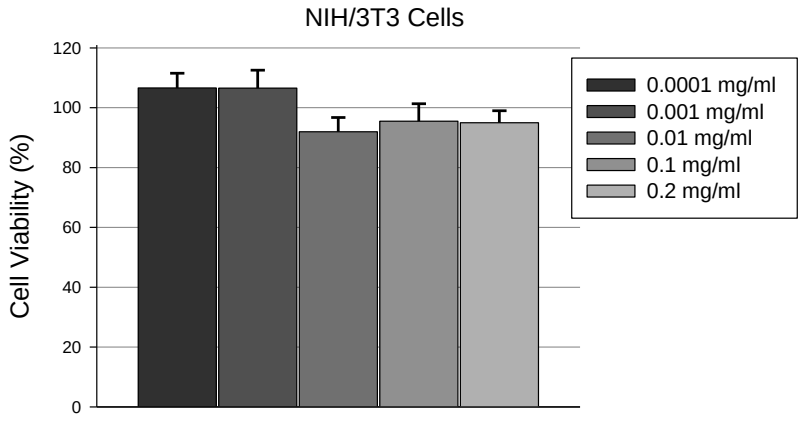


**Fig 6.11.** Cell viability of NIH/3T3 after incubation for 48 hr with 0.1-200 mg/ml Deg-XG nanoparticles.

*Interaction with camptothecin*

Due to its hydrophobic character, Deg-XG could profitably serve to vehicle hydrophobic active molecules. Deg-XG hydrogels have been already proposed as in situ forming drug delivery depots, [146-155] but there are only a few studies concerning the use of Deg-XG nanoparticles prepared with the native or partially degalactosylated polymer and evaluated as drug nanocarriers. [128, 130] We tested the potential use of Deg-XG aggregates as particles to vehicle camptothecin, a cytotoxic quinoline alkaloid that inhibits the DNA enzyme topoisomerase I (topo I) and has a potent antitumor activity against a wide spectrum of human malignancies (stomach, lung, prostate, breast, colon). [174] The incorporation of this molecule in a protective medium is essential for therapeutic uses as the drug is only slightly soluble in water (2.5 µg/ml), [175] it shows toxic effects after long administration times, [176, 177] and, most of all, it can be inactivated by hydrolysis of its lactone ring at neutral and basic pH. Indeed, in these conditions the drug becomes more toxic and 10-fold less pharmacologically active. [178] Because of the considerable self-aggregation phenomenon observed upon dilution from DMSO stock solution to water, we worked with very low CPT concentration. An aqueous dispersion of Deg-XG was loaded with

$2*10^{-5}$ M CPT and let dwell at 20°C for other 24 hours ("as prepared" system). An aliquot was incubated at 37°C for 24 hours ("incubated" system). The drug in excess was then removed from both the "as prepared" and "incubated" system by subsequent liquid-liquid extractions with diethyl-ether. The amount extracted was determined by UV-vis absorption measurements. Similar liquid-liquid extractions were also performed on CPT dispersed at the same concentration in pure water. CPT entrapment efficiency as a function of the extraction number is shown in Fig. 6.12.

Results show that the "as prepared" Deg-XG system retained about 40% of the loaded drug, while the "incubated" system released all the loaded drug, thus suggesting that Deg-XG aggregates tend to release the drug when incubated at 37°C. The drug load content calculated according to Eq. 5.1 is about 0.3% for the "as prepared" system. The amount of CPT retained before incubation, though quite small, is comparable with that obtained for solid lipid nanoparticles. [179]

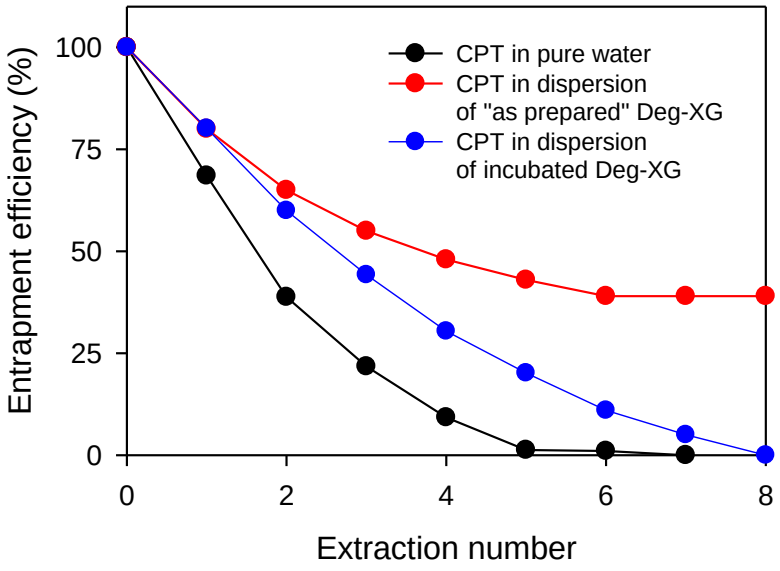


**Fig. 6.12:** CPT entrapment efficiency as function of the extraction number from pure water, "as prepared" Deg-XG dispersion and incubated Deg-XG dispersion.

# 7 GAMMA-IRRADIATION EFFECTS ON DEG-XG SELFASSEMBLY: FROM NANO TO MACROSCALE

## 7.1 Aim and introduction

In this chapter, the possibility to tailor degalactosylated xyloglucan molecular and/or chemical properties and functionality through the application of gamma-irradiation treatment is discussed. Generally, natural biopolymers show high average molecular weight, broad molecular weight distribution and poor water solubility, as large and compact aggregates usually form via inter-molecular hydrogen bonding. Differently from other natural biopolymers, such as cellulose, [45] starch [43] and chitosan, [44] there are few studies concerning the application of irradiative methods on xyloglucans. [132-134] These studies have been already described in Section 3.5. Briefly, high energy irradiation treatments performed on polysaccharides usually promote chain scission and partial degradation, thus reducing the polymer average molecular weight. Indeed, the possibility to modify the polymer molecular weight distribution can be very useful because self-assembly properties could be affected by these modifications and the comprehension of the mechanisms that rule the self-assembly process is mandatory to exploit this behavior for the production of stimuli-responsive (in this case temperature-responsive) materials. Besides, there is a growing interest in lower molecular weight polymers in the biomedical field, thanks to their improved properties of compatibility and adhesion.

The irradiation effects on molecular and chemical properties and on polymer solubility were investigated by gel filtration chromatography (GFC), Fourier-transform infrared spectroscopy (FT-IR) and dynamic light scattering (DLS) studies. Then, the repercussions on Deg-XG temperature-triggered self-assembly behavior were analyzed. In particular, this behavior has been studied in two concentration regimes, dilute (0.1 polymer wt%) and concentrated (2-6 polymer wt%), for their impact onto two possible domains of application of this polymer, as drug nanocarrier and as scaffold for tissue engineering, respectively. Besides, the combination of

different characterization techniques performed on the two concentration ranges enables us to elucidate the self-assembly mechanisms on different length scales.

In the low concentration regime thermally induced aggregation kinetics of dispersions prepared with either irradiated or nonirradiated polymers were comparatively analyzed. Dynamic light scattering measurements have been performed both in isothermal conditions (37°C) as function of time, and by the imposition of a temperature ramp (from 15 to 40°C), to determine the onset of thermal gelation, $T^0_{gel}$, and the initial rate of scattered light increase, $\Delta I/\Delta t_{20\%}$. SAXS measurements were performed both before and after prolonged incubation at 37°C to elucidate the polymer supramolecular organization in water as function of the irradiation dose. Indeed, the observation of the polymer organization on small length scale (tens of Angstrom) can be very useful for the comprehension of the polymer structural rearrangement upon temperature variations, both before and after the irradiation treatment.

Concentrated systems were analyzed in terms of shear viscosity, dynamic-mechanical properties and morphology. In particular, rheological properties were evaluated at the variance of irradiation dose, polymer concentration in water and incubation times at 37°C (5 and 30 minutes). Results provided insights into the suitability of these systems as *in situ*-forming gels to be employed as scaffolds for regenerative medicine.

## 7.2 Materials and methods

Xyloglucan with a galactose removal ratio of 44% (Deg-XG) was kindly provided by DSP Gokyo, Food and Chemical Co, Japan.

Deg-XG powder was γ-irradiated in air at room temperature using a $^{60}$Co source (Gamma Chamber 5000, Institute of Nuclear Chemistry and Technology, Warsaw, Poland) at 8 kGy/h and irradiation doses of 10, 20, 40 and 60 kGy, as described in Section 5.8.1.

0.1 wt% Deg-XG aqueous dispersions preparation is described in Section 5.4.2, while Deg-XG macrogels preparation is reported in Section 5.7.

***Gel filtration chromatography***

Gel filtration chromatography measurements were performed on 0.1 wt% Deg-XG aqueous dispersions after 1.2 µm filtration as described in Section 5.11.2.

***Fourier transform infrared spectroscopy***

FT-IR spectra were collected as reported in Section 5.11.1. They have been normalized with respect to the peak correspondent to the stretching of methylene groups (2956 $cm^{-1}$).

***Dynamic light scattering***

All samples were filtered through 5 or 1.2 µm cellulose acetate (Millipore) syringe filters to remove gross contaminants and DLS measurements were performed as reported in Section 5.11.4 at 90° scattering angle. Data were analyzed by the stretched exponential method, according to Eqs. 6.2 and 6.3.

***Small angle X-ray scattering***

SAXS experiments were performed as described in Section 5.11.3. The collected data were fitted according to Debye equation:

$$I(q) = \frac{2I_0}{(q^2a^2)^2}(exp(-q^2a^2) - 1 + q^2a^2) \qquad \textbf{Eq. 7.1}$$

where *a* is a structural parameter, that is a measure of the characteristic size of structural inhomogeneity (in Angstrom) of the system.

***Shear viscosity measurements***

Shear viscosity measurements were performed according to Section 5.11.5. The flow curves have been fitted to a power law in the shear-rate range 1-500 $sec^{-1}$ according to Eq. 7.2, also known as Ostwald-de Waele model: [180, 181]

$$\eta = K \times \dot{\gamma}^{n-1} \qquad \textbf{Eq. 7.2}$$

where $\eta$ is the shear viscosity and $\dot{\gamma}$ is the shear rate.

***Dynamic-mechanical stress rheometry***

The elastic modulus *G'* and the loss modulus *G''* were measured through frequency sweep tests performed after 5 and 30 minutes of incubation at 37°C of the high concentrated Deg-XG systems. Measurements are more in detail described in Section 5.11.5.

***Scanning electron microscopy***

SEM imaging was performed according to Section 5.11.6.

## 7.3 Results

### 7.3.1 Effect of gamma-irradiation on Deg-XG molecular and chemical properties.

GFC measurements were performed at 15°C on the 0.1 wt% Deg-XG aqueous dispersions to gather information on the molecular weight distributions before and after irradiation. The evident effect of the absorbed dose on the molecular weight distribution is presented in Fig. 7.1. In particular, the broad and complex signal of the refractive index as function of the elution volume gradually shifts toward smaller values at the increase of the dose absorbed by the polymer, as a clear evidence of the decrease in molecular weight. The weight-average molecular weights ($M_w$) for the different irradiation doses, based on pullulan and dextran standards calibration, are reported in Tab. 7.1, together with the numerical-average molecular weight ($M_n$) and the polydispersity index PI. These values should be considered for comparative purposes only, in consideration of the structural differences among the two polymers used for calibration and Deg-XG: pullulan and dextran are linear polymers, while xyloglucan is highly branched. Furthermore, for the difficulty encountered in the

molecular dissolution of Deg-XG in water, especially the high molecular weight tails probably describe aggregates of more than one macromolecule. For this reason, the observed polydispersity cannot be unequivocally attributed to different chain lengths, in consideration of the well-known self-aggregation propensity of the polymer. [165] For these reasons we will refer to those values as "apparent" $M_n$ and $M_w$. Notwithstanding these limitations, the calculated values of $M_n$ and $M_w$ are in good agreement with the values reported in the literature for native XG ($M_w$ range: 650,000 to 2,500,000 Da). [98] By increasing the dose, a progressive decrease in average molecular weight and the attainment of a condition of minimum polydispersity at 40 kGy can be observed. A higher imparted dose leads to a further molecular weight reduction accompanied by a broadening of the molecular weight distribution.

The decrease in the average molecular weight at the increase of the irradiation dose can be better appreciated through the deconvolution of raw data in different families (Fig. 7.2 a-f). The most significant families are the blue and the red one, and the relative area percentage of these curves as function of the irradiation dose is reported in Panel f of Fig. 7.2. It is possible to observe a noticeable decrease of the relative area percentage of the blue family with the concomitant increase of the population represented by the red family. Therefore, it can be concluded that gamma irradiation is surely an effective tool in reducing the molecular weight of the polymer in the range of hundreds of kDa, but the absorbed dose should be carefully controlled to avoid undesired broadening of molecular weight distributions. In particular, 40 kGy dose ensures a reduction of both molecular weight and polydispersity index (see Tab. 7.1).

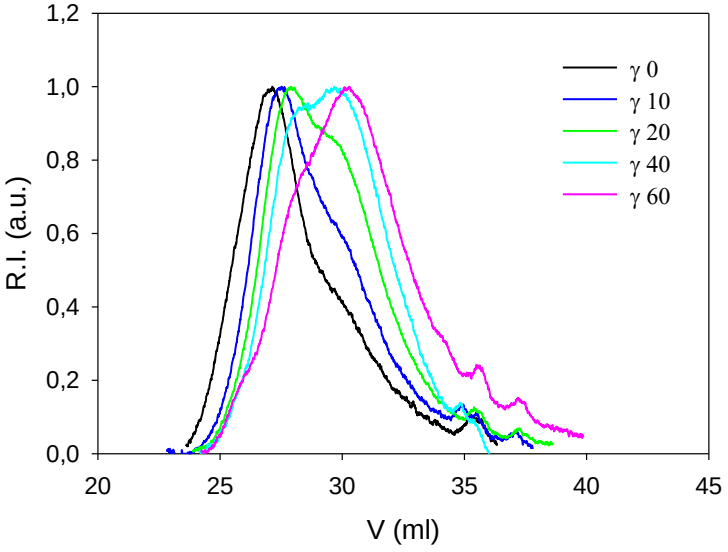


**Fig. 7.1:** Chromatograms of irradiated Deg-XG obtained by GFC measurements.

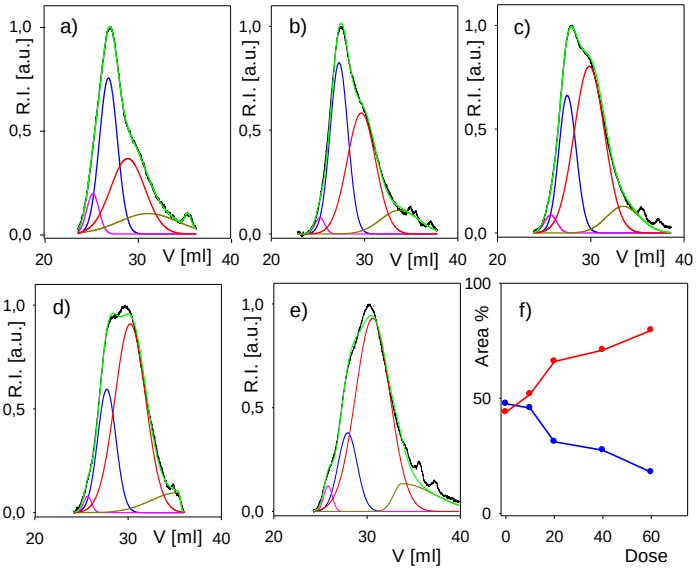


**Fig. 7.2:** GFC results for the polymer dispersed in water at 0.1 wt% irradiated with a) 0 kGy (non irradiated); b) 10 kGy c) 20 kGy d) 40 kGy e) 60 kGy f) area % under the blue and the red

curves as function of the dose. The chromatographic profile (black line) was deconvoluted using four different families (I: pink; II: blue, III: red, IV: dark green).

**Tab. 7.1:** $M_n$, $M_w$ and PI for the irradiated samples.

| Dose [kGy] | $M_n$ [kDa] | $M_w$ [kDa] | PI |
|---|---|---|---|
| 0 | 342 | 1280 | 3.74 |
| 10 | 226 | 911 | 4.03 |
| 20 | 181 | 732 | 4.04 |
| 40 | 247 | 637 | 2.58 |
| 60 | 96 | 500 | 5.20 |

The dynamics of irradiated Deg-XG dispersed in water in the semidilute regime have been investigated by DLS, with measurements performed at 15°C and best fitted with a stretched exponential. This model is well suited to describe systems with "heterogeneities" at the scale of a few hundred of nanometers, each relaxing exponentially with a characteristic structural relaxation time. The nature of these "heterogeneities" has been addressed in detail in Chapter 6. Here, we can succinctly say that they can either refer to the presence of clusters of different size, i.e. system polydispersity, or to motional constraints imposed by inter-particle interactions. The autocorrelation functions reported in Fig. 7.3 were fitted according to the stretched exponential method: the average relaxation time $\tau_c$ and the exponent of the stretched exponential $\beta$ are reported in Tab. 7.2.

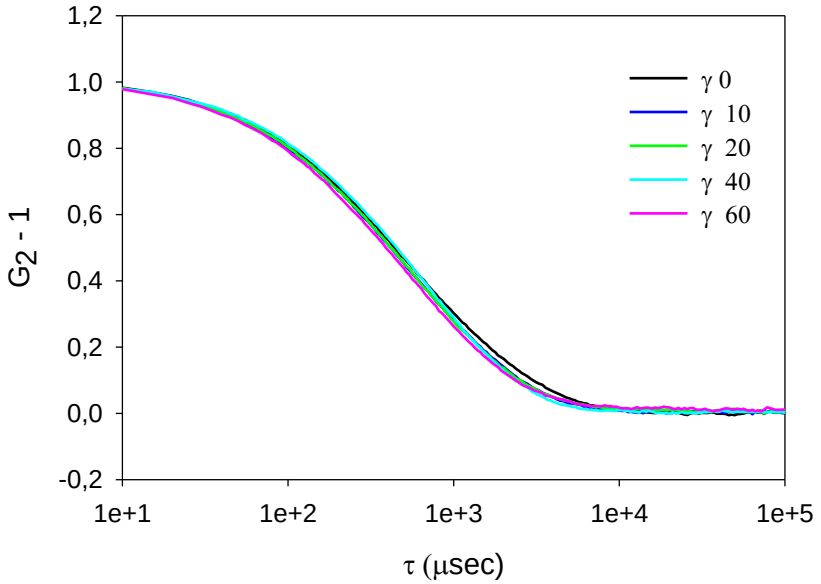


**Fig. 7.3:** Auto-correlation functions measured by DLS at 15°C

**Tab. 7.2:** Stretched exponential fitting parameters estimated for aqueous dispersions equilibrated at 15°C (upon filtration with 5 μm pore size filters) and for dispersions incubated for 40 minutes ($t_{in}$), 5 hours ($t_2$), 10 hours ($t_3$) and 18 hours ($t_f$) at 37°C (upon filtration with 1.2 μm pore size filters).

| **Dose (kGy)** | **$\tau_{c\ 15°C}$ (μsec)** | **$\beta_{15°C}$** | **$\tau_{c\ 37°C}$ (μsec)** | | | | **$\beta_{37°C}$** | | | |
|---|---|---|---|---|---|---|---|---|---|---|
| | | | $t_{in}$ | $t_2$ | $t_3$ | $t_f$ | $t_{in}$ | $t_2$ | $t_3$ | $t_f$ |
| 0 | 2535 | 0.64 | 979 | 1127 | 1153 | 1214 | 0.84 | 0.84 | 0.84 | 0.84 |
| 10 | 2069 | 0.68 | 870 | 1013 | 1065 | 1111 | 0.88 | 0.87 | 0.87 | 0.86 |
| 20 | 1858 | 0.70 | 900 | 1009 | 1018 | 1082 | 0.87 | 0.87 | 0.87 | 0.86 |
| 40 | 1995 | 0.74 | 773 | 792 | 824 | 855 | 0.86 | 0.88 | 0.88 | 0.88 |
| 60 | 1633 | 0.71 | 691 | 776 | 799 | 802 | 0.89 | 0.89 | 0.89 | 0.90 |

The observed trends for $\tau_c$ and $\beta$ are remarkably similar to those observed for the average molecular weight and polydispersity, respectively. The monotonic decrease of $\tau_c$ increasing the dose indicates that the dynamics become progressively faster, i.e.

associated to objects of smaller apparent hydrodynamic diameter; this result is well in agreement with the observed progressive reduction of "apparent" molecular weight. The initial increase of the exponent $\beta$ up to a dose of 40 kGy, followed by its decrease at 60 kGy, can be interpreted as an initial reduction of structural heterogeneity, that is in agreement with the observed initial decrease of polydispersity with the dose, followed by its increase when the irradiation is continued beyond 40 kGy. As pointed out before, the stretched exponential, $\beta$, cannot be unequivocally related to polydispersity, since it may also reflect a change in the interactions as a result of the structural and molecular modifications induced to Deg-XG upon irradiation. In this frame, we would be witnessing a progressive attenuation of inter-particle interaction at the increase of dose up to 40 kGy, to rise again at 60 kGy.

Functional groups analysis of the irradiated samples has been carried out by FT-IR spectroscopy. As shown in Figure 7.4, FT-IR spectra do not present new vibration bands, but only a progressive reduction of the height of the broad absorption band associated to the hydroxyl groups stretching (3600-3200 $cm^{-1}$), also visible in the attenuation of the bands associated to C-O and C-C stretching vibrations (1200-800 $cm^{-1}$). A reduction of hydroxyl groups content upon irradiation in the presence of air can be associated to oxidation and dehydrogenation of glycosidic rings with formation of ketones and aldehydes (–CH(OH)– to >C=O or of $–CH_2OH$ to –CHO), as supported by the increase of the carbonyl band shown in the inset of Figure 7.4.

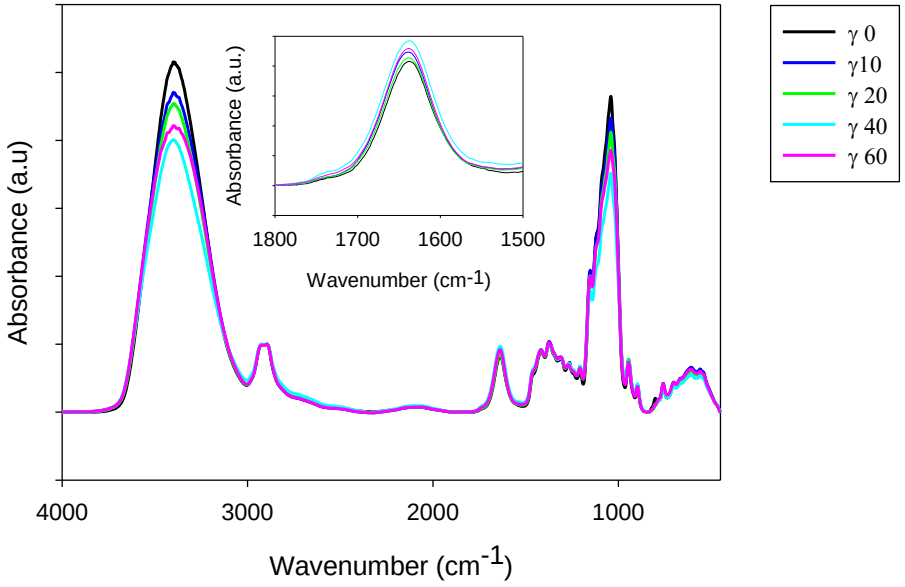


**Figure 7.4**: FT-IR analysis at the variance of the irradiation dose; inset: detail of the carbonyl band.

### 7.3.2 Effect of gamma-irradiation on thermally-induced aggregation in semi-dilute conditions

The scattered light intensity measured in the temperature range 15-40°C when imposing a temperature ramp of 10°C/h, for the dispersions prepared with irradiated Deg-XG at various doses, is shown in Figure 7.5. In Table 7.3, the onset of thermal gelation, $T^0_{gel}$, and the initial rate of scattered light increase, $\Delta I/\Delta t_{20\%}$, are reported as function of the dose. It can be observed that $T^0_{gel}$ slightly increases with the dose, as it is greatly affected by the size (and molecular weight) of the already present macromolecular clusters. Indeed, by reducing the molecular weight and/or cluster size with higher radiation doses imparted to the solid polymer, the onset of gelation occurs at higher temperature. Conversely, $\Delta I/\Delta t_{20\%}$ is related to the driving force of the different systems to self-aggregation. Interestingly, for this parameter we obtain a trend that is remarkably similar to the one for $\beta$ at 15°C: by reducing the initial

polydispersity and/or the extent of inter-particle interactions the driving force to aggregation is attenuated and particle size growth is less pronounced. This finding is well in agreement with a picture of the self-assembly of these polymers, where aggregation is mainly occurring by hydrophobic interactions driving single chains or smaller clusters to fuse into larger clusters.

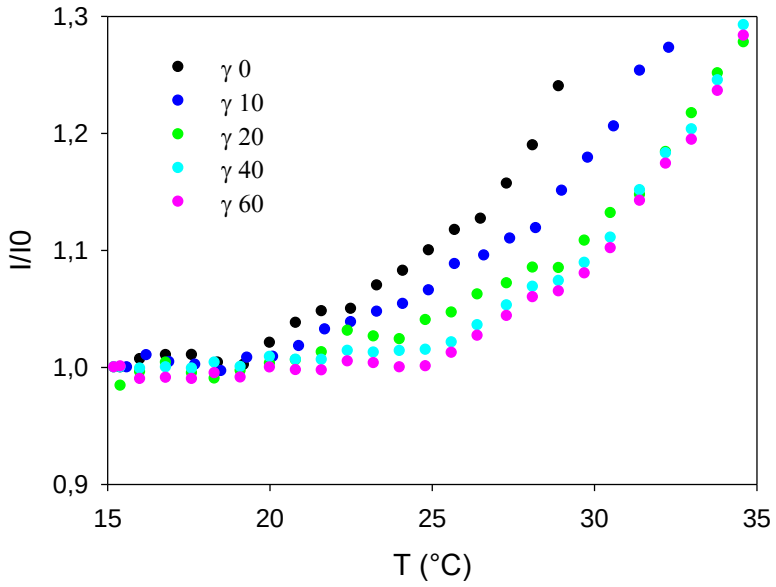


**Figure 7.5:** Normalized scattered light intensity as function of the temperature for different irradiation doses.

**Tab. 7.3:** $T^0_{gel}$ *(°C)* and $\Delta I/\Delta T_{20\%}$ values as function of the irradiation dose.

| Dose (kGy) | $T^0_{gel}$ (°C) | $\Delta I/\Delta T_{20\%}$ |
|---|---|---|
| 0 | 20 | 0.020 |
| 10 | 21 | 0.018 |
| 20 | 25 | 0.018 |
| 40 | 25.5 | 0.024 |
| 60 | 26.5 | 0.025 |

The organization of irradiated Deg-XG at 37°C has been investigated by carrying out DLS measurements at different incubation times. These measurements pose some challenges, since the systems stored below $T^0_{gel}$ (4°C) are suddenly brought at 37°C, i.e. within their instability region. Some large clusters may form, especially if the systems present some residual impurities. For this reason, prior to the light scattering measurements, samples were filtered with 1.2 µm pore size filters and let equilibrate for 40 min in the cuvette. As a consequence, the initial phase of self-assembly has not been tracked. The autocorrelation functions collected after 40 minutes ($t_1$), 5 hours ($t_2$), 10 hours ($t_3$) and 18 hours ($t_f$) of incubation at 37°C have been fitted with a stretched exponential and the corresponding fitting parameters are reported in Tab. 7.2. All systems experiment an increase of average relaxation time over time, that can be related to a cluster size increase.

Interestingly, $\beta$ values are very similar for the different irradiated systems; they are also significantly higher at 37°C than at 15°C. As we might expect, the self-assembly process leads to more homogenous and/or less interacting particles of a characteristic size, this size being strongly affected by the initial size or polymer molecular weight as resized by the interaction with the ionizing radiation.

In order to withdraw information on polymer chains organisation at a smaller scale, SAXS measurements have been carried out both before and after prolonged incubation at 37°C on selected irradiated systems: the scattered intensity as function of the scattering vector are shown in Fig. 7.6. Data have been fitted with the Debye

model to determine the structural parameter, *a*, that is a measure of the characteristic size of structural inhomogeneity (in Angstrom) of the system, according to Eq. 7.1; *a* values are reported in Tab. 7.4.

The larger is *a*, the larger are the "condensed" domains, constituted by ordered portions of material. Before incubation, this parameter increases with the dose up to 20 kGy, and slightly decreases for 60 kGy. A decrease of macromolecule chain length or branching degree, by increasing segmental mobility and/or reducing steric hindrance, can favour chain stacking and formation of larger clusters. The process does not imply any significant configurational entropy loss for the polymeric segments involved into the formation of these supramolecular aggregates, owing to their inherent stiffness, while their association leads to a significant entropy gain for the solvent. Therefore, the process that leads to more homogeneous systems at the mesoscale also drives macromolecular segments to a higher degree of structural organisation at the sub-nanometer scale. But, if the imparted dose is high and sequence defects are introduced, for example as a result of ring opening reactions, the stacking process is no longer favored and solvation forces may take over hydrophobic association forces. Indeed, upon incubation at 37°C, *a* increases for all systems, except for 60 kGy.

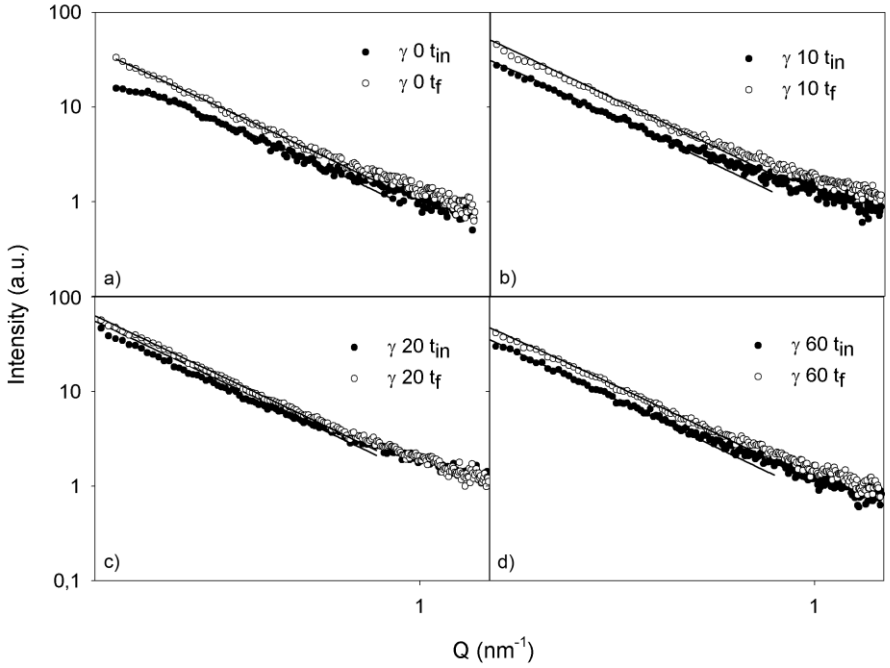


**Fig. 7.6:** SAXS measurements performed before and after incubation at 37°C on a) the nonirradiated polymer and the polymer irradiated with b) 10 kGy, c) 20 kGy, d) 60 kGy.

**Tab. 7.4:** Debye fitting results on nonirradiated and irradiated Deg-XG dispersions before and after incubation at 37°C.

| **Sample** | ***a* ($t_{in}$)** (Å) | ***a* ($t_f$)** (Å) |
|---|---|---|
| γ 0 | 10 | 23 |
| γ 10 | 21 | 45.5 |
| γ 20 | 44 | 61.5 |
| γ 60 | 38 | 24 |

### 7.3.3 Temperature-triggered macroscopic gelation of irradiated xyloglucans

In order to form macroscopic gels both nonirradiated and irradiated Deg-XG were dispersed in the concentrated regime as it is known to yield strong physical gels upon incubation at a temperature above the LCST. [119] Deg-XG aqueous dispersions were subjected to rotational shear viscosity measurements at 20°C: results are shown in Fig.

7.7. All systems show a typical non-Newtonian behavior of the shear thinning type. The Newtonian viscosity plateau at low shear rate is not accessible. This situation is typical of the flow behavior of anisotropic solutions of stiff chains. [182]

Indeed, the critical shear rate for the onset of non-Newtonian behavior decreases steeply as the concentration increases, becoming very low in value. All irradiated systems show shear viscosities lower than the non-irradiated system and decreasing with dose up to 40 kGy. Further irradiation up to 60 kGy does not produce significant effects.

The power law index, *n*, in Eq. 7.2 and the constant *K*, also known as consistency index, are shown in Table 7.5. The consistency decreases to about 25% of the original value at 10 kGy of absorbed dose and to 25% of this value by prolonging irradiation to 40 kGy and beyond. The exponent *n* decreases with the irradiation dose, in good agreement with the effect observed for the same systems studied in semi-dilute regime of an attenuation of interactions upon irradiation. The only exception is represented by the 20 kGy system, whose fitting with equation is not particularly good.

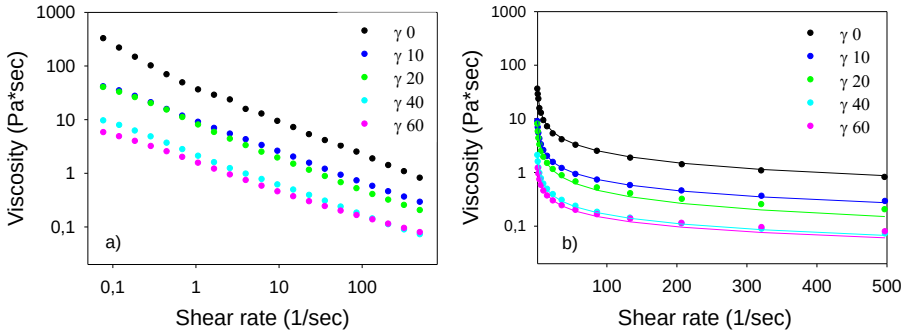


**Fig. 7.7:** a) Shear viscosity measurements performed on 4 wt% Deg-XG aqueous dispersions (20°C), b) Power law fitting of the flow curves.

**Tab. 7.5:** Power law fitting parameters obtained from shear viscosity measurements performed on the 4 wt% systems.

| Dose (kGy) | Power law exponent, n | Consistency k (Pa*sec) |
|---|---|---|
| γ 0 | 0.39 | 38.5 |
| γ 10 | 0.43 | 9.3 |
| γ 20 | 0.36 | 8.2 |
| γ 40 | 0.44 | 2.1 |
| γ 60 | 0.48 | 1.5 |

Deg-XG aqueous dispersions were incubated at 37°C for 5 minutes and then their viscoelastic properties were tested by dynamic-mechanical stress rheometry. In particular, the shear elastic modulus, *G'*, and the loss modulus, *G''*, were obtained as function of the oscillation frequency, in the 0.01-100 Hz range (Fig. 7.8). All the Deg-XG systems retain the propensity to promptly form "strong" gels after incubation at physiological temperature. Indeed, for all systems *G'* is almost invariant with frequency and higher than the corresponding *G''*. Values of *G'* and *G"* at 1 Hz frequency as function of the irradiation dose are reported in Table 7.6: it can be observed that they both decrease at the increase of the irradiation dose, resulting in a progressive loss of mechanical strength of the network. Differences in the dynamic-mechanical spectra diminish to fade with the dose increasing above 40 kGy. These effects will be further discussed after an analysis of the micrographs of freeze-dried gel samples as they provide some useful complementary information.

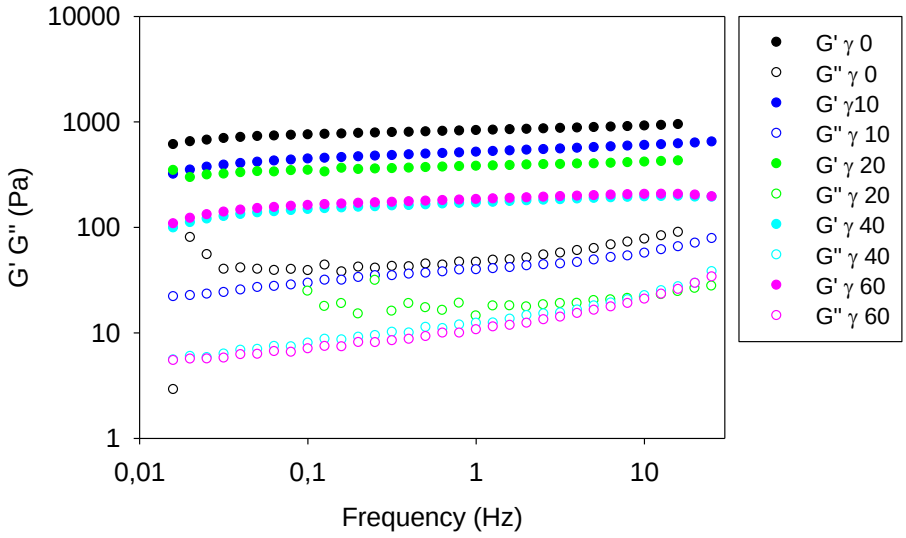


**Fig. 7.8:** Frequency sweep tests after 5 minutes at 37°C performed on 4 wt% Deg-XG gels at the variance of the irradiation dose.

**Tab. 7.6:** Values of elastic modulus, *G´*, and loss modulus, *G´´*, at 1 Hz from dynamic mechanical frequency sweep tests.

| Sample | G´(Pa) | G´´ (Pa) |
|---|---|---|
| γ 0 | 829.1 | 46.7 |
| γ 10 | 516.0 | 39.6 |
| γ 20 | 379.3 | 20.5 |
| γ 40 | 170.5 | 12.3 |
| γ 60 | 183.6 | 10.7 |

The concentration of polymer in water is the most significant parameter to tune the network density and, in turn, the mechanical properties of the gels. In Fig. 7.9 the influence of this parameter on the mechanical spectra of the gels has been investigated for the 40 kGy irradiated system. *G'* values span over two decades by varying the concentration from 2 wt% to 6 wt%. The effect of prolonging the incubation from 5 min to 30 min has been also investigated for the same system and concentration range (see Fig. 7.9 b). A slight increase both in *G'* and *G''* with incubation time can be

noticed together with a shift towards the higher frequencies of the *G"/G'* crossover, when the gel loses its structural integrity.

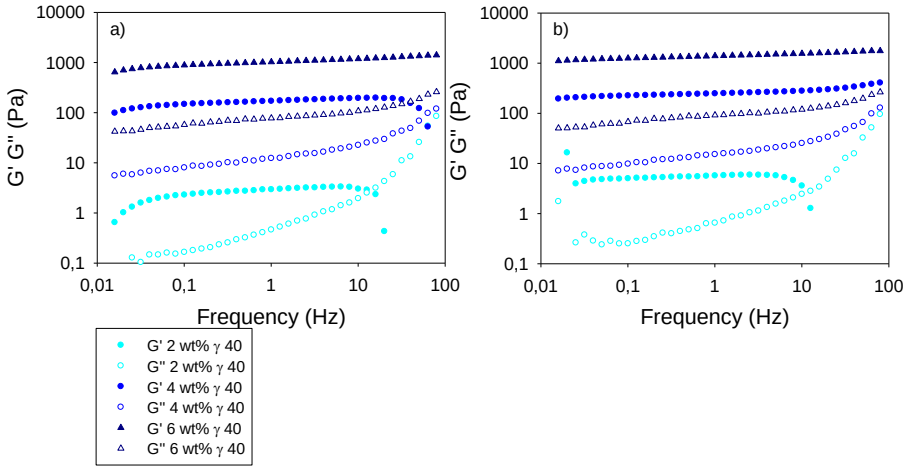


**Fig. 7.9:** Frequency sweep tests after a) 5 minutes and b) 30 minutes of incubation at 37°C for the 40 kGy irradiated systems at the variance of Deg-XG concentration.

Morphology studies on the gels prepared both with nonirradiated and irradiated Deg-XG were performed through the acquisition of SEM images: results are shown in Fig. 7.10 a-d.

The Deg-XG gel prepared with the nonirradiated polymer is characterized by dense and uneven porosity with pores ranging from about 5 to 10 μm, while the irradiated gels at the same polymer concentration show the appearance of a more ordered microstructure consisting of stacked lamellae with connecting filaments. This characteristic feature of the irradiated Deg-XGs morphology in the scale of tens to hundred of microns can be possibly related to the differences in the structure and properties of the mesoscopic building blocks (i.e. the clusters of tens to hundred of nanometers). The reduction of cluster size and of their polydispersity and/or the attenuation of their mutual interactions achieved upon irradiation up to a given dose

enable the attainment of a higher degree of structural order also due to slower self-aggregation process leading to a stratified and hierarchically organized microstructure.

The influence of irradiation dose on the morphology is mainly in the number of interconnections between lamellas, that seems to gradually decrease at the increase of the dose, probably as a results of the reduction of cluster size and connectivity. It is worth noticing that 40 kGy and 60 kGy irradiated Deg-XG show very similar morphologies, for this reason only the 40 kGy is represented in Fig. 7.10.

A lamellar morphology is particularly interesting for a possible use of these gels as scaffolds for the reconstruction of ordered biological tissues, such as tendons and ligaments etc. [183]

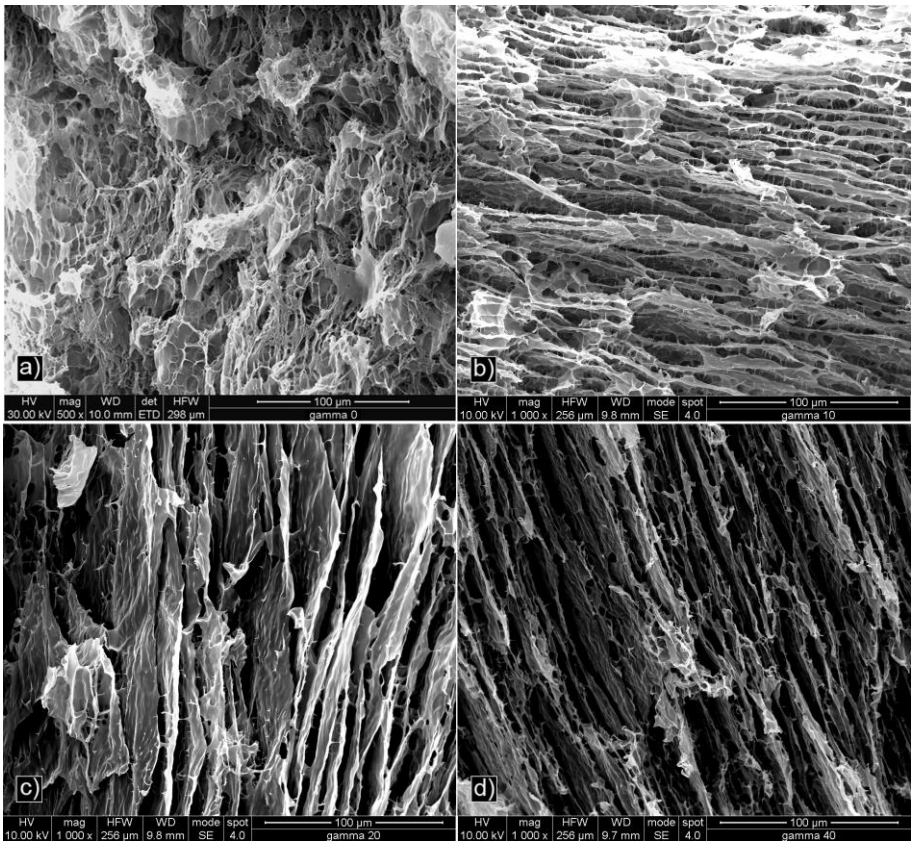


**Fig. 7.10:** SEM micrographs of 4 wt% Deg-XG gels prepared with the a) nonirradiated; b) 10 kGy; c) 20 kGy; d) 40 kGy irradiated polymers by incubation at 37°C for 5 min.

# 8 STUDY OF THE INFLUENCE OF DIFFERENT IRRADIATION CONDITIONS ON DEG-XG

## 8.1 Aim and introduction

In order to better understand the influence of irradiation conditions on Deg-XG properties, a different set of irradiation experiments was conducted using a Gammacell 1000 Elite $^{137}$Cs-source (School of Chemical Science and Engineering, Royal Institute of Technology, Stockholm, Sweden). In particular, the following irradiation conditions were systematically investigated:

- Influence of different gaseous atmospheres during the irradiation process: samples were irradiated both in presence of air and nitrogen in order to understand the role of oxygen and oxidative reactions during the degradation process.
- Influence of impurities and moisture content in the solid state: impurities or other components can act as "electron traps", thus altering the irradiation efficacy in reducing the polysaccharide molecular weight. [47] Besides, moisture content can strongly influence the reaction pathways, due to contribution of water radiolysis. Indeed, in presence of water yields of radicals are significantly higher than for polysaccharides in the dry state, so the contribution of the "indirect effect" (that is due to absorption of radiation energy by water and not by the polysaccharide itself), may be greater.
- Influence of the physical state of the material (solid vs aqueous solution): when dilute aqueous solutions are irradiated, water absorbs most of the radiation energy and indirect effects prevail over direct ones, leading to the formation of water-derived radicals and their subsequent attack on polysaccharide molecules.

All the irradiated samples were analyzed by size exclusion chromatography to compare irradiation effects on the polymer molecular weight distribution.

## 8.2 Materials and methods

Xyloglucan was purchased from Megazyme International (Ireland) and degalactosylated according to Section 5.3.

Nonpurified, purified Deg-XG powders and purified Deg-XG aqueous dispersions (0.1 wt%) were gamma-irradiated both in air and in $N_2$ atmosphere using a Gammacell 1000 Elite $^{137}$Cs-source (School of Chemical Science and Engineering, Royal Institute of Technology, Stockholm, Sweden) as described in Section 5.8.2. Deg-XG aqueous dispersions were freeze-dried to recover the solid products. All the irradiated samples were then dispersed in aqueous NaOH 10 mM at 0.2 wt% polymer concentration and analyzed by SEC measurements as described in Section 5.11.2. All samples were centrifuged at 8000g and 5°C for 45 min and then filtered with 0.2 pore size filters to remove insoluble parts and gross contaminants prior to analysis.

Irradiation conditions and samples codes in the solid state and in the solution state are summarized in Tabs. 8.1 and 8.2.

**Tab. 8.1:** Irradiation conditions and samples codes for Deg-XG irradiated in the solid state.

| Polymer state | Nominal Dose (kGy) | Eff. Dose (kGy) | Dose rate (kGy/h) | Irradiation time (h) | Atmosphere | Sample code |
|---|---|---|---|---|---|---|
| Dry, NP | 0 | 0 | // | // | // | γ 0 |
| Dry, P | 0 | 0 | // | // | // | Pγ 0 |
| Dry, NP | 10 | 10.26 | 0.4104 | 25 | air | γ 10_air |
| Dry, NP | 20 | 21.51 | 0.8964 | 24 | air | γ 20_air |
| Dry, NP | 40 | 38.59 | 0.4824 | 80 | air | γ 40_air |
| Dry, NP | 60 | 59.87 | 1.0692 | 56 | air | γ 60_air |
| Dry, NP | 10 | 9 | 0.36 | 25 | $N_2$ | γ 10_$N_2$ |
| Dry, NP | 20 | 19.35 | 0.6048 | 32 | $N_2$ | γ 20_ $N_2$ |
| Dry, NP | 40 | 38.88 | 0.486 | 80 | $N_2$ | γ 40_ $N_2$ |
| Dry, NP | 60 | 58 | 0.558 | 104 | $N_2$ | γ 60_ $N_2$ |
| Dry, P | 20 | 20.52 | 0.4104 | 50 | air | ' γ20_ air |
| Dry, P | 60 | 62.29 | 0.6048 | 103 | air | ' γ60_ air |
| Dry, P | 20 | 21.94 | 0.4824 | 45.5 | $N_2$ | 'γ 20_ $N_2$ |
| Dry, P | 60 | 58.27 | 1.0692 | 54.5 | $N_2$ | 'γ 60_ $N_2$ |

NP: non purified; P purified

**Tab. 8.2:** Irradiation conditions and samples codes for the purified Deg-XG aqueous dispersions.

| Dose (kGy) | Dose rate (kGy/h) | Irradiation time (h) | Atmosphere | Sample code |
|---|---|---|---|---|
| 0.01 | 0.36 | 0.0278 | Air | 0.01 kGy |
| 0.05 | 0.4824 | 0.103 | Air | 0.05 kGy |
| 0.1 | 0.486 | 0.206 | Air | 0.1 kGy |
| 0.5 | 0.8964 | 0.558 | Air | 0.5 kGy |
| 2 | 0.4104 | 4.87 | Air | 2 kGy |
| 20 | 0.36 | 54.5 | Air | 20 kGy |
| 60 | 0.558 | 103 | Air | 60 kGy |

## 8.3 Results

### 8.3.1 Influence of different gaseous atmospheres on the molecular modifications of Deg-XG upon irradiation of the polymer in the solid state.

Molecular weight distributions of the nonpurified polymer, irradiated at various integrated doses in the solid state, are shown in Fig. 8.1: in particular, Panel a reports chromatograms obtained upon irradiation in $N_2$ and Panel b shows chromatograms obtained upon irradiation in air. Irradiation effects are in good agreement with what was already observed in Chapter 7 for the proprietary Deg-XG polymer irradiated with a $^{60}$Co gamma cell at a dose rate of 8 kGy/h for the same doses: a progressive shift of the maximum of the chromatogram toward higher elution times (corresponding to lower average molecular weights) is observed at the increase of the irradiation dose for both the atmospheres. In Fig. 8.2 a-d a comparison between the two different atmospheres for each of the investigated irradiation doses is reported. All chromatograms show little or no modification of the main broad peak, when irradiation is carried out either in air or $N_2$. Only a slight shift of the maximum of the chromatograms can be observed at the lower irradiation doses (namely, 10 and 20 kGy).

The apparent average molecular weight values $M_w$ were calculated by performing calibration with pullulan standards to better appreciate the molecular modifications induced by irradiation: results are shown in Tab. 8.3. These values can be only considered for comparison purposes because of the structural differences between xyloglucan and pullulan. Nevertheless, they provide a clue on the very strong effects that gamma-irradiation has on the polymer molecular weight: the average molecular weight is decreased of 25% of the original value for the polymer irradiated in $N_2$ at 10 kGy, and of almost 30% when the same irradiation dose is absorbed in air. This value increases up to more than 75% at 60 kGy and almost no differences can be observed between the two irradiation atmospheres.

In Tab. 8.4 the average molecular weight decrease obtained by performing irradiation in air is compared with the already discussed results of the irradiation performed on Deg-XG with a $^{60}$Co source in the same dose range (see Chapter 7). It

is important to underline that, although many differences occur between the two irradiation sets, results are in good agreement, especially for the lower investigated irradiation doses. At higher dose this comparison is probably invalidated by the different filtration performed prior to chromatographic analysis (Deg-XG systems irradiated with the $^{60}Co$ source were filtered with 1.2 µm pore filters, while the systems irradiated with the $^{137}Cs$ source were filtered with 0.2 µm pore filters). At the higher irradiation doses, the bigger clusters that are not removed by the 1.2 µm filtration probably conceal the more marked irradiation effects on the polymer average molecular weight.

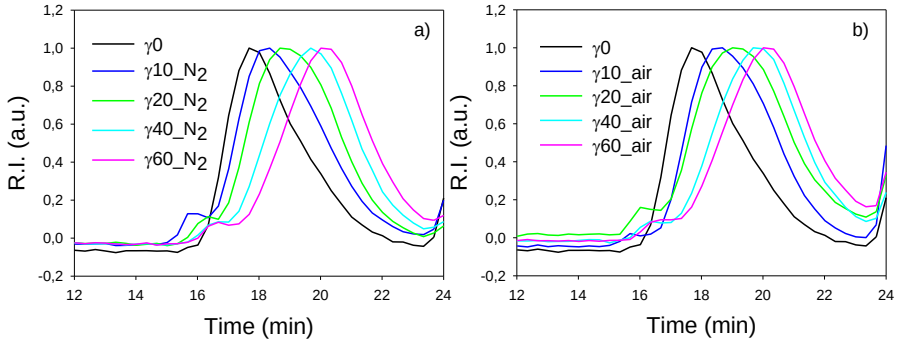


**Fig. 8.1:** Chromatograms of nonpurified Deg-XG irradiated in the solid state a) in $N_2$ atmosphere; b) in air atmosphere.

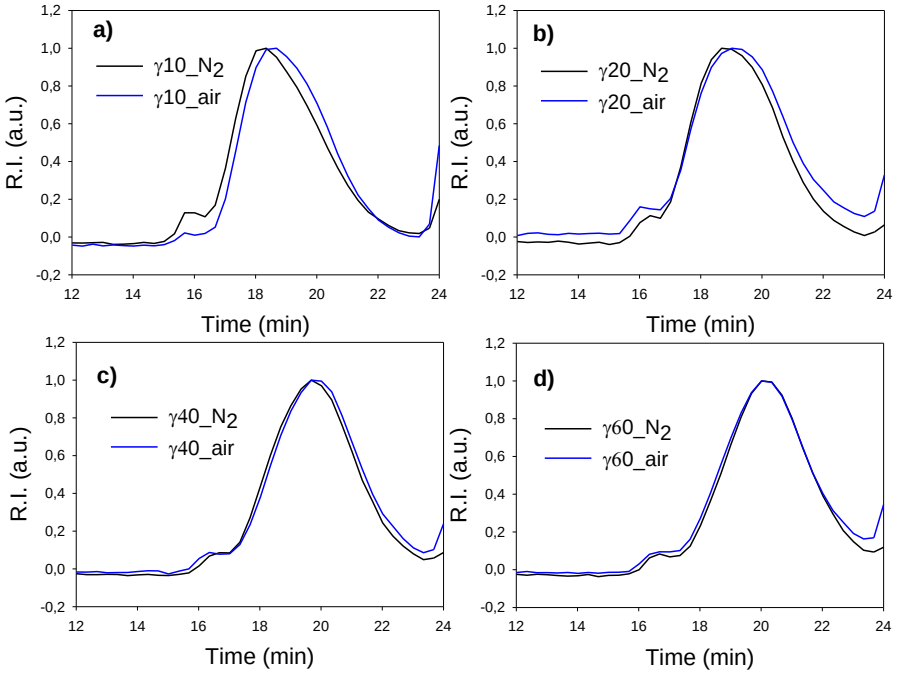


**Fig. 8.2:** Chromatograms of the nonpurified polymer irradiated in $N_2$ and in air atmosphere at a) 10 kGy; b) 20 kGy; c) 40 kGy; d) 60 kGy.

**Tab. 8.3:** Apparent average molecular weight values calculated from pullulan calibration for nonpurified, irradiated Deg-XG.

| Sample | Mw [Da] | Average Mw decrease [%] |
|---|---|---|
| γ 0 | 440592 | - |
| γ 10_air | 309101 | 29.8 |
| γ 20_air | 205403 | 53.4 |
| γ 40_air | 116707 | 73.5 |
| γ 60_air | 101244 | 77 |
| γ 10_$N_2$ | 330506 | 25 |
| γ 20_ $N_2$ | 251695 | 42.9 |
| γ 40_ $N_2$ | 141493 | 67.9 |
| γ 60_ $N_2$ | 102262 | 76.8 |

**Tab. 8.4:** Comparison of the apparent average molecular weight values calculated by pullulan calibration for Deg-XG samples gamma-irradiated with a $^{137}Cs$ source and with a $^{60}Co$ source (the latter were already reported in Chapter 7 and they are here indicated as "γ dose*"). All samples have been irradiated in air atmosphere.

| Sample | Average Mw decrease [%] |
|---|---|
| γ 10_air | 29.8 |
| γ 20_air | 53.4 |
| γ 40_air | 73.5 |
| γ 60_air | 77 |
| γ 10* | 28.8 |
| γ 20* | 42.8 |
| γ 40* | 50.2 |
| γ 60* | 60.9 |

The purified polymer in the solid state was gamma-irradiated at two different doses (20 and 60 kGy): chromatograms are shown in Fig. 8.3 for the polymer irradiated in nitrogen and in air. The nonirradiated purified polymer is also reported for comparison. The effect of the different atmosphere is more pronounced at lower irradiation dose (20 kGy).

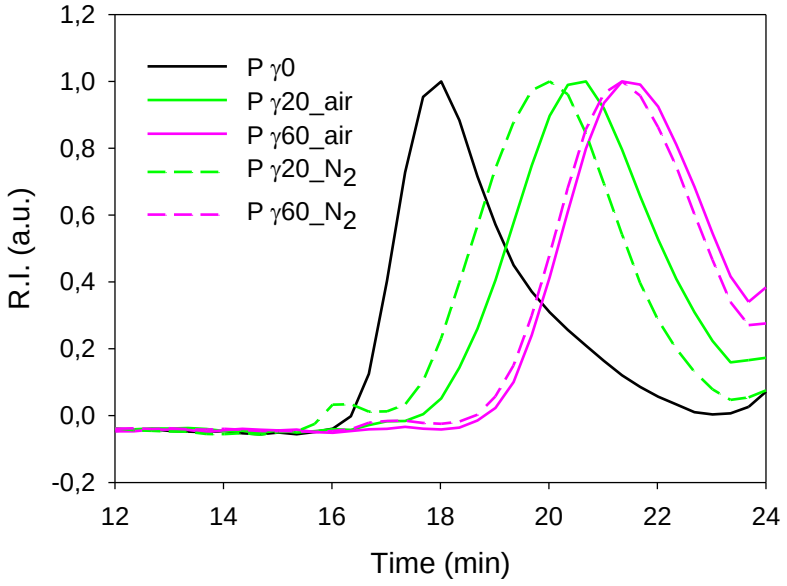


**Fig. 8.3:** Chromatograms of the purified polymer irradiated in $N_2$ and in air atmosphere at 20 kGy and 60 kGy. The nonirradiated, purified polymer chromatogram is reported for comparison.

In Fig. 8.4, the purified polymer irradiated in air is compared with the nonpurified polymer irradiated at the same irradiation doses.

At both the investigated doses, the purified polymer is more severely degraded than the nonpurified one. It is already known that impurities present in the material during irradiation can act as "electron traps" and alter the irradiation efficacy in degrading the polysaccharide. [47]

However, in our case the observed effect could be due to higher moisture content or bound water of the purified polymer (which is irradiated after freeze-drying), rather than to impurities present in the nonpurified material and removed after the purification process. Indeed, the floccular, porous solid obtained after freeze-drying is probably more hygroscopic than the powdered raw material.

The apparent average molecular weight values $M_w$ from pullulan calibration were also calculated for these systems: results are shown in Tab. 8.5 and confirm the already discussed effects.

**Tab. 8.5:** Apparent average molecular weight values calculated from pullulan calibration for purified, irradiated Deg-XG.

| Sample | Mw [Da] | Average Mw decrease [%] |
|---|---|---|
| P γ 0 | 440483 | - |
| P γ 20_air | 94981 | 78.4 |
| P γ 60_air | 41997 | 90.5 |
| P γ 20_$N_2$ | 127032 | 71.2 |
| P γ 60_$N_2$ | 46886 | 89.3 |

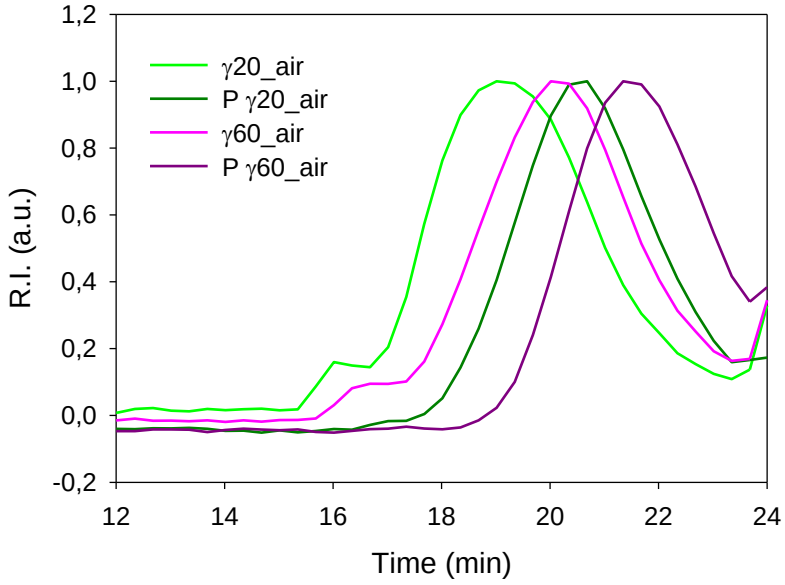


**Fig. 8.4:** Comparison of chromatograms of nonpurified and purified polymer irradiated in air at 20 kGy and 60 kGy.

### 8.3.2 Modifications induced by irradiation of polymer aqueous dispersions

In order to better appreciate the influence of residual water or moisture on the molecular modifications observed upon gamma irradiation of the "dry" polymers, irradiation of dilute Deg-XG aqueous dispersions (polymer concentration: 0.1 wt%) was performed in a broad range of irradiation doses: 0.01, 0.05, 0.1, 0.5, 2, 20 and 60 kGy. Results of chromatographic analysis are shown in Fig. 8.5, Panel a (comparison of the different irradiation doses up to 2 kGy) and Panel b (effects of the highest irradiation doses, 20 and 60 kGy). As expected, in this case radiation-induced degradation is much more severe due to the involved water radiolysis processes that lead to higher radical yield. The shift of the maximum of the chromatograms toward higher elution time values (corresponding to lower values of the average molecular weight) progressively increases at the increase of the irradiation dose and together with the amplitude of the polymer molecular weight distribution, thus indicating a polydispersity increase. At the highest irradiation doses (20 and 60 kGy), the typical molecular weight distribution of a polymer is no longer present and only narrow peaks corresponding to low molecular weight fragments can be observed. Their identification will be investigated in the follow up of this research. This result supports a possible role of moisture on the more pronounced effects of irradiation observed for the purified polymer.

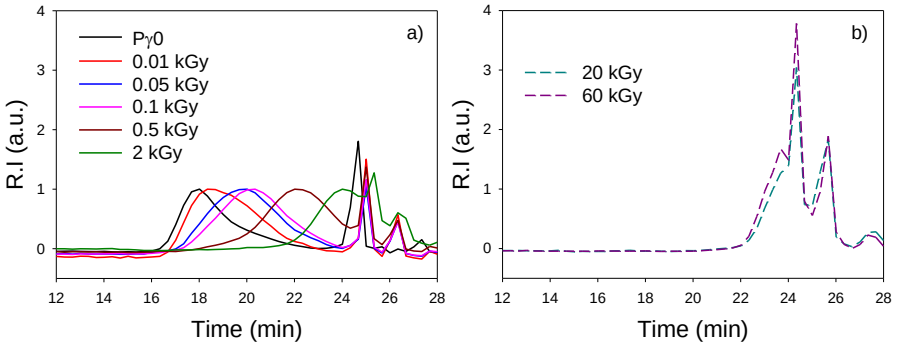


**Fig. 8.5:** a) Comparison of the different irradiation doses; b) effects of the highest irradiation doses on 0.1 Deg-XG wt% aqueous dispersions.

# 9 IRRADIATION EFFECTS ON NATIVE XG

## 9.1 Aim and introduction

Irradiation treatment in the same range of doses explored for Deg-XG (10-60 kGy) was also performed on the native polymer (XG).

In its native form, xyloglucan is more soluble in water than its degalactosylated variant, thanks to the higher galactose content. The higher degree of branching prevents the polymer to undergo gelation in water, but it can form gels if its branches are dehydrated (i.e. by addition of alcohols or sugars) or engaged in interactions with other substances, such as polyphenols or other polysaccharides. [91, 107-110, 113, 114]

The irradiation effects on molecular and chemical properties and on polymer solubility were investigated by gel filtration chromatography (GFC), Fourier-transform infrared spectroscopy (FT-IR) and dynamic light scattering (DLS) studies.

Then, the propensity of the polymer to aggregation when dispersed in water at relatively low concentration (0.1, 0.5 wt%) upon addition of ethanol (XG dispersion/ethanol volumetric ratio = 1:1 or 4:1) was analyzed at the variance of the irradiation dose by DLS and shear viscosity measurements.

## 9.2 Materials and methods

Tamarind seeds xyloglucan (XG) was purchased from Megazyme International (Ireland). Ethanol was purchased from Sigma Aldrich and used without further purification.

***Irradiation treatments and sample preparation***

XG powder was irradiated with the linear electron accelerator of *"Lodz University of Technology"* (Lodz, Poland) as described in Section 5.8.3.

XG aqueous dispersions (both with the nonirradiated and the irradiated polymer, 0.1-0.5 wt% polymer concentration) were prepared by overnight magnetic stirring at room temperature, followed by autoclaving at 121°C and 1 bar for 20 minutes.

XG dispersions were mixed with ethanol in 1:1 or 4:1 polymer dispersion/alcohol volumetric ratios.

***Dynamic light scattering***

Dynamic light scattering measurements were performed both by using a Brookhaven BI-9000 correlator and with a Zetasizer Nano ZS, as described in Section 5.11.4. The apparent average hydrodynamic diameter from DLS measurements performed with the Brookhaven instrument was calculated by the method of cumulant, [164] as shown by Eq. 6.1. Measurements performed with the Zetasizer Nano ZS were fitted according to the CONTIN (or Non-negative least squares, NNLS) method, that consists in fitting the correlation function with a multiple exponential to obtain the particle size distribution.

All samples were filtered with 0.45 µm cellulose acetate filters to remove gross contaminants.

***Gel filtration chromatography***

After 0.45 µm filtration, the molecular weight distributions were obtained by GFC measurements according to Section 5.11.2.

***Fourier transform infrared spectroscopy***

FT-IR analysis was carried out as in Section 5.11.1. All spectra have been normalized with respect to the peak correspondent to the stretching of methylene groups (2956 $cm^{-1}$).

***Shear viscosity measurements***

Shear viscosity measurements were performed at 25°C with a Haake Rheometer RT 20 (Lodz, Poland), as described in Section 5.11.5.

## 9.3 Results

### 9.3.1 Effects of irradiation treatments on XG molecular and chemical properties

GFC measurements were performed at 15°C on 0.1 wt% XG aqueous dispersions, both before and after autoclaving, to gather information about the modifications induced by high energy irradiation on the molecular weight distribution. The effect of irradiation dose is shown in Fig. 9.1 both for the nonautoclaved (Panel a) and the autoclaved systems (Panel b): in both cases the chromatograms shift towards higher elution times, which correspond to lower molecular weights, at the increase of the irradiation dose. These results suggest radiation-induced molecular degradation phenomena (main chain and/or side chains breakage) and different organisation of the irradiated biopolymer chains in the eluting medium.

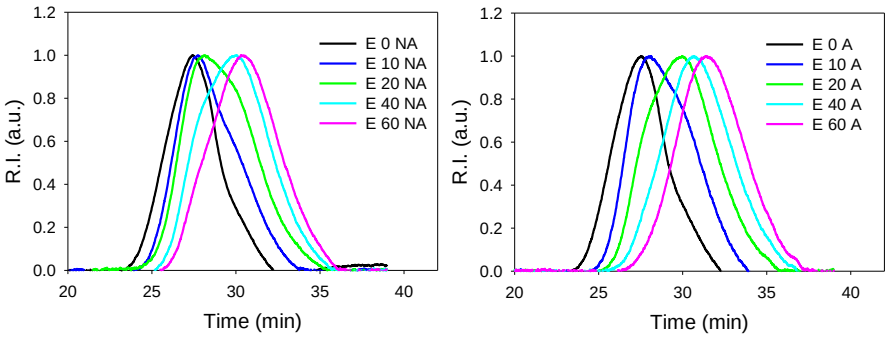


**Fig. 9.1:** GFC results on a) nonautoclaved XG samples and b) autoclaved XG samples.

In Fig. 9.2 b-e comparisons of the chromatograms obtained for nonautoclaved and autoclaved systems irradiated with the same doses are reported. In Panel a, the nonirradiated system chromatogram before and after autoclaving is shown: the

autoclaving treatment does not have any significant effect on polymer molecular weight distribution. Results are quite different for the irradiated systems (Panels b-e): a shift towards higher elution times upon autoclaving is observed for all the different doses, the more pronounced the higher is the irradiation dose. These results are in good agreement with the already observed average molecular weight reduction of the degalactosylated polymer: irradiation causes decrease in macromolecular chain length and/or branching degree, thus favouring chain stacking and aggregation (hydrophobic forces prevail). However, at higher imparted doses, polymer clusters are progressively damaged by the introduction of sequence defects: solvation forces prevail over hydrophobic ones and polymer clusters tend to dissolve. These phenomena are more marked when the polymer is autoclaved after irradiation, because the autoclaving process favours dissolution of the already damaged clusters.

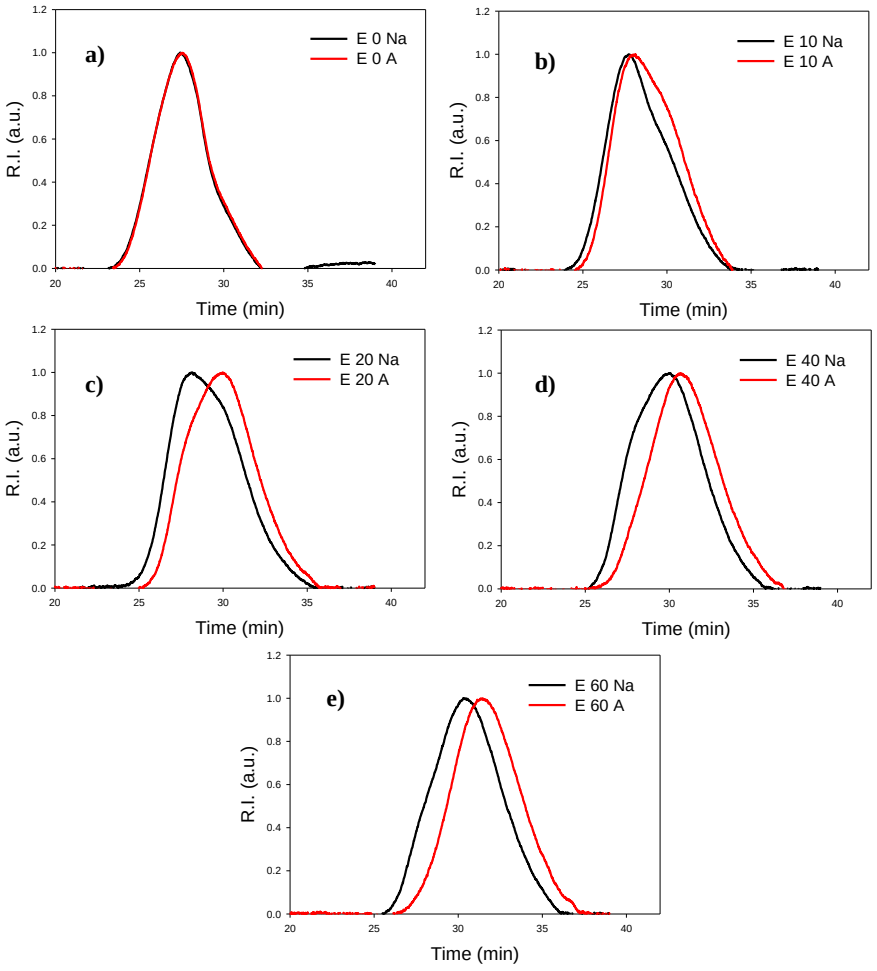


**Fig. 9.2:** Autoclaving effect at different irradiation doses: a) nonirradiated samples, b) 10 kGy, c) 20 kGy, d) 40 kGy, e) 60 kGy. Na: nonautoclaved; A: autoclaved.

In order to understand if this phenomenon is correlated to chemical modifications induced by the combined effect of irradiation treatment and autoclaving on polymer functionality, FT-IR measurements were performed. Fig. 9.3 reports FT-IR spectra collected for the nonirradiated polymer before and after

autoclaving and Fig. 9.4 shows spectra collected for the nonirradiated, nonautoclaved polymers (a) and irradiated, autoclaved polymers (b) (the nonirradiated XG is always reported as a comparison).

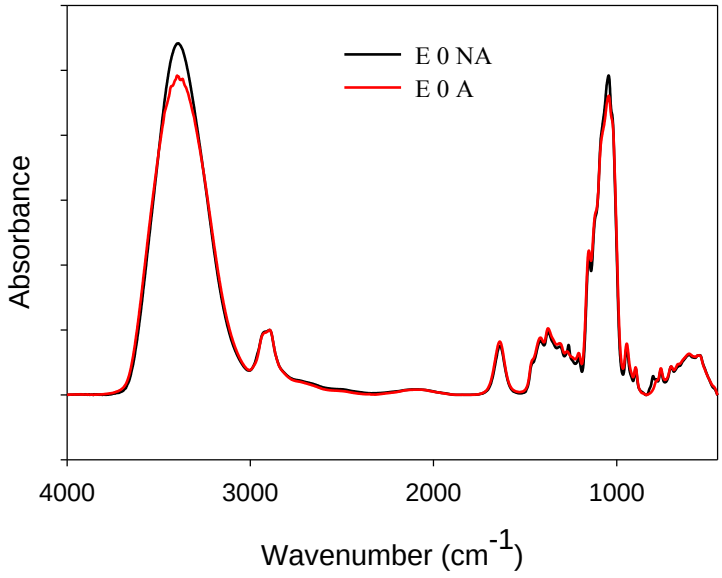


**Fig. 9.3:** FT-IR spectra of the nonirradiated polymer before and after autoclaving.

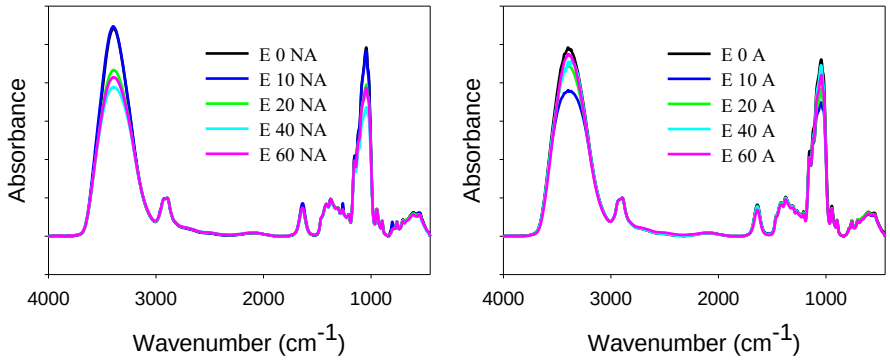


**Fig. 9.4:** FT-IR spectra collected for a) nonautoclaved, b) autoclaved XG irradiated samples (the nonirradiated sample is also reported as comparison, both before and after autoclaving).

FT-IR spectra do not show either appearance of new vibration bands or disappearance of the characteristic peaks of the nonirradiated polymer. The only noticeable effect is a reduction of the heights of the broad absorption band associated to the stretching vibration of hydroxyl groups (3600-3200 $cm^{-1}$) and of the bands associated to C-O stretching of alcohols and/or ethers. No evident effect regarding the carbonyl band is observed. This may suggest a chain scission of the galactose ring-carrying side branches induced by irradiation, since these lateral units are richer in hydroxyl groups in comparison with the glucan-based backbone, thus indicating the possibility of a partial degalactosylation induced by irradiation.

DLS studies were conducted to investigate the irradiation effects on the apparent average hydrodynamic diameter ($D_h$) of the polymer clusters in aqueous solvent. The decay curves reported in Fig. 9.5 were fitted according to the cumulant method: results are shown in Tab. 9.1. Only a small reduction of $D_h$ before and after irradiation can be observed, but no significant effects of the irradiation doses are displayed.

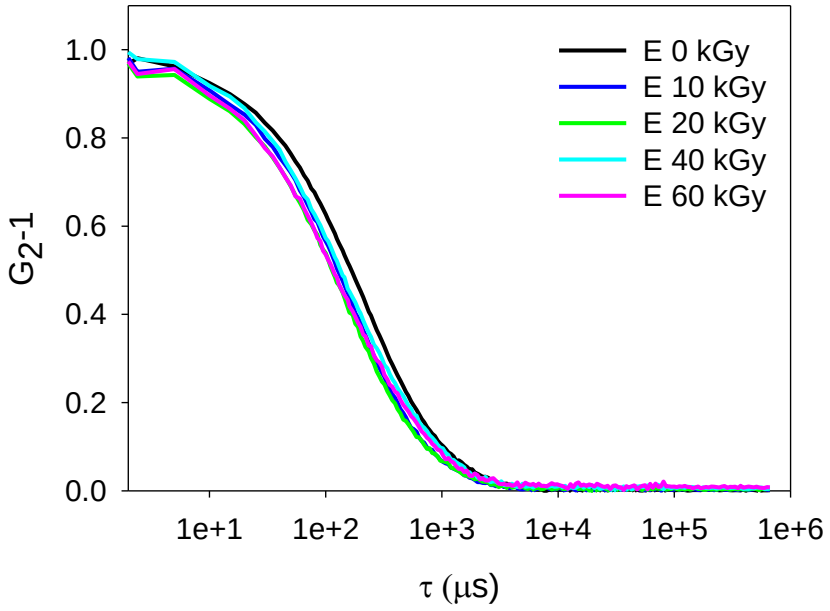


**Fig. 9.5:** Decay curves obtained by DLS measurements performed on 0.1 wt% polymer aqueous dispersions.

**Tab. 9.1**: Average hydrodynamic diameter ($D_h$) and polydispersity index (PDI) calculated by cumulant analysis.

| **Cumulant analysis results** | | | | | |
|---|---|---|---|---|---|
| Dose (kGy) | 0 | 10 | 20 | 40 | 60 |
| Dh (nm) | 101± 38 | 84± 27 | 82± 30 | 84± 32 | 83± 30 |
| PDI | 0.55 | 0.46 | 0.49 | 0.5 | 0.5 |

### 9.3.2 Irradiation effects on XG aggregation induced by mixing with ethanol

When concentrated XG aqueous dispersions (1 polymer wt% and above) are mixed with appropriate amounts of alcohols, gelation occurs because of the partial polymer dehydration caused by the alcohol, that competes with XG in the interactions with water molecules. [113, 114] Here, the aggregation propensity of nonirradiated and irradiated XGs in presence of ethanol is analyzed. In particular, dilute/semi-dilute polymer aqueous dispersions (0.1 – 0.5 polymer wt%) are mixed with ethanol in 1:1 and 4:1 volumetric ratios.

Indeed, as already observed for the partially degalactosylated variant, the gelation propensity at higher polymer concentration is related to the polymer tendency to aggregate when dispersed in water at lower concentration (see Chapter 6). The final composition of the analyzed systems is reported in Tab. 9.2.

**Table 9.2:** Samples codes.

| Sample code | Polymer concentration (wt %) | Water/EtOH (vol:vol) |
|---|---|---|
| XG(0.1)/EtOH-DOSE(1:1) | 0.1 | 1:1 |
| XG(0.1)/EtOH-DOSE(4:1) | 0.1 | 4:1 |
| XG(0.5)/EtOH-DOSE(1:1) | 0.5 | 1:1 |
| XG(0.5)/EtOH-DOSE(4:1) | 0.5 | 4:1 |

*DOSE = 0, 10, 20, 40, 60 kGy.

Xyloglucan aggregation propensity after mixing with alcohol was firstly evaluated upon a visual inspection. The XG(0.1)/EtOH-DOSE(1:1) systems appear homogeneous, transparent and colourless, while all the other systems appear cloudy, with a higher turbidity at the increase of the alcohol content and at the decrease of the irradiation dose. Some selected samples were also subjected to a tilting-tube test: flow behaviors are shown in Tab. 9.3 for the 0.5 wt% systems. These systems cannot be considered as “macrogels”: they flow as single body and fill completely the

container once at rest. However, at the increase of the irradiation dose, it is possible to observe the presence of macrogels fragments which adhere to the tube.

**Tab. 9.3:** Visual inspection of XG(0.5)/EtOH-DOSE at different irradiation dose and alcohol content after tilting-tube test.

| v:v | E0 | E 10 | E 20 | E 40 | E 60 |
|---|---|---|---|---|---|
| 4:1 |  | | | | |
| 1:1 |  | | | | |

The apparent hydrodynamic size of polymer clusters formed upon mixing with ethanol has been measured via DLS (with the Nanosizer), as function of time for the XG(0.1)/EtOH-0(4:1), XG(0.1)/EtOH-20(4:1) and XG(0.1)/EtOH-60(4:1) systems, both "as prepared" and after ten times dilution with the 4:1 $H_20$/EtOH solution. Data are reported in Tabs. 9.4 and 9.5, respectively. The turbidity of higher concentrated systems impaired their DLS analysis. The corresponding values at t=0 for the XG dispersions at 0.1 wt% is 92 nm. In general, as expected, the measured $D_h$ values are higher after mixing with ethanol, thus confirming that further aggregation of the polymer clusters is induced by the presence of alcohol and its competition with the polymer towards water molecules.

Besides, the nonirradiated systems hydrodynamic diameter also increases with the storage time, while for the irradiated systems there is no further aggregation of

polymer clusters. This suggests that the irradiation treatment improves XG storage stability.

**Table 9.4:** $D_h$ and PDI of XG(0.1)/EtOH-0(4:1), XG(0.1)/EtOH-20(4:1) and XG(0.1)/EtOH-60(4:1) by CONTIN data analysis.

| **XG(0.1)/EtOH-DOSE(4:1)** | **0 Kgy** | | **20 kGy** | | **60 kGy** | |
|---|---|---|---|---|---|---|
| Time (h) | $D_h$ (nm) | PDI | $D_h$ (nm) | PDI | $D_h$ (nm) | PDI |
| 0 | 162.4 | 0.5 | 166.9 | 0.7 | 120.3 | 0.8 |
| 1 | 186.2 | 0.6 | 191.8 | 0.6 | 147.6 | 0.6 |
| 2 | 191.2 | 0.5 | 193.7 | 0.7 | 146.4 | 0.6 |
| 3 | 234.9 | 0.8 | 253.4 | 0.6 | 148.3 | 0.6 |
| 4 | 229.7 | 1 | 206.5 | 0.5 | 158.3 | 0.6 |
| 5 | 281.2 | 0.8 | 200.1 | 0.6 | 144.7 | 0.6 |
| 6 | 290.5 | 0.8 | 183.3 | 0.6 | 145 | 0.6 |
| 7 | 258.1 | 1 | 188.4 | 0.4 | 183.5 | 0.4 |
| 8 | 261.5 | 1 | 174.9 | 0.5 | 150.4 | 0.6 |
| 23 | 586.8 | 1 | 184.2 | 0.3 | 180.2 | 0.6 |
| 25 | 593.7 | 1 | 178.5 | 0.2 | 177.9 | 0.6 |
| 27 | 599 | 1 | 171.8 | 0.3 | 197.4 | 0.6 |
| 29 | 616.9 | 1 | 177.8 | 0.2 | 190.9 | 0.6 |
| 31 | 767.3 | 1 | 166.5 | 0.2 | 198.2 | 0.6 |
| 47 | 1067 | 1 | 204.8 | 0.5 | 211.2 | 0.7 |
| 49 | 1327 | 1 | 170.7 | 0.4 | 213.4 | 0.7 |
| 51 | 1288 | 1 | 177.5 | 0.4 | 204.1 | 0.6 |
| 53 | 1250 | 1 | 194.9 | 0.6 | 199.8 | 0.6 |

**Table 9.5:** $D_h$ and PDI of XG(0.01)/EtOH-0(4:1), XG(0.01)/EtOH-20(4:1) and XG(0.01)/EtOH-60(4:1) by CONTIN data analysis.

| **XG(0.01)/EtOH-DOSE(4:1)** | **0 kGy** | | **20 kGy** | | **60 kGy** | |
|---|---|---|---|---|---|---|
| Time (h) | $D_h$ (nm) | PDI | $D_h$ (nm) | PDI | $D_h$ (nm) | PDI |
| 0 | 149.3 | 0.7 | 190.7 | 0.5 | 146.7 | 0.9 |
| 1 | 157.4 | 077 | 171.6 | 0.5 | 142.1 | 0.8 |
| 2 | 163.5 | 0.7 | 162.7 | 0.6 | 165.4 | 0.6 |
| 3 | 179.3 | 0.7 | 157.5 | 0.6 | 177.6 | 0.7 |
| 4 | 174.4 | 0.7 | 168.2 | 0.7 | 154.1 | 0.8 |
| 5 | 193 | 0.6 | 193.8 | 0.4 | 148.3 | 0.8 |
| 6 | 204.8 | 0.7 | 176.8 | 0.5 | 179 | 0.4 |
| 7 | 206 | 0.6 | 183.5 | 0.4 | 167.8 | 0.5 |
| 8 | 207 | 0.6 | 182.7 | 0.3 | 118.6 | 0.9 |
| 23 | 218.7 | 0.7 | 149.4 | 0.8 | 151.5 | 0.8 |
| 25 | 217.7 | 0.7 | 137 | 0.5 | 165.7 | 0.6 |
| 27 | 207.2 | 0.6 | 204.3 | 0.6 | 224.4 | 0.7 |
| 29 | 240.7 | 0.7 | 155.4 | 0.6 | 205.5 | 0.5 |
| 31 | 267.2 | 0.7 | 144.4 | 0.6 | 147.9 | 0.7 |
| 47 | 647.1 | 0.7 | 147 | 0.6 | 190.6 | 0.9 |
| 49 | 712.6 | 0.7 | 172.4 | 0.4 | 133.9 | 0.7 |
| 51 | 651.3 | 0.7 | 160.4 | 0.7 | 299.5 | 0.4 |
| 53 | 650.7 | 0.8 | 185.2 | 0.5 | 164.2 | 0.9 |

The nonirradiated, the 20 kGy and the 60 kGy irradiated systems, both at 0.1 and 0.5 wt% polymer concentration and at different alcohol content, were subjected to shear viscosity measurements: results are shown in Fig 9.6. As a general trend, the shear viscosity increases and the non-Newtonian behavior of the shear thinning type becomes more pronounced at the increase of both polymer concentration and alcohol content, the polymer concentration effect being the most significant one. An influence of irradiation dose on shear viscosity is only evident at lower polymer concentration (0.1 wt%) and higher alcohol content (1:1 vol:vol). Indeed, for these

systems a decrease of both viscosity and curves slope is observed at the increase of irradiation dose. This result is in good agreement with the DLS data which showed a reduction in polymer cluster size with irradiation dose, without and with alcohol.

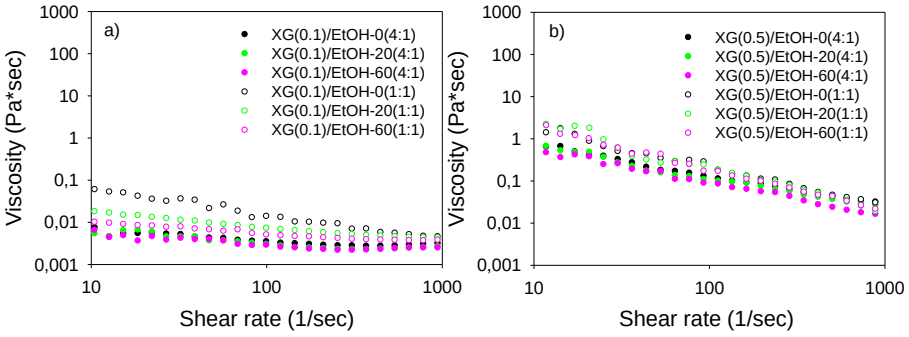


**Fig. 9.6:** Shear viscosity as function of shear rate for a) 0.1 wt% polymer concentration and b) 0.5 wt% polymer concentration at different irradiation doses and alcohol content.

# 10 CHEMICAL MODIFICATIONS OF XYLOGLUCAN FUNCTIONALITY

## 10.1 Aim and introduction

The possibility of functionalizing xyloglucan with groups that can be used for bio-conjugation reactions or that can modify its solubility or self-assembly properties has been assessed. There are a few studies concerning the replacement of xyloglucan hydroxyl groups with different moieties, such as carboxyl, amino, alkyloamino, sulphonic and carboxymethyl groups, but they are mainly focused on the native polymer, due to its better water solubility. [126-129] At the best of our knowledge, only one functionalization reaction on the degalactosylated variant of the polymer has been reported in the literature: Deg-XG hydroxyl-groups were replaced by carboxylic derivatives for grafting doxorubicin. They were also covalently attached to a targeting unit, in this case galactosamine. [130]

Similarly to Ref. 129, chemical functionalization protocols have been here developed in order to specifically graft carboxyl groups onto XG and Deg-XG, as a way to chemically anchor biomolecules with targeting or therapeutic functions. In particular, repercussions on the temperature-triggered self-assembly behavior have been evaluated when these protocols were applied to the partially degalactosylated polymer.

For the introduction of carboxyl groups, 2,2,6,6-tetramethyl-1-piperidinyloxy (TEMPO) is used to promote selective oxidation at C-6 position of glucose or galactose rings. This protocol was already found effective in the oxidation of a large number of polysaccharides, [184-188] including xyloglucan extracted from *Hymanea Courbaril* seeds. [129]

The reaction is conducted in inert atmosphere and in aqueous solvent with catalytic amounts of TEMPO and halide. [185] The first step is the oxidation of primary alcohols to aldehydes, followed by oxidation of aldehydes to carboxyl acids. Sodium hypochlorite acts as regenerating oxidant for TEMPO. Then, the reaction is stopped by adding $NaBH_4$ as a reducing agent.

Reaction and catalytic pathways are shown in Fig. 10.1 and Fig. 10.2

The modified polymer produced is an anionic polyelectrolyte having a greater solubility in aqueous solvents than the original material.

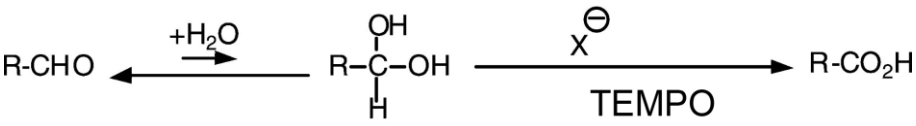


**Fig. 10.1:** Reaction pathway of carboxylation.

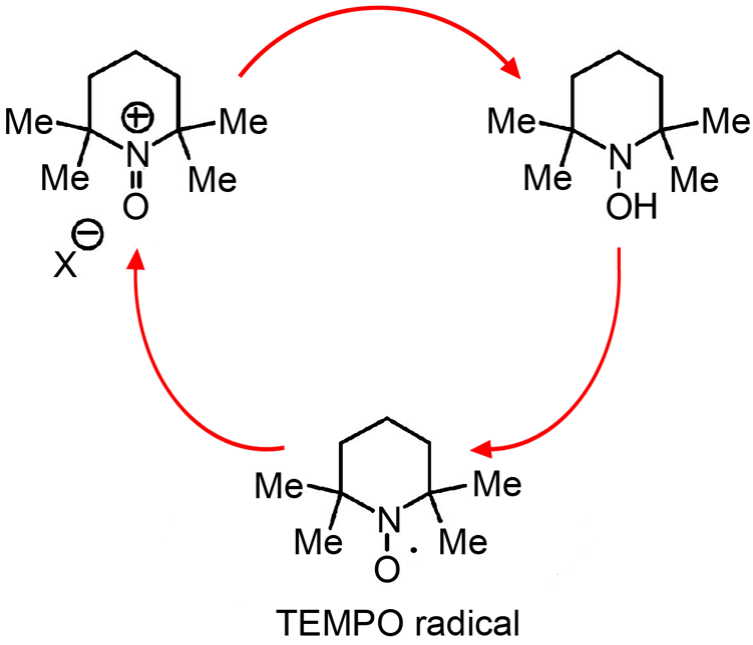


**Fig. 10.2:** Catalytic cycle of TEMPO.

Carboxyl groups were here introduced onto both the native and the partially degalactosylated polymer and different carboxylation degrees were achieved by varying the reaction time. The occurrence of these reactions was evaluated by FT-IR measurements. DLS studies were conducted to investigate the modifications in the dynamics of polymer aggregates after these reactions.

Modifications induced in the molecular weight distributions and in the polymers flow behavior in water were analyzed by gel filtration chromatography and shear viscosity measurements, respectively.

When the functionalization reactions were carried out onto Deg-XG, the effects on the temperature-triggered polymer self-assembly were studied both in the low concentration regime, by dynamic light scattering measurements performed at 37°C as function of time, and in the high concentration regime, by dynamic-mechanical stress rheometry performed after incubation of the 4 wt% Deg-XG aqueous dispersions at 37°C.

## 10.2 Materials and Methods

Tamarind seeds xyloglucan (XG) was purchased from Megazyme International (Ireland) and the partially deglactosylated variant was produced according to Section 5.3.

2,2,6,6-Tetramethyl-1-piperidinyloxy (TEMPO), sodium bromide (NaBr), sodium hypochlorite solution, sodium borohydride ($NaBH_4$) and ethanol were purchased from Sigma Aldrich and used without further purification.

***Functionalization protocols and sample preparation***

Functionalization protocols are described in Ref. 129 and in Section 5.9. Table 10.1 reports samples codes for this chapter.

**Tab. 10.1:** Sample codes of functionalized polymers.

| Polymer | Reaction, reaction time | Code |
|---|---|---|
| XG | Carboxylation, 2 h | XG-COOH_2 |
| XG | Carboxylation, 4 h | XG-COOH_4 |
| Deg-XG | Carboxylation, 2 h | Deg-XG-COOH_2 |
| Deg-XG | Carboxylation, 4 h | Deg-XG-COOH_4 |

XG-COOH_2 and XG-COOH_4 0.1 wt% aqueous dispersions were prepared by prolonged magnetic stirring at room temperature, while Deg-XG-COOH_2 and Deg-XG-COOH_4 0.1 wt% aqueous dispersions were prepared by prolonged magnetic stirring at 5°C. All samples were centrifuged for 45 minutes at 8000 rpm and 5°C to remove insoluble parts.

Concentrated Deg-XG-COOH aqueous dispersions (4 wt% polymer concentration) were prepared by homogenization for 5 hours at 13500 rpm and 5°C.

***Fourier transform infrared spectroscopy***

FT-IR analysis was carried out as described in Section 5.11.1. All spectra have been normalized with respect to the peak correspondent to the stretching of methylene groups (2956 $cm^{-1}$).

***Gel filtration chromatography***

The chromatographic profile was obtained as reported in Section 5.11.2. All samples were filtered through 1.2 µm pore filters prior to analysis to remove gross contaminants.

***Dynamic light scattering***

DLS measurements were performed at 90° scattering angle and 15°C, as described in Section 5.11.4. All samples were filtered through 1.2 µm cellulose acetate

(Millipore) syringe filters to remove gross contaminants. DLS data were fitted according to the stretched exponential method, that is expressed by Eqs. 6.2 and 6.3. Repeated DLS runs were also performed at the constant temperature of 37°C to collect the scattered intensity as function of time and evaluate Deg-XG propensity to temperature-triggered aggregation.

***Shear viscosity measurements***

Shear viscosity measurements were performed according to Section 5.11.5, at 25°C, on 0.1 wt% Deg-XG aqueous dispersions prepared both with the nonfunctionalized and functionalized polymers.

***Dynamic-mechanical stress rheometry***

Rheological measurements were performed according to Section 5.11.5 on 4 wt% Deg-XG, Deg-XG-COOH_2 and Deg-XG-COOH_4 aqueous dispersions after 5 minutes of incubation at 37°C.

## 10.3 Results

### 10.3.1 Carboxylated XG and Deg-XG characterization

Functionalization reactions for the introduction of carboxyl groups were conducted both on XG and Deg-XG dispersed in water at the same polymer concentration (0.2 wt%).

The presence of carboxyl groups after the already described reactions was evaluated by FT-IR spectroscopy measurements (Fig. 10.3).

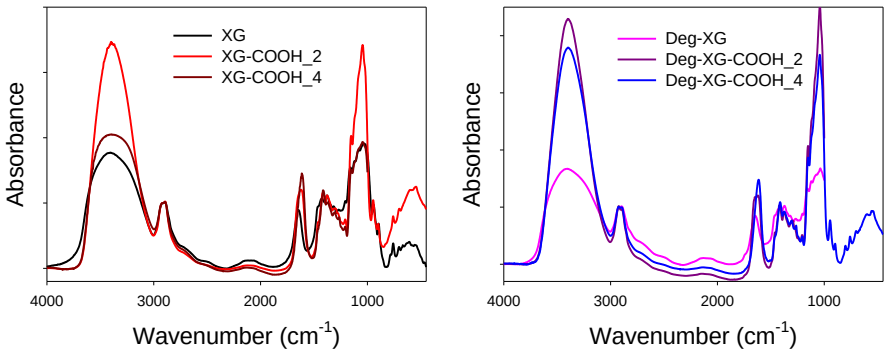


**Fig. 10.3:** FT-IR spectra collected after carboxylation reactions for a) XG and b) Deg-XG

All spectra are qualitatively similar, the most significant bands being at 3700-3000 $cm^{-1}$ (OH stretching vibration), 2920-2887 $cm^{-1}$ (symmetric CH stretching) and 1200-800 $cm^{-1}$ (C-O and C-C stretching vibrations). Differences in the OH stretching vibration band among the nonfunctionalized and the functionalized polymers are probably due to the different moisture content (the functionalized polymers are recovered after freeze-drying).

The occurrence of carboxylation reactions is qualitatively confirmed by the appearance of the band at about 1650 $cm^{-1}$, arising from the stretching vibration of carbonyl groups. In Fig. 10.4 a-b, FT-IR spectra in the 2000-1300 $cm^{-1}$ range are reported.

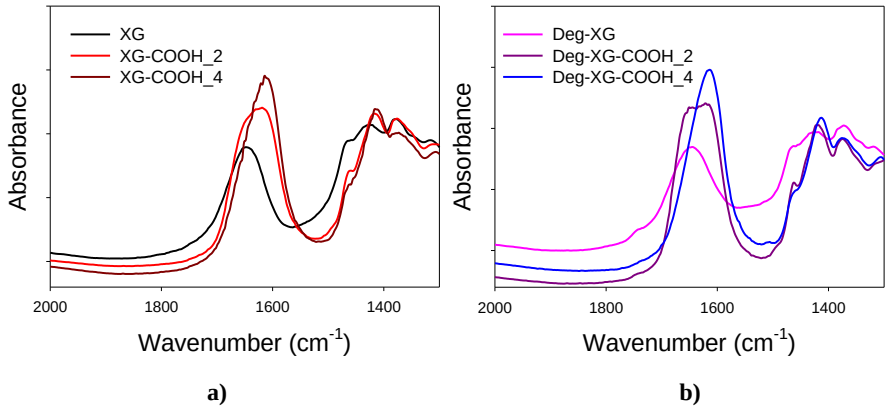


**Fig. 10.4:** Zoom of FT-IR spectra collected after carboxylation reactions for a) XG and b) Deg-XG in the 2000-1300 $cm^{-1}$ range.

FT-IR spectra collected for nonfunctionalized polymers show a vibrational peak at approximately 1650 $cm^{-1}$, associated with the aldehydic form of glucose rings. After 2 hours of carboxylation reaction, a peak at ~1620 $cm^{-1}$ appears, associated with the presence of $COO^-$ groups, and the peak at 1650 $cm^{-1}$ reduces its intensity. After 4 hours of carboxylation, the decrease of the intensity associated to the peak at 1650 $cm^{-1}$ is concomitant with the increase of the intensity of the 1620 $cm^{-1}$ peak, thus indicating an increase in the number of the $COO^-$ groups.

A similar result is reported in the literature for the carboxylation reaction conducted on the native polymer extracted from different plant seeds. [129]

The eventual modifications induced by carboxylation reactions on molecular weight distributions were investigated by GFC measurements (see Fig. 10.5). Only a slight shift of the maximum of the chromatograms can be observed, corresponding to a very modest reduction in the average molecular weight. This average molecular weight reduction is smaller than the one observed by Lucyszyn et al. for carboxylated XG extracted from *Hymanaea Courbaril* seeds. [129] The authors attributed this phenomenon to chain scission and degradation phenomena induced by the TEMPO-

mediated oxidation. In our case (xyloglucan extracted from Tamarind seeds) these phenomena seem to be attenuated.

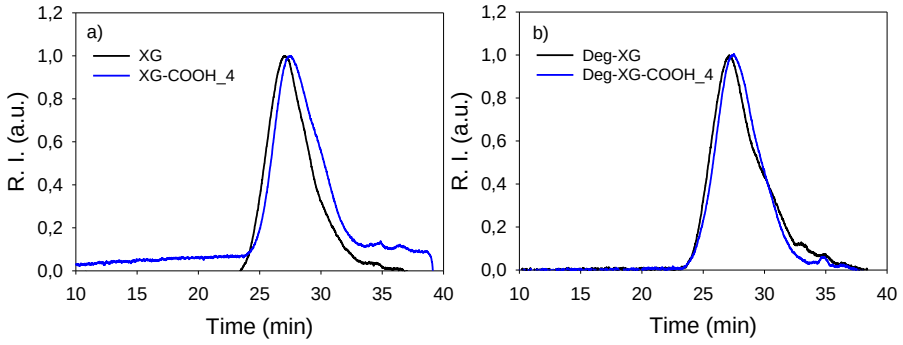


**Fig. 10.5:** GFC results for a) functionalized XG and b) functionalized Deg-XG. Nonfunctionalized polymers chromatograms are also included for comparison.

The average relaxation time $\tau_c$ and the stretched exponent $\beta$ of polymer clusters after carboxylation reactions were evaluated by DLS measurements. In Fig. 10.6 decay curves for both XG and Deg-XG are reported, and parameters obtained after the stretched exponential fit are shown in Tab. 10.2. The effect of carboxylation is quite evident in the average relaxation time increase.

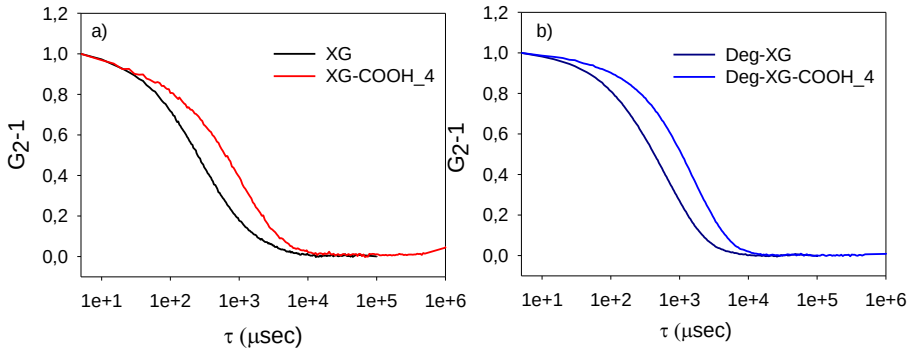


**Fig. 10.6:** Decay curves of functionalized XG and Deg-XG obtained by DLS measurements. Nonfunctionalized polymers are also reported for comparison.

**Tab. 10.2:** Stretched exponential fitting parameters for nonfunctionalized polymers and after carboxylation reactions (4 hours).

| System | β | $\tau_c$ (μsec) |
|---|---|---|
| XG | 0.6342 | 1274.9 |
| XG-COOH_4 | 0.633 | 5565.9 |
| Deg-XG | 0.7485 | 1844.7 |
| Deg-XG-COOH_4 | 0.8452 | 3845.5 |

### 10.3.2 Effects of carboxylation on temperature-triggered Deg-XG self-assembly

The presence of carboxyl groups enhances Deg-XG water solubility because it modifies the balance between hydrophobic and hydrophilic character of the polymer. The effects of these modifications on Deg-XG self-assembly triggered by temperature were studied in the low concentration regime in terms of polymer self-aggregation induced by the temperature increase: the scattered intensity growth with time at 37°C is shown in Fig. 10.7.

The presence of carboxyl groups impairs the polymer propensity to aggregation at 37°C. Besides, we attempted to alter the pH of polymer dispersion to 3, but even in this case Deg-XG did not shown thermal responsiveness anymore (data not shown).

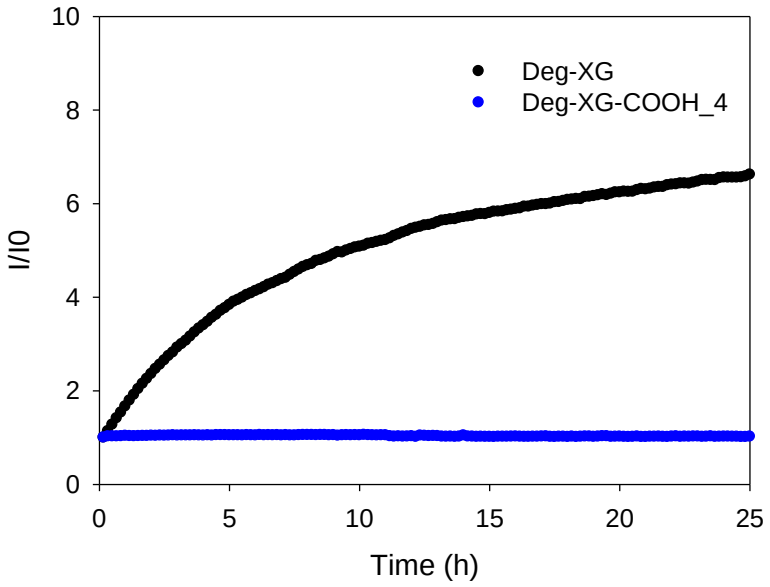


**Fig. 10.7:** Timecourse of normalized scattered intensity for 0.1 wt% Deg-XG aqueous dispersions.

More concentrated polymer dispersions (4 wt%) were subjected to frequency sweep tests after 5 minutes of incubation at 37°C: results are shown in Fig. 10.8.

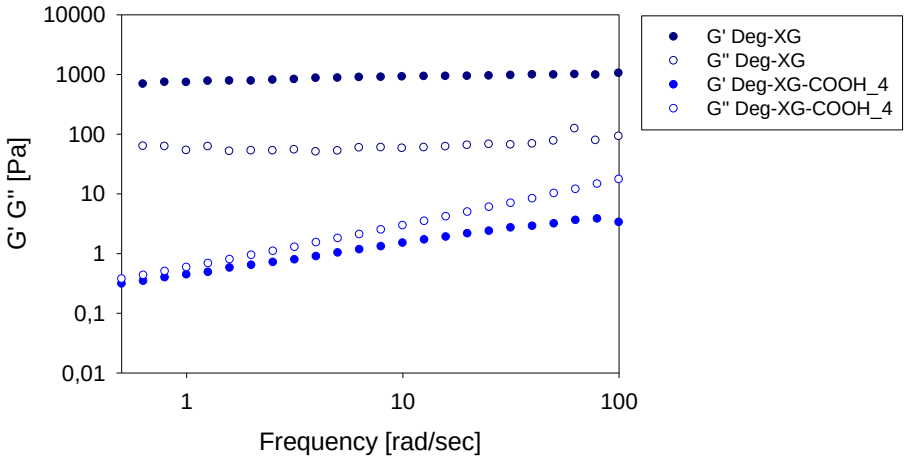


**Fig. 10.8:** Frequency sweep tests results for 4 wt% Deg-XG aqueous dispersions after 5 minutes conditioning at 37°C.

While the nonfunctionalized Deg-XG displays the typical "strong gel" behavior, with the elastic modulus *G'* higher than the loss modulus *G''* and both almost invariant with frequency in the explored range, the carboxylated polymer dispersion behavior is that typical of very viscous polymer solutions: both *G'* and *G''* increase with frequency and *G''* is always higher than *G'*. No cross-over between *G'* and *G''* plots can be observed, thus indicating that a gel point is not reached.

# 11 PRELIMINARY INVESTIGATION OF ENZYMATIC DEGRADATION STRATEGIES

## 11.1 Aim and introduction

In a biological environment, xyloglucan could be subjected to both hydrolytic and enzymatic degradation. Xyloglucan-active enzymes belong to the glycoside hydrolases (GH) family: they all split glycosidic bonds and can degrade xyloglucan to monosaccharides. Several *β-galactosidases* [136, 137] and *xylosidases* [138, 139] have been studied for their ability to degrade xyloglucan by cutting down branches, while the polymer glucose backbone can be broken down by *endoglucanases* in the same way as for cellulose (see also Section 3.6). [140-142]

Here, a partially degalactosylated xyloglucan variant with a galactose removal ratio in the range 40-45% was produced starting from a commercially available polymer, by adapting the procedure described in Ref. 88 (see also Section 5.3). The obtained material showed molecular and self-assembly properties that are at all similar to the partially degalactosylated polymer named after Deg-XG and whose properties were already described in Chapter 6, 7, 8 and 10.

In this chapter, the ability of the complex *Cellulase* and of the single enzyme *β-Glucosidase* to degrade the home-made partially degalactosylated variant is discussed. The commercially available *Cellulase* from *Trichoderma reesei* is a multi-enzymatic system composed of the so-called *C1* ($M_w$ = 57 kDa), that degrades crystalline cellulose, an *endogucanase* ($M_w$ = 52 kDa), an *exoglucanase* ($M_w$ = 61 kDa) and a *β-glucosidase* (*Mw* = 76 kDa). [189]

After the enzymatic reactions, modifications induced in the polymer molecular weight distributions were investigated by size exclusion chromatography measurements.

## 11.2 Materials and methods

Xyloglucan was purchased from Megazyme International (Ireland) and degalactosylated according to Section 5.3.

Enzymatic reactions with *Cellulase* and *β-Glucosidase* are described in Section 5.10. The enzymatically degraded polymer was recovered after freeze-drying, redispersed in aqueous NaOH 10 mM (polymer concentration: 0.2 wt%), filtered with 0.2 pore filters and analyzed by SEC according to Section 5.11.2. Enzymatic degradation conditions and samples codes are reported in Tab. 11.1.

**Tab. 11.1:** Enzymatic degradation conditions and samples codes.

| **Enzyme** | **Enzyme concentration [U/ml]** | **Reaction time (h)** | **Sample code** |
|---|---|---|---|
| *Cellulase* | 0.084 | 1 | C_1 |
| *Cellulase* | 0.084 | 2 | C_2 |
| *β-Glucosidase* | 0.084 | 1 | β_1 |
| *β-Glucosidase* | 0.084 | 2 | β_2 |
| *β-Glucosidase* | 0.084 | 24 | β_24(1) |
| *β-Glucosidase* | 0.084 | β_1 | β_48(1) |
| *β-Glucosidase* | 0.168 | 24 | β_24(2) |
| *β-Glucosidase* | 0.168 | 48 | β_48(2) |

## 11.3 Results

The chromatograms obtained after degrading the polymer with the complex *Cellulase* are shown in Fig. 11.1 together with the nondegraded polymer for comparison.

Results are in good agreement with Ref. 142: after two hours of enzymatic reaction, the polymer is almost completely degraded.

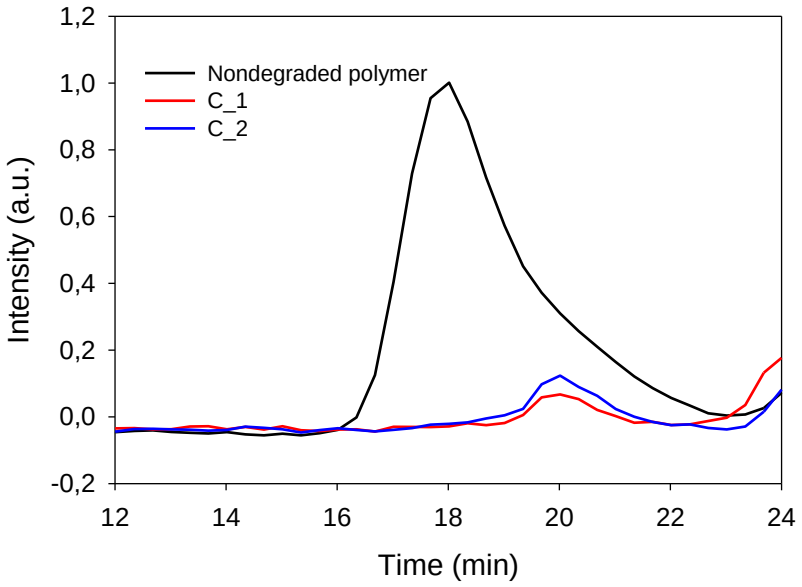


**Fig. 11.1:** Chromatograms of nondegraded Deg-XG and after degradation with *Cellulase* for 1 and 2 hours.

The ability of one single component of Cellulase, *β-Glucosidase* (*Mw* = 135 kDa), was also tested. Results are reported in Fig. 11.2. In this case, a higher enzyme concentration and longer degradation times were also evaluated. In all the investigated reaction conditions the only appreciable effect is a slight shift of the maximum of the chromatograms toward higher elution time values, together with a broadening of the

distribution. Therefore, the single enzyme is not able to degrade xyloglucan completely like the complex *Cellulase*, but its effects are not negligible and they will be further investigated in the follow-up of this research.

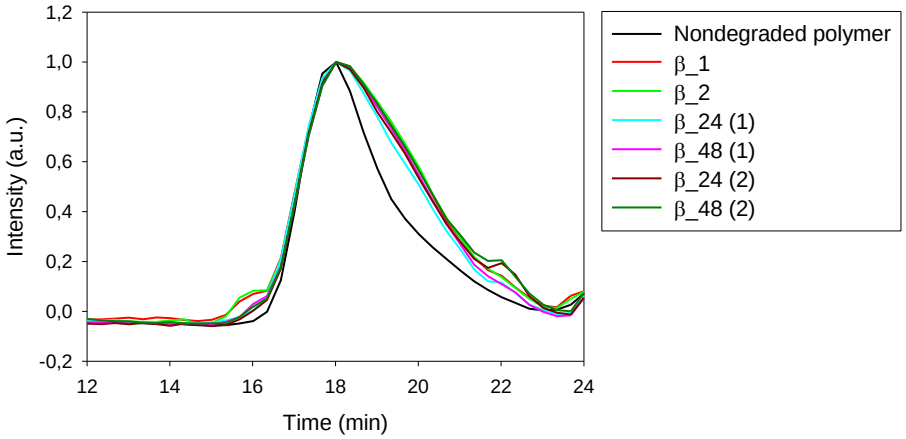


**Fig. 11.2:** Chromatograms of the polymer degraded with *β-glucosidase* at different concentrations and for different reaction times. The nondegraded polymer chromatogram is reported for comparison.

# 12 DISCUSSION

The main topic of the present dissertation is the study of xyloglucan self-assembly. Results from a multi-scale analysis conducted by the combination of several experimental techniques at the variance of polymer concentration showed that Deg-XG self-assembly in an aqueous solvent is a hierarchical and multi-step process: polymer segments (that are already somewhat aggregated as formed by the enzymatic reactions occurring in nature) form "condensed domains" that, in turn, assemble into "clusters" and, at appropriate polymer concentration and environmental conditions, clusters can form macroscopic hydrogels. The structural and physico-chemical features of Deg-XG that rule this process must be individuated, as well as the forces involved. Indeed, a self-assembly process is the result of the balance between a driving and an opposing force (or more than one of each type) that have to be identified at any scale of observation of the phenomenon. When two opposing forces balance, the system falls into a metastable state (or "kinetic trap") and a structure or a characteristic size is fixed.

## 12.1 Description of naturally occurring XGs structural organization

Xyloglucans are enzymatically synthetized by higher plants in the form of multi-stranded aggregates, with regions characterized by high packing ability and hence high density. This structural feature is related to the main function of XG in the plant as storage material. XG is initially synthesized in form of amorphous linear chains constituted by β-D glycoside units, then it forms branches. Branching reduces chain flexibility due to steric hindrance. Branches can actually form and be cleaved; the result is that they change position along the backbone. When a few neighboring segments reach structural order and complementarity, they self-assemble into flat supra-molecular aggregates. Due to limited accessibility and restrained mobility, these aggregates are no longer subjected to molecular and chemical modifications due to enzymatic reaction.

At the increase of the branching degree, the polymer loses flexibility. In water, the statistical Kuhn length and the radius of gyration were estimated to be 150 nm and 148 ± 5 nm, respectively. [99]

XG is constituted by four different monomer units (see Fig. 3.2), represented by specific sequences that differ for the number and the distribution of xylose and galactose residues: $Glc_4Xyl_3$ heptasaccharide (XXXG), two types of Glc4Xyl3Gal octasaccharide (XLXG, XXLG), and Glc4Xyl3Gal2 nonasaccharide (XLLG). In this abbreviation, X represents a Xylp(α1→6)-Glcp unit, L represents a Galp(β1→2) Xylp(α1→6)Glcp unit, and G represents a Glcp residue.

The cross-sectional radius of gyration, $R_{gc}$, of native XG for xyloglucan oligomers determined from SAXS is reported in the literature. [99] In particular, SAXS profiles from xyloglucan heptamer, octamer and nonamer were fitted to those calculated from tri-axial bodies with an ellipsoid well representing the scattering profile from each xyloglucan oligomer. The smaller semi-axis of the ellipsoid is about 0.22 nm for all the monomers, while the width of the cross-section is 0.62, 0.71 and 0.75 nm for the heptamer, octamer and nonamer, respectively. This suggests that branches are mainly located on the larger semi-axis of the ellipsoid.

Some of these monomer units (or macromolecular segments) are more suitable than others to establish mutual interactions (hydrogen bonds and hydrophobic interactions). More specifically, the heptamer (XXXG) and the two octamers (XLXG and XXLG) undergo aggregation, while the nonamer (XLLG) does not form aggregates, due to high steric hindrance of the two galactose residues. [99] Sequences of heptamer and octamer units assemble in ribbons, interconnected by kinked chain segments. We can consider these flat aggregates as the *primary building units* in the multi-scale, hierarchical self-assembly of the polymer. A pictorial representation of these structures is shown in Fig. 12.1.

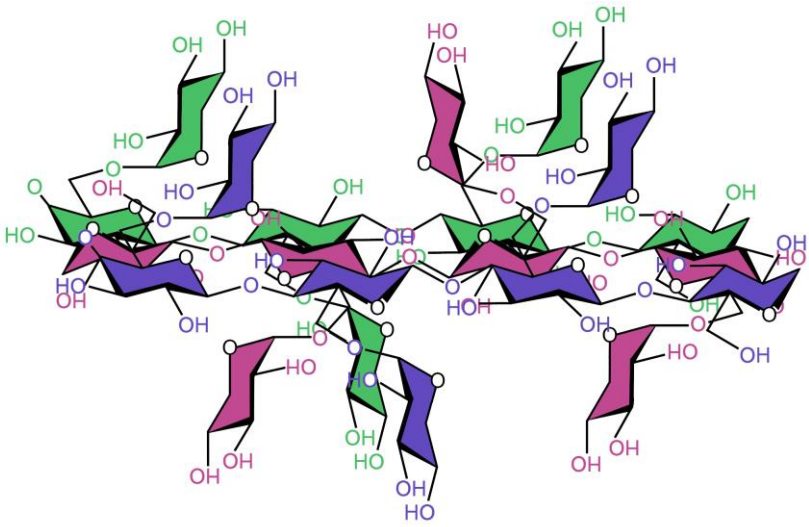

**Fig. 12.1:** Structure of xyloglucan ribbon-like multistranded aggregates.

Regarding the energetics of the stacking of ordered sequences constituted by a few monomer units, it can be argued that this process does not lead to any significant enthalpy gain (since approximately the same number of hydrogen bonds are broken and reformed), it does not cause entropic loss (since these sequences are already ordered) but it leads to an entropy gain for the solvent (indeed, hydration water is released). The hydrophobic interaction is therefore the main driving force for the macromolecular self-assembly at this scale.

On the other hand, the presence of polymer segments with longer branches favors the dissolution (by increasing their conformational entropy) and contrasts the attractive hydrophobic interaction.

According to SAXS studies performed on the native polymer dispersed in water in the high concentration regime (data here not shown), the system can be described as composed of condensed domains (*secondary building units*) of stacked polymer chains dispersed in the aqueous medium with a characteristic size *a*. The polymer chains are organized in cylindrical polymer aggregates (ribbons or *primary building units*) of cross-sectional gyration radius $R_{G,C}$ (Fig. 12.2, Panel c). SAXS data fitting

gives $R_{G,C}$ = ~10 Å and $a$ = ~80 Å. The parameter $a$ decreases by increasing the polymer concentration in water, which suggests that the system is more ordered at higher concentration on this scale, while $R_{G,C}$ remains constant. It can be concluded that the primary building units, formed by 3-4 chains, are not affected by polymer concentration, probably because they result from the original organization of the macromolecules. The condensed domains can be thought as made of clusters of rods (or ribbons) associated in a multi-stranded higher aggregate which shrinks at the increase of concentration (Fig. 12.2, Panel b). We can expect the interface between two "condensed domains" to be spatially diffuse, since it has thermally mobile surface groups or chains. Branches and irregular segments suffer from being constrained. When two of such interfaces approach each other, their protrusions become increasingly confined into a smaller region of space and, in the absence of any other interaction, a *repulsive force* arises associated with the unfavorable entropy of confinement.

The characteristic size of the condensed domains (the *secondary building blocks* probed by SAXS measurements) is affected by the polymer concentration in water. Upon dispersion (at the most favorable temperature and by providing shear) these primary structural units change in size. Their growth is the more favored the higher is the concentration because the probability of polymer-polymer interaction increases. It is arrested when an adequate coverage of their surfaces by hydrophilic groups or chains is achieved (this last process being controlled by hydration kinetics and molecular mobility). A pictorial sketch of the supramolecular organization of the native polymer in aqueous solvent is suggested in Fig. 12.2.

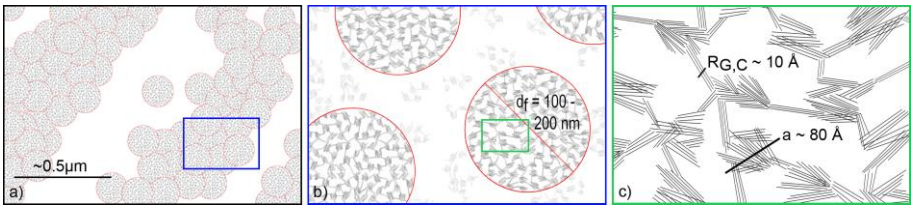


**Fig. 12.2:** Pictorial sketch of xyloglucan supramolecular organization in aqueous solvent, probed on different length scales. a) length scale probed by small angle light scattering (1500-

500 nm); b) length scale probed by large angle light scattering (100-30 nm); c) length scale probed by small angle x-ray scattering (10-1 nm).

## 12.2 Supra-molecular self-assembly of Deg-XG triggered by temperature

The steric stabilization mechanism is very efficient for native XG. Indeed, native XG does not gel (in the high concentration regime) unless its stabilizing moieties are dehydrated (i.e. by addition of alcohols or sugars [107, 113]) or engaged in interactions with other polymers, such as polyphenols or other polysaccharides. [91, 108]

Partial degalactosylation makes the surface of condensed domains less efficiently covered by flexible branches rich in hydrophilic groups and thereby more susceptible of aggregation (indeed, the presence of aggregates is always observed, even in very dilute aqueous dispersions) in conditions that reduce their surface hydration and increase their mobility, such as upon a temperature increase.

When the galactose content is partially removed from xyloglucan by an enzymatic reaction, the polymer becomes temperature-responsive: this has repercussions on the structures of Deg-XG building blocks on all the probed length scales. At the molecular scale, the condensed domains formed by a number of individual chains increase in size with prolonged incubation in water at 37°C. Indeed, 100% increase of their characteristic dimension has been observed by fitting data obtained from SAXS measurements for the nonpurified system ($\gamma 0$).

At the mesoscale, in dilute conditions, Deg-XG condensed domains are organized in *terziary aggregates* (compact clusters) with a gyration radius $Rg$ = 230 nm and a fractal dimension of 2.7 (close to 3, that is the hard sphere fractal dimension). Their dynamics contain vibrational motions contribution as reveled by dynamic light scattering measurements. Upon incubation in water at temperatures above 20-25°C, Deg-XG clusters grow in size. Their dynamics studied by dynamic light scattering measurements display a stretched exponential behavior with both $\tau_c$ and $\beta$ growing with time. This indicates that the system dynamics become progressively slower but, at the same time, more homogeneous, at least on the length scale of a few tens of

nanometers. The change of the dynamic properties may equally refer to a decrease of polydispersity or of inter-particle interactions, or more likely to both conditions. It appears that the temperature triggered self-assembly process mainly involves the smaller, yet more interacting single chains and/or clusters that coalesce into existing or newly formed larger and less mutually interacting clusters.

Upon temperature-triggered aggregation, shear viscosity increases and polymer clusters display non-Newtonian, shear-thinning flow behavior.

No influence of the rate of the temperature increase (jump vs ramp treatments lead to same structures at the mesoscale) or of different conditioning temperatures (above 37°C) had been observed. The irreversibility of the self-assembled nanostructures suggests that the system soon approaches a metastable state condition.

A pictorial representation of these mesoscopic aggregates at 15°C and after prolonged incubation at 37°C is shown in Fig. 12.3 a-b. As already observed, both the condensed domains and the clusters grow in size upon prolonged incubation at 37°C.

At the scale of tens to hundreds of microns, that has been probed by SEM, a solid residue composed by bigger, compact and roundly shaped nanoparticles forms upon drying from the incubated sample, while the one obtained from the freshly prepared system forms a more compact layer with smaller nanoparticles and filamentous structures. Such structural difference at microscopic scale provides a clue on the origin of the dynamical properties change. Indeed, it is reasonable that the compact, yet larger, aggregates can move more freely than entangled clusters.

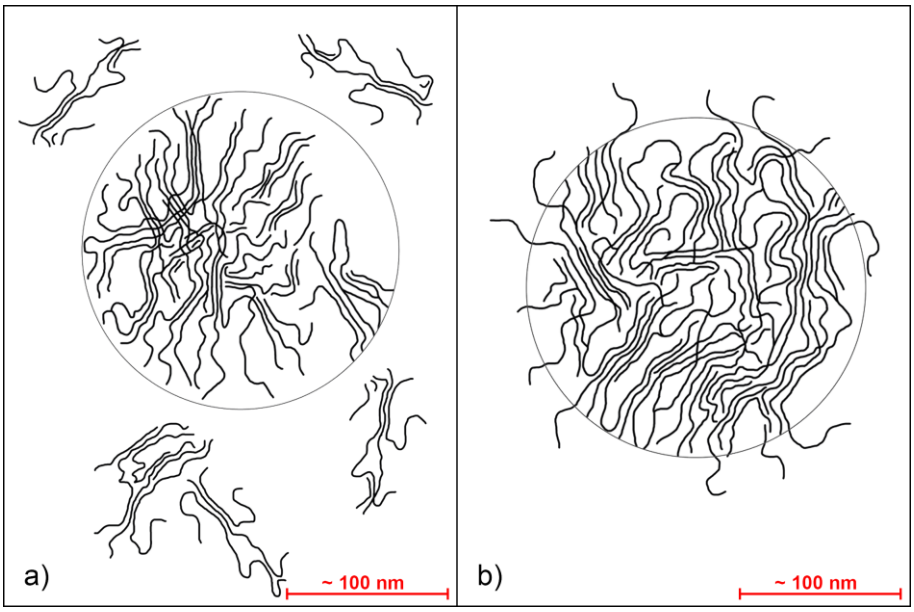


**Fig. 12.3**: Pictorial representation of Deg-XG aggregates at a) 15°C and b) after prolonged incubation at 37°C.

At even larger scale, but provided that the polymer concentration is sufficiently high, the tertiary self-aggregates further assemble into entangled filaments or align into surfaces forming *quaternary self-aggregates* (scaffolds of tens of microns, as observed by SEM analysis).

Fig. 12.4 shows a representation of the aggregation of polymer tertiary building blocks that leads to the formation of macrogels at highly enough polymer concentration in aqueous solvent (above 2 wt%).

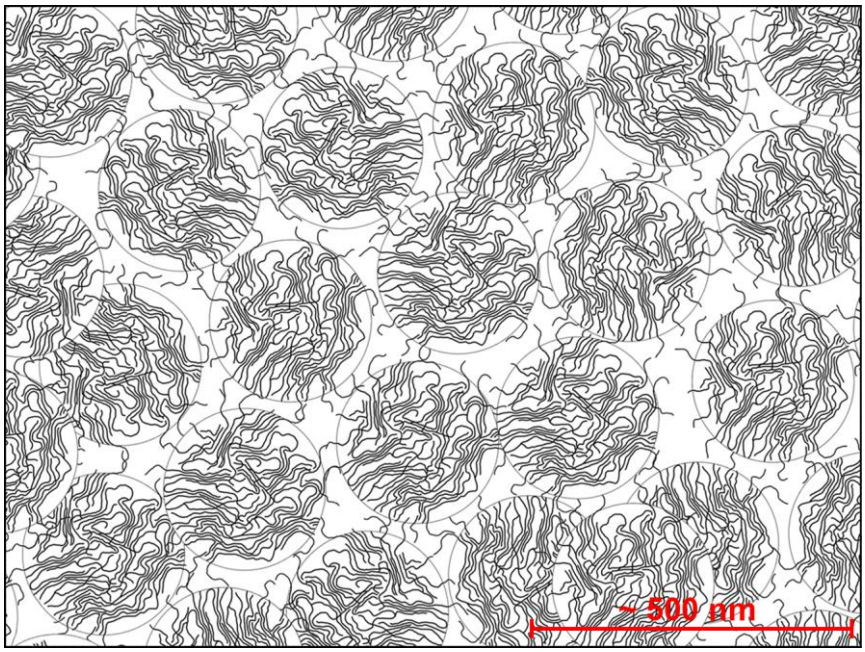


**Fig. 12.4:** Pictorial representation of a Deg-XG macrogel.

## 12.3 Influence of irradiation

Gamma irradiation effects on Deg-XG molecular properties, supramolecular organization and self-assembly have been investigated in Chapter 7.

From FT-IR analysis it can be concluded that irradiated polymers show a significant lower content of hydroxyl groups and a modest increase of the carbonyl group. These modifications can be associated both to the loss of hydroxyl groups due to oxidation and chain scission phenomena, as also suggested by the modest but evident increase of carbonyl groups, and to a reduction of bound water. Molecular weight decreases with dose over the entire explored dose range, while polydispersity decreases up to given irradiation dose (40 kGy). Indeed, in this self-assembly process two competitive phenomena should be considered: “condensation”, that implies growth of the building blocks, and “dissolution”, that causes their shrinking.

Condensation is favored the more the lower is the molecular weight or the lower is the branching degree, and therefore it is favored by irradiation-induced chain scission up to a given dose. When high doses are imparted, "defects" are introduced (open rings, etc…) and dissolution prevails. A pictorial representation of nonirradiated and irradiated systems at low (10-20 kGy) and high (40-60 kGy) doses is shown in Fig. 12.5 a-c.

After gamma irradiation at low doses (10, 20 kGy, see Panel b of Fig. 12.5), the condensed domains grow in size, while the size of clusters decreases as well as the polymer average molecular weight. At higher doses (40-60 kGy, see Panel c of Fig. 12.5), tertiary clusters are even smaller, while defects appear in the structure of the condensed domains.

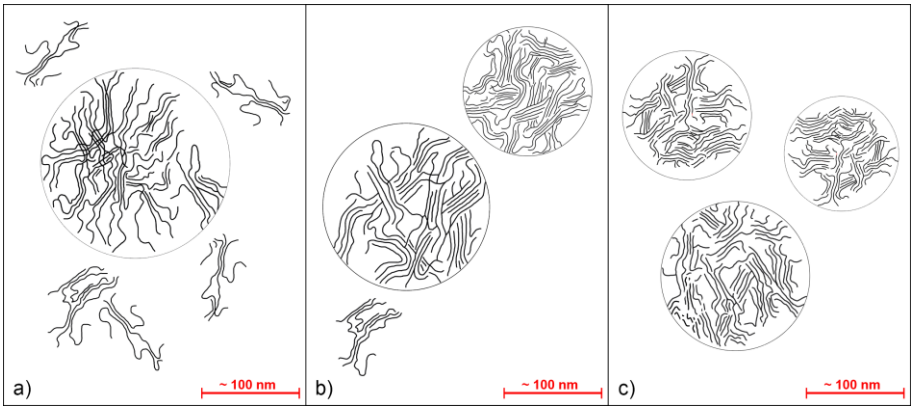


**Fig. 12.5:** Pictorial representation of a) nonirradiated system, b) low doses (10-20 kGy) irradiated systems and c) high doses (40-60 kGy) irradiated systems.

The characteristic temperature of the onset of self-aggregation is only slightly increased by dose. In the dilute regime, the temperature triggered self-assembly process leads to the formation of more homogenous and/or less interacting clusters, whose size is strongly affected by the reduction of polymer molecular weight due to gamma-irradiation. The self-assembly process also drives macromolecular segments to form large condensed domains having a higher degree of structural organisation on

the scale of a few Angstrom probed by SAXS (see Fig. 12.6). However, if the imparted dose is high enough to introduce sequence defects, the stacking process is no longer favored and solvation forces take over the hydrophobic association forces (see Fig. 12.7): the clusters growth with incubation at 37°C is less pronounced and condensed domains become smaller and more defective.

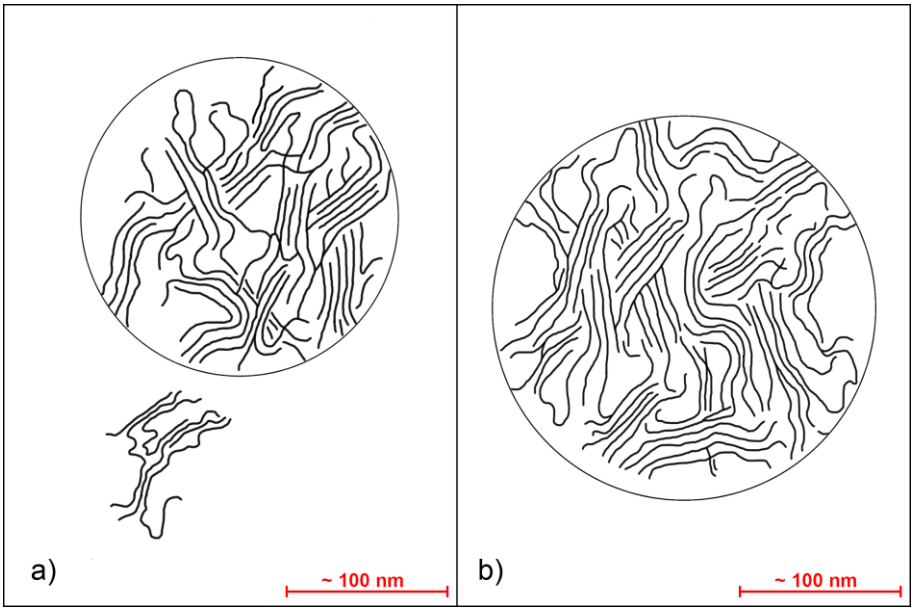


**Fig. 12.6**: Pictorial representation of lower doses (10-20 kGy) irradiated systems at a) 15°C and b) after prolonged incubation at 37°C.

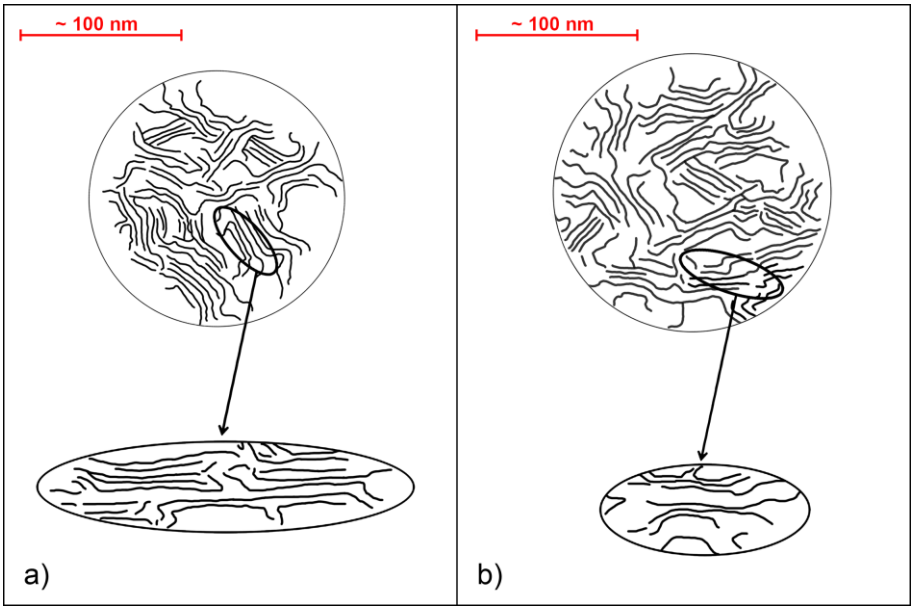


**Fig. 12.7**: Pictorial representation of higher doses (40-60 kGy) irradiated systems at a) 15°C and b) after prolonged incubation at 37°C.

At the micro-scale probed by SEM, the reduction of cluster size and polydispersity or the attenuation of their mutual interactions can be considered responsible for the obtainment of a higher degree of structural order after incubation at 37°C. The quaternary self-aggregates characterized by a lamellar structure are schematically represented in Fig. 12.8.

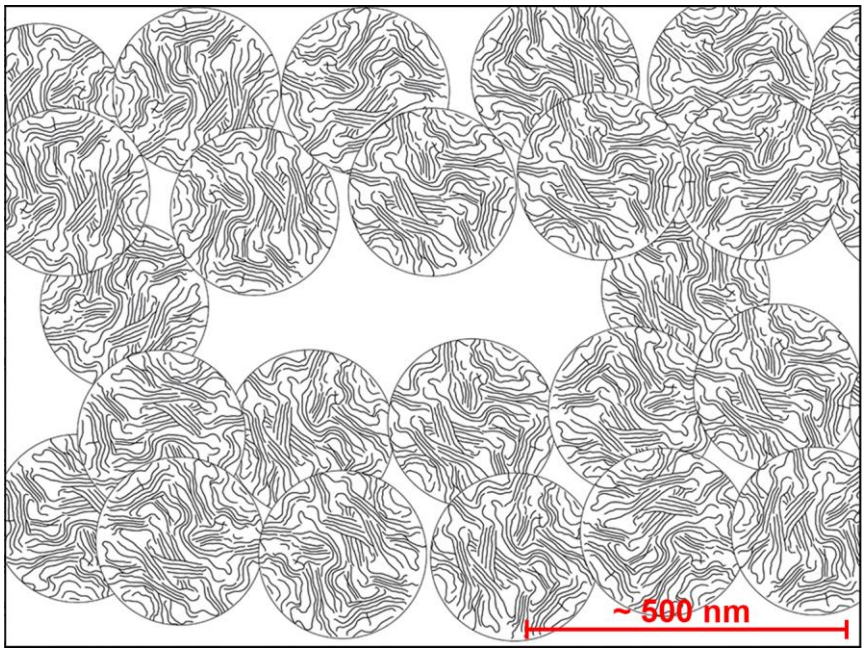


**Fig. 12.8:** Pictorial representation of a macrogel prepared with the irradiated polymer.

Irradiation in the same range of doses was performed at high dose-rates with an electron beam on the native XG. Qualitatively similar results were observed, although the extent of modification both in the molecular properties of the material and in its structure is higher. This is probably due to the higher moisture content and/or bound water of the galactosylated polymer. Irradiations of the purified Deg-XG lead to a similar result. Indeed, some preliminary irradiations carried out in aqueous medium and in the dilute regime (0.1 wt% polymer concentration) point out to a complete degradation of the polymer at 20 kGy, suggesting an important role of hydroxyl radicals in this process.

# CONCLUSIONS

A major part of my research was dedicated to the elucidation of the mechanisms that are at the basis of xyloglucan self-assembly in water, whose comprehension is crucial for the design of "smart" biomedical devices. Indeed, a multi-scale analysis - conducted with a combination of different scattering techniques - provided information on the supramolecular polymer organization on a very broad length scale, ranging from a few Angstrom, to the mesoscale up to the macroscale. As a result, xyloglucan self-assembly has been described as a multi-step and hierarchical process and different levels of organizations have been identified. The *primary building blocks* are constituted by stacked sequences of a few macromolecular segments belonging to the same or to different chains, interconnected by kinked chain portions, which altogether form the *secondary aggregates* or condensed domains. *Tertiary aggregates* are compact clusters of these domains, that can undergo further aggregation when their surface hydration is reduced and/or their mobility is increased. In the case of the partially degalactosylated variant of xyloglucan (Deg-XG), the aggregation is triggered by a temperature increase above a threshold value: in the low polymer concentration regime this leads to the formation of roundly-shaped polymer nanoparticles that can be conveniently employed for the incorporation and delivery of hydrophobic drugs, while in the high concentration regime it leads to thermo-responsive gels that can be employed as drug delivery depots or as *in-situ* forming scaffolds for tissue engineering. Gamma irradiation has been applied on solid Deg-XG as a tool to tailor the polymer molecular weight and self-assembly properties and, at the same time, in order to assess the eventual degradation phenomena induced by radiation-based sterilization protocols. Indeed, high energy irradiation in the sterilization dose range induces noticeable modifications in the polymer molecular weight distribution without dramatically altering the polymer chemical structure and, most of all, without hampering the ability of the polymer to undergo a sol-gel transition at about body temperature. Nevertheless, the aggregation kinetics at the mesoscale and macroscopic gelation are both significantly affected by this

treatment and higher polymer concentrations are required at the higher irradiation doses to obtain similar mechanical properties of the corresponding gels. Furthermore, Deg-XG gels prepared with the irradiated polymers show an ordered, lamellar morphology that could be very useful for mimicking the extracellular matrix of ordered human tissues, thus opening an interesting application field of this materials as minimally invasive scaffold for tissue engineering. Additionally, suitable chemical modification protocols have been developed to modify the xyloglucan functionality, introducing active moieties that can be employed for drug bioconjugation and targeting.

Finally, it is important to emphasise that, besides the specific results on a very interesting biopolymer, this dissertation proposes a powerful approach to unravel the intrinsic complexity of the natural polymers behavior in aqueous solution, whose application in the biomedical field, although strongly encouraged by their biocompatibility, biodegradability and low cost, is not always developed due to the lack of a clear understanding of their supramolecular organization and self-assembly mechanisms.

## FUTURE DEVELOPMENTS

A more detailed *in vitro* degradation and *in vivo* resorption study is required for the application of xyloglucan-based biomedical devices. In particular, the combined effects of hydrolytic and enzymatic degradation are currently under evaluation. The low molecular weight degradation products obtained both after irradiation and enzymatic reactions will be studied.

Regarding Deg-XG nanoparticles loaded with camptothecin, a biological analysis on cancer cells will be performed to evaluate the bioavailability of the loaded drug.

Protocols to further enhance or tailor Deg-XG macrogels mechanical properties will be developed for their use as scaffolds for tissue engineering.

Finally, bio-conjugation strategies for functionalized XG and Deg-XG will be developed in the view of their inclusion into *in-situ* gelling formulations with the parent XG and Deg-XG.

## APPENDIX

### Development of specific protocols to purify Deg-XG and enhance its dispersibility.

The preparation of homogenous aqueous dispersions of Deg-XG is a difficult task due to the strong intermolecular interactions that prevent a fully solubilization of the individual polymer chains. [103, 104, 165] Indeed, xyloglucan is composed of multistranded aggregates in the form of flat ribbons, as already described in Section 3.2.

The solubility issue is even worse for the partially degalactosylated variant, because of the lower galactose content: indeed, water is a solvent of lower quality for glucose and xylose than for galactose.

For these reasons polymer aggregates were still present in solution even after a prolonged homogenization at sub-ambient temperature (5°C) and precipitated upon storage at 5°C. A comparative investigation by DLS measurements was conducted to choose the best dispersion protocols for the degalactosylated polymer. In particular, after prolonged homogenization at 5°C, polymer aqueous dispersions were subjected to centrifugation at 8000 rpm for 45 min, autoclaving for 20 min at 121°C and 1 bar, and the extensive purification protocol described in Section 5.2.

Centrifugation at 8000 rpm for 45 minutes was found effective in inducing the phase separation of a solid deposit, that was estimated to be about 4 wt% of the initial polymer content. Centrifuged samples remained stable against deposit formation even after a prolonged storage at 5°C. DLS measurements at 15°C were done to evaluate the average apparent hydrodynamic size of Deg-XG in water at three concentrations. The measurements on noncentrifuged samples were performed immediately after cold homogenization (5°C) for 5 h. Table 1 reports the average value and standard deviation of the apparent diameter distribution of Deg-XG in water before centrifuging (NP) and in the supernatant solution after centrifuging (NP-C). All samples were filtered through 5 μm cellulose filters to remove gross contaminants.

The apparent hydrodynamic diameter increases significantly with polymer concentration, and it is always much smaller in centrifuged samples even though the percentage reduction is lower at higher concentration.

The purification protocol described in Section 5.2 was developed to remove the impurities present in the feedstock material. The purification process yields about 75 % of recovered product. Aqueous dispersions of purified polymer proved more stable since the sediment formation was no longer observed. The apparent hydrodynamic size of the purified polymer was found slightly smaller than that of the untreated polymer, as shown in Table 2. This suggests that the large value of the hydrodynamic size mainly reflects the strong inter-chain interactions that establish in the dry state and cannot be easily reverted by water addition. As next step, we checked if very high temperatures have some effect in reducing the average size, as suggested by the existence of an UCST at~100°C in the phase diagram of Deg-XG aqueous dispersions at 44% galactose removal ratio. Dispersions of both untreated and purified variants were autoclaved at 121°C and the apparent average hydrodynamic diameter was determined at 15°C by DLS measurements. Data reported in Table 2 show that autoclaving always caused a significant reduction of the particles' size for both the purified and non-purified systems, even though the effect was lower than that of the centrifugation. Indeed, the smallest cluster size was observed in centrifuged system, which did not show further reduction upon autoclaving.

From this preliminary investigation it can be concluded that the measured hydrodynamic diameter in water in systems tested immediately after cold homogenization likely refers to supramolecular Deg-XG clusters. Centrifugation is efficient in knocking down the largest clusters, whereas autoclaving only partially dissolves them. It should be also emphasized that upon the purification protocol or prolonged centrifugation, the colloidal dispersions remain stable over a prolonged storage at 5°C.

**Tab. 1:** Dependence of the apparent average hydrodynamic diameter and width of size distribution on Deg-XG concentration before (b.c) and after centrifuging (a.c).

| **Concentration [wt%]** | **Dh [nm] (Std Dev [%]) b.c.** | **Dh [nm] (Std Dev [%]) a.c** | **$-(Dh_f-Dh_i)/Dh_i(\%)$** |
|---|---|---|---|
| 0.1 | 407 (36.8) | 204 (33.7) | 49.9 |
| 0.25 | 704 (44.9) | 516 (48.4) | 26.7 |
| 0.5 | 2192 (40.1) | 1791 (46.9) | 18.3 |

**Tab. 2:** Influence of purification and autoclaving treatments on the apparent average hydrodynamic diameter and width of size distribution for 0.1 wt% Deg-XG aqueous dispersions.

| **System** | **Dh [nm] (Std Dev [%]) before autoclaving** | **Dh [nm] (Std Dev [%]) after autoclaving** | **$-(Dh_f-Dh_i)/Dh_i(\%)$** |
|---|---|---|---|
| NP | 407 (36.85) | 307 (30.6) | 24.6 |
| P | 373 (33.8) | 265 (29) | 28.9 |
| NP-C | 204 (33.7) | 195 (35.4) | 4.4 |

**REFERENCES**


1. Persini Z., Stana-Kleinschek K., Foster T. J., Van Dam J. E. G., Boeriu C. G., Navard P. "Challenges and opportunities in polysaccharides research and technology: The EPNOE views for the next decade in the areas of Materials, Food and Health Care". Carbohyd Polym 84, 1 (2011), 22-32.
2. Coviello T., Matricardi P., Marianecci C., Alhaique F. "Polysaccharide hydrogels for modified release formulations". J Control Release 119, 1 (2007), 5-24.
3. Van Vlierberghe S., Dubruel P., Schacht E. "Biopolymer-based hydrogels as scaffolds for tissue engineering applications: a review". Biomacromolecules 12 (2011), 1387-1408.
4. Zonghua L., Yanpeng J., Yifei W., Changren Z., Ziyong Z., "Polysaccharides-based nanoparticles as drug delivery systems". Adv Drug Deliv Rev 60 (2008), 1650-1662.
5. Sintov A., Dicapua N., Rubinstein A. "Cross-Linked Chondroitin Sulfate Characterization for Drug Delivery Purposes". Biomaterials 16 (1995) 473-478.
6. Pieper J. S., Oosterhof A., Dijkstra P. J., Veerkamp J. H., van Kuppevelt T. H. "Preparation and characterization of porous crosslinked collagenous matrices containing bioavailable chondroitin sulphate". Biomaterials 20 (1999), 847-858.
7. Cai S. S., Liu Y. C., Shu X. Z., Prestwich G.D. "Injectable glycosaminoglycan hydrogels for controlled release of human basic fibroblast growth factor". Biomaterials 26, 57 (2005), 6054-6067.
8. Li Q., Wang D. A., Elisseeff J. H. "Heterogeneous-phase reaction of glycidyl methacrylate and chondroitin sulfate: Mechanism of ring-opening-transesterification competition". Macromolecules 36 (2003), 2556-2562.

9. Bick A, Gomez E, Shin H, Brigham M, Vu M, Khademhosseini A. “Fabrication of Microchannels in Methacrylated Hyaluronic Acid Hydrogels”. In 2009 IEEE 35th Annual Northeast Bioengineering Conference; Institute of Electrical and Electronics Engineers, Piscataway, NJ (2009), 28-29.
10. Nam H. S., An J, Chung D. J, Kim J. H, Chung C. P. “Controlled release behavior of bioactive molecules from photo-reactive hyaluronic acid-alginate scaffolds”. Macromol Res 14 (2006), 530-538.
11. Wei Y. T, Sun X. D, Xia X., Cui F. Z., He Y., Liu B. F., Xu Q. Y. “Hyaluronic acid hydrogel modified with Nogo-66 receptor antibody and poly(L-lysine) enhancement of adherence and survival of primary hippocampal neurons”. J Bioact Compat Polym 24 (2009), 205-219.
12. Ruel-Gariepy E., Chenite A., Chaput C., Guirguis S., Leroux, J. C. “Characterization of thermosensitive chitosan gels for the sustained delivery of drugs”. Int J Pharm 203 (2000), 89-98.
13. Bagnaninchi P. O., Yang Y., Zghoul N., Maffulli N., Wang R. K., El Haj A. J. “Chitosan microchannel scaffolds for tendon tissue engineering characterized using optical coherence tomography”. Tissue Eng 13 (2007), 323-331.
14. Crompton K. E., Goud J. D., Bellamkonda R. V., Gengenbach T. R., Finkelstein D. I., Horne M. K., Forsythe J. S. “Polylysine functionalised thermoresponsive chitosan hydrogel for neural tissue engineering”. Biomaterials 28 (2007), 441-449.
15. Jiao H. S., Yao J., Yang Y. M., Chen X., Lin W. W., Li Y., Gu X. S., Wang X. D. “Chitosan/polyglycolic acid nerve grafts for axon regeneration from prolonged axotomized neurons tochronically denervated segments”. Biomaterials 30 (2009), 5004-5018.
16. Sarkar N. “Thermal gelation properties of methyl and hydroxypropyl methylcellulose”. J Appl Polym Sci 24 (1979), 1073-1087.

17. Tate M. C., Shear D. A., Hoffman S. W., Stein D. G., LaPlaca M. C. "Biocompatibility of methylcellulose-based constructs designed for intracerebral gelation following experimental traumatic brain injury". Biomaterials 22 (2001), 1113-1123.
18. Zhao S. P., Cao M. J., Li H., Li L.Y., Xu W. L. "Synthesis and characterization of thermo-sensitive semi-IPN hydrogels based on poly(ethylene glycol)-co-poly(epsilon-caprolactone) macromer, N-isopropylacrylamide, and sodium alginate". Carbohydr Res 345 (2010), 425-431.
19. Yang S. W., Liu G. Q., Cheng Y. Q., Zheng Y. H. "Electroresponsive behavior of sodium alginate-g-poly (acrylic acid) hydrogel under DC electric field". J Macromol Sci, Part A: Pure Appl Chem 46 (2009), 1078-1082.
20. Bernhardt A., Despang F., Lode A., Demmler A., Hanke T., Gelinsky M. "Proliferation and osteogenic differentiation of human bone marrow stromal cells on alginate-gelatine-hydroxyapatite scaffolds with anisotropic pore structure". J Tissue Eng Regener Med 3 (2009), 54-62.
21. Peppas N. A., Bures P., Leobandung W., Ichikawa H. "Hydrogels in pharmaceutical formulations". Eur J Pharm Biopharm 50, 1 (2000), 27-46.
22. Osada Y., Gong J. P., Tanaka Y. "Polymer gels". J Macromol Sci, Part C: Polym Rev 44, 1 (2004), 87-112.
23. Chung H. J., Park T. G. "Self-assembled and nanostructured hydrogels for drug delivery and tissue engineering". Nano Today 4 (2009), 429-437.
24. Oh J. K., Lee D. I., Park J. M. "Biopolymer-based microgels/nanogels for drug delivery applications". Prog Polym Sci 34 (2009), 1261-1282.
25. Ebringerovà A., Hromàdkovà Z., Vodenicàrovà M., Dvoaàkovà D., Gregusòvà K., Velebny´ V.. Abstr. XXIst ICS, Cairns, Australia, 2002, 237.
26. Strickland F. M., Darvill A., Albersheim P., Eberhard S., Pauly M., Pelley R. P. "Inhibition of UV-induced immune suppression and interleukin-10 production by plant oligosaccharides and polysaccharides". Photochem Photobiol 69 (1999), 141-147.
27. Galema S. A. "Microwave chemistry". Chem Soc Rev 26 (1997), 233-238.

28. Kingston H., Haswell S. J. “Microwave-enhanced chemistry: fundamentals, sample preparation, and applications”. American Chemical Society, Washington, DC (1997).
29. Basedow A., Ebert K. “Ultrasonic degradation of polymers in solution”. Adv Polym Sci 22 (1977), 83-148.
30. Lorimer J. P., Mason T. J., Cuthbert T. C., Brookfield E. A. “Effect of ultrasound on the degradation of aqueous native dextran”. Ultrason Sonochem 2 (1995), 55-57.
31. Kojima T., Tabata K., Ikumoto T., Yanaki T., Itoh W. Proc Res Jpn Sugar Refn Technol 31 (1982) 105.
32. Yanaki T., Nishi K., Tabata K., Kojima T. “Ultrasonic degradation of *schizophyllum commune* polysaccharide in dilute aqueous solution”. J Appl Polym Sci 28 (1983), 873-878.
33. Koda S., Mori H., Matsumoto K., Nomura H. “Ultrasonic degradation of water-soluble polymers”. Polymer 35 (1994), 30.
34. Ebringerovà A., Pruzinec J., Kacuràkovà M., Hromàdkovà Z. “Effect of gamma-radiation on a water-insoluble arabinoxylan”. J Appl Polym Sci 38 (1989), 1919-1928.
35. Ebringerovà A., Kacuràkovà M., Pruzinec J. “The effect of gamma-radiation on yeast cell-wall glucans”. J Radioanal Nucl Chem Lett 144 (1990), 287-295.
36. Chen R.H., Chang J.R., Shyur J.S. “Effect of ultrasonic conditions and storage in acidic solutions on changes in molecular weight and polydispersity of treated chitosan”. Carbohydr Res 299 (1997), 287-294.
37. Miyazaki T., Yomota C., Okada S. “Ultrasonic depolymerization of hyaluronic acid”. Polym Degr Stab 74 (2001), 77-85.
38. Gura E., Huckel M., Muller P.-J. “Specific degradation of hyaluronic acid and its rheological properties”. Polym Degrad Stab 59 (1998) 297-302.
39. Grönroos A., Pirkonen P., Ruppert O. “Ultrasonic depolymerization of aqueous carboxymethylcellulose”. Ultrason Sonochem 11 (2004), 9-12.

40. Phillips G. O. “Radiation chemistry of carbohydrates”. Adv Carbohydr Chem 16 (1961), 13-58.
41. Phillips G. O. “Effects on carbohydrate systems”. Radiat Res Rev 3 (1972), 335-351.
42. Ershov B.G., Klimentow A.S. Usp. Khim. 53 (1984), 2056.
43. Michel J.P., Raffi J., Saint-Lebe L. “Experimental study of the radio depolymerization of starch”. Starch 32 (1980), 295-298.
44. Choi W.S., Ahn K.J., Lee D.W., Byun M.W., Park H.J. “Preparation of chitosan oligomers by irradiation”. Polym Degrad Stab 78 (2002), 533-538.
45. Charlesby A. “Atomic Radiation and Polymers” Pergamon Press, Oxford, 1960.
46. Löfroth G. “Yields in the radiation degradation of solid carbohydrates”. Acta chemica Scandinavica 21, 8 (1967), 1997-2006.
47. Jumel K., Harding S. E., Mitchell J. R., “Effect of gamma irradiation on the macromolecular integrity of guar gum”. Carbohyd Res 282 (1996) 223-236.
48. Von Sonntag C. “Free radical reactions of carbohydrates as studied by radiation techniques”. Adv Carbohydr Chem Biochem 37 (1980), 7.
49. Dziedziela W. M., Rosiak J. “Some aspects of radiation-induced transformations of cellulose”. Cellulose Chem Technol 11 (1977), 261.
50. Phillips G. O. Polym Photochem 6 (1985), 135.
51. Delides G., Panagiotalidis C. Z., Legapanagiotalidis O. C. Textile Res J 51 (1981) 31.
52. Williams D.F., Zhong S.P. “Biodeterioration/biodegradation of polymeric medical devices in situ”. Int Biodeter Biodegrad 95 (1994).
53. Azevedo H. S., Rui L. R. “Understanding the Enzymatic Degradation of Biodegradable Polymers and Strategies to Control Their Degradation Rate”. Chapter 12 in: “Biodegradable Systems in Tissue Engineering and Regenerative Medicine”. CRC Press LLC (2005).
54. Göpferich A. “Mechanisms of polymer degradation and erosion”. Biomaterials, 17 (1996), 103.

55. Mainil-Varlet P., Curtis R., Gogolewski S. “Effect of in vivo and in vitro degradation on molecular and mechanical properties of various low-molecular-weight polylactides”. J Biomed Mater Res, 36 (1997), 360.
56. Agrawal C.M., Athanasiou K.A. “Technique to control pH in vicinity of biodegrading PLA-PGA implants”. J Biomed Mater Res (Appl Biomater), 38 (1997), 105.
57. Tsuji H., Muramatsu H. “Blends of aliphatic polyesters: V Non-enzymatic and enzymatic hydrolysis of blends from hydrophobic poly(L-lactide) and hydrophilic poly(vinyl alcohol)”. Polym Degrad Stabil 71 (2001), 403.
58. Göpferich A. “Erosion of composite polymer matrices” Biomaterials, 18 (1997), 397.
59. Burkoth A.K., Burdick J., Anseth K.S. “Surface and bulk modifications to photocrosslinked polyanhydrides to control degradation behavior”. J Biomed Mater Res 51 (2000), 352.
60. Tamada J.A., Langer R. “Erosion kinetics of hydrolytically degradable polymers”. Proc Natl Acad Sci U.S.A., 90 (1993), 552.
61. Langer R. “Biomaterials and biomedical engineering”. Chem Eng Sci 50, (1995), 4109.
62. Li S. “Hydrolytic degradation characteristics of aliphatic polyesters derived from lactic and glycolic acids”. J Biomed Mater Res (Appl Biomater), 48 (1999), 342.
63. Rahmouni M. et al. “Enzymatic degradation of cross-linked high amylose starch tablets and its effect on in vitro release of sodium diclofenac”. Eur J Pharm Biopharm 51 (2001), 191.
64. Griffiths M.M., Langone J.J., Lightfoote, M.M. “Biomaterials and granulomas, Methods: A Comparison to Methods”. Enzymol 9 (1996), 295.
65. Stephanopoulos N., Ortony J. H., Stupp S. I. “Self-assembly for the synthesis of functional biomaterials”. Acta Mater 61, 3 (2013) 912-930.
66. Stupp S. I., LeBonheur V., Walker K., Li L. S., Huggins K. E., Keser M., Amstutz A. Science 276 (1997) 384-389.

67. Zubarev E. R., Pralle M. U., Sone E. D., Stupp S. I. J. Am. Chem. Soc. 123 (2001), 4105-4106.
68. Hill J., Jin W., Kosaka A., Fukushima T., Ichihara H., Shimomura T., Ito K., Hashizume T., Ishii N., Aida T. Science 304 (2004), 1481-1483.
69. Hirschberg J. H., Brunsveld L., Ramzi A., Vekemans J. A., Sijbesma R.P., Meijer E.W. Nature 407 (2000), 167-170.
70. Stupp S. I., Zha R. H., Palmer L. C., Cui H., Bitton R. "Self-assembly of biomolecular soft matter". Faraday Discuss. 166 (2013), 9–30.
71. Whitesides G. M., Grzybowski B. "Self-assembly at all scales". Science 295 (2002), 2418-2421.
72. Rinaudo M. "Non-covalent interactions in polysaccharide systems". Macromol Biosci 6 (2006), 590-610.
73. Aseyev V., Tenhu H., Winnik F. M. "Non-ionic thermoresponsive polymers in water". Adv Polym Sci 242 (2011), 29-89.
74. Hassani L. N., Hendra F., Bouchemal K. "Auto-associative amphiphilic polysaccharides as drug delivery systems" Drug Discov Today 17 (2012), 608-614.
75. Halperin A., Tirrell M., Lodge T. P. "Tethered chains in polymer microstructures". Adv Polym Sci 100 (1992), 31-71.
76. Riess G. "Micellization of block copolymers". Prog Polym Sci 28 (2003), 1107.
77. Choucair A., Eisenberg A. "Control of amphiphilic block copolymer morphologies using solution conditions". Eur Phys J E 10 (2003), 37.
78. Foerster S., Antonietti M. "Amphiphilic block copolymers in structure-controlled nanomaterial hybrids". Adv Mater 10 (1998), 195-217.
79. Discher D. E., Eisenberg A. "Polymer vesicles". Science 297 (2002), 967-973.
80. Lifson S., Katchalsky A. J Polym Sci 13 (1953), 43.
81. Manning G. S. J Chim Phys 51 (1969), 924-933.
82. Blanchard D., Auzély-Velty R. "Associating biopolymer systems and hyaluronate biomaterials", Chapter 9 in Thomas S., Durand D., Chassenieux

C.,. Jyotishkumar P Eds. “Handbook of Biopolymer-Based Materials: From Blends and Composites to Gels and Complex Networks”, 2013, 235-278.

83. Gil E. S., Hudson S. M. “Stimuli-reponsive polymers and their bioconjugates”. Prog. Polym. Sci. 29 (2004), 1173–1222.
84. McNaught A. D., Wilkinson A. (1997) Gold book. Compendium of chemical terminology: IUPAC recommendations, 2nd edn. Blackwell Scientific Publications, Oxford; XML on-line corrected version: http://goldbook.iupac.org (2006) created by Nic M, Jirat J, Kosata B, updates compiled by Jenkins A. Accessed 17 November, 2009.
85. Wang X., Qiu X., Wu C. “Comparison of the Coil-to-Globule and the Globule-to-Coil Transitions of a Single Poly(*N*-isopropylacrylamide) Homopolymer Chain in Water”. Macromolecules 31 (1998), 2972-2977.
86. Hoare T. R., Kohane D. S. “Hydrogels in drug delivery: progress and challenges”. Polymer 49 (2008), 1993-2007.
87. Fang Y., Takahashi R., Nishinari K. “A gel network constituted by rigid schzophyllan chains and nonpermanent crosslinks”. Biomacromolecules 5, 1 (2004), 126-136.
88. Brun-Graeppi Andriola Silva A. a K., Richard C., Bessodes M., Scherman D., Narita T., Ducouret G., Merten O-W. “Study on the sol-gel transition of xyloglucan hydrogels”. Carbohyd Polym 80, 2 (2010), 555-562.
89. Nirmal H.B., Bakliwal S.R., Pawar S.P. “In-situ gel: new trends in controlled and sustained drug delivery system”. Int J Pharm Tech Res 2, 2 (2010), 1398-1408.
90. Overstreet D. J., Dutta D., Stabenfeldt S. E., Vernon B. L. “Injectable Hydrogels”. J Polym Sci B: Polym Phys 50 (2012), 881-903.
91. Nishinari K., Kim B., Fang Y., Nitta Y., Takemasa M. “Rheological and related study of gelation of xyloglucan in the presence of small molecules and other polysaccharides”. Cellulose 13 (2006), 365-374.
92. Fry S.C. “The growing plant cell wall. Chemical and metabolic analysis”. Longman Scientific & Technical Editor, Harlow, UK (1988).

93. Carpita N., Gibeaut C. “Structural models of primary cell walls in flowering plants: consistency of molecular structure with the physical properties of the walls during growth”. Plant J 3, 1 (1993), 1-30.
94. Hoffman M., Jia Z. H., Pena M. J., Cash M., Harper A., Blackburn A. R., Darvill A., York W. S. “Structural analysis of xyloglucans in the primary cell walls of plants in the subclass *Asteridae*”. Carbohydr Res 340 (2005), 1826-1840.
95. Shankaracharya N. B. “Tamarind – chemistry, technology and uses – a critical appraisal”. J Food Sci Technol 35, 3 (1998), 193-208.
96. Dea I.C.M., “Industrial Polysaccharides” Pure & Appl Chem 61 (1989), 7, 1315-1322.
97. Mishra A., Malhotra A. V., “Tamarind xyloglucan: a polysaccharide with versatile application potential”. J Mater Chem 19 (2009), 8528-8536.
98. Nishinari K., Takemasa M., Zhang H., Takahashi R. “Storage Plant Polysaccharides. Xyloglucans, Galactomannans, Glucomannans. Elsevier 2007.
99. Nishinari K., Yamatoya M., Shirakawa M. “Xyloglucan”, Chapter 14 in “Handbook of Hydrocolloids”. Woodhead Publishing Limited and CRC Press LLC, 2000.
100. Gidley M. J., Lillford P. J., Rowlands D. W., Lang P., Dentini M., Crescenzi V., Fanutti C., Grant Reid J. S. “Structure and solution properties of tamarind seed polysaccharide”. Carbohyd Res 214 (1991) 299-314.
101. Picout D. R., Ross-Murphy S. B., Errington N., Harding S. E. “ Pressure Cell Assisted Solubilization of Xyloglucans: Tamarind Seed Polysaccharide and Detarium Gum” Biomacromolecules 4 (2003), 799-807.
102. de Freitas R. A., Drenski M. F., Alb A. M., Reed W. F.“Characterization of Stability, Aggregation, and Equilibrium Properties of Modified Natural Products; The Case of Carboxymethylated Chitosans,". Mat Sci & Eng C 30 (2010), 234-241.
103. Muller F., Manet S., Jean B., Chambat G., Boué F., Heux L., Cousin F., “SANS measurements of semiflexible xyloglucan polysaccharide chains

reveal their self-avoiding statistics." Biomacromolecules, 12 (2011), 3330-3336.

104. Muller F., Jean B., Perrin P., Heux L., Boué F., Cousin F. "Mechanism of association of neutral semiflexible biopolymers in water: the xyloglucan case reveals inherent links." Macromol Chem Phys 214 (2013), 2312-2323.
105. Esquenet C., Buhler E. "Aggregation behavior in semidilute rigid and semirigid polysaccharide solutions". Macromol 35 (2002), 3708-3716.
106. Kochumalayil J., Houssine S., Qi Z., Berglund L. "Xyloglucan films", Patent application number 20120216706 (2012).
107. Ogawa K., Hayashi T., Okamura K. "Conformational analysis of xyloglucans". Int J Biol Macromol 12 (1990), 218-222.
108. Nitta Y, Fang Y., Takemasa M., Nishinari K., "Gelation of Xyloglucan by Addition of Epigallocatechin Gallate as Studied by Rheology and Differential Scanning Calorimetry". Biomacromolecules 5 (2004), 1206-1213.
109. Yuguchi Y., Fujiwara T., Miwa H., Shirakawa M., Yajima H. "Color Formation and Gelation of Xyloglucan Upon Addition of Iodine Solutions". Macromol Rapid Commun 26 (2005), 1315-1319.
110. Yuguchi Y., Hirotsu T., Hosokawa J. "Structural Characteristics of Xyloglucan – Congo Red Aggregates as Observed by Small Angle X-ray Scattering". Cellulose 12, 5 (2005), 469-477.
111. Giacomazza D., Sabatino M. A., Catena A., Leone M., San Biagio P. L., Dispenza C. "Maltose-conjugated chitosans induce macroscopic gelation of pectin solutions at neutral pH". Carbohyd Polym 114 (2014), 141-148.
112. Tanaka T., Swislow G., Ohmine I. "Phase Separation and Gelation in Gelatin Gels". Phys Rev Lett 42 (1979), 1556-1559.
113. Yamanaka S., Yuguchi Y., Urakawa H., Kajiwara K., Shirakawa, M., Yamatoya K. "Gelation of tamarind seed polysaccharide xyloglucan in the presence of ethanol". Food Hydrocoll 14 (2000), 125-128.
114. Yuguchi Y., Kumagai T., Wu M., Hirotsu T., Hosokawa J. "Gelation of xyloglucan in water/alcohol systems". Cellulose 11 (2004), 203-208.

115. Nishi N., Takahashi S., Matsumoto M., Tanaka A., Muraya K., Takamuku T., Yamaguchi T. "Hydrogen-bonded cluster formation and hydrophobic solute associations in aqueous solutions of ethanol". J Phys Chem 99, 1 (1995), 462-468.
116. Stillinger F. H. "Water revisited". Science 209 (1980), 451-457.
117. Noskov S. Y., Lamoureux G., Roux B. "Molecular dynamics study of hydration in ethanol–water mixtures using a polarizable force field". J Phys Chem B 109 (2005), 6705-6713.
118. Umemura M., Yuguchi Y. "Solvation of XG in water-alcohol systems by molecular dynamics simulation". Cellulose 16 (2009), 361-371.
119. Shirakawa M., Yamatoya K., Nishinari K., "Tailoring of xyloglucan properties using an enzyme". Food Hydrocoll 12 (1998), 25-28.
120. Ruel-Gariépy E., Leroux J. C. "In situ-forming hydrogels-review of temperature-sensitive systems". Eur J Pharm Biopharm 58 (2004) 409-426.
121. Ruan D., Lue A., Zhang I. "Gelation behaviors of cellulose solution dissolved in aqueous NaOH/thiourea at low temperature". Polymer 49 (2008), 1027-1036.
122. Weng I., Zhang I., Ruan D., Shi I., Xu J. " Thermal gelation of cellulose in a NaOH/thiourea aqueous solution. Langmuir 20 (2004), 2086-2093.
123. de Freitas R. A., Busato, A. P., Mitchell D. A., Silveira J.L.M. "Degalatosylation of xyloglucan: Effect on aggregation and conformation, as determined by time dependent static light scattering, HPSEC–MALLS and viscosimetry". Carbohyd Polym 83 (2011), 1636-1642.
124. Yamanaka S., Yuguchi Y., Urakawa H., Kajiwara K., Shirakawa, M., Yamatoya K. "Gelation of enzymatically degraded xyloglucan extracted from tamarind seeds". Transaction 55, 11 (1999), 528-532.
125. Lang, P., Masci, G., Dentini, M., Crescenzi, V., Cooke, D., Gidley, M.J., Fanutti, C., Reid, J.S.G. "Tamarind seed polysaccharide: preparation, characterisation and solution properties of carboxylated, sulphated and alkylaminated derivatives". Carbohyd Polym 17, 3 (1992), 185-198.

126. Lang P., Kajiwara K., Burchard W. ": "Investigations on the solution architecture of carboxylated tamarind seed polysaccharide by static and dynamic light scattering". Macromol 26, 15 (1993), 3992-3998.
127. Pal S., Sen G., Mishra S., Dey R. K., Jha U. "Carboxymethyl Tamarind: Synthesis, Characterization and Its Application as Novel Drug-Delivery Agent". J Appl Polym Sci 110 (2008), 392-400.
128. Lucyszyn N., Lubambo A. F., Matosk F., Marvilla I., Souza C. F., Sierakowski M. R. "Specific modifications of xyloglucan from Hymenaea courbaril seeds". Mat Sci Eng C 29 (2009), 552-558.
129. Chandroth K. S., Tholath E. A. "Physico-chemical properties of aminated tamarind xyloglucan". Colloids Surf B: Biointerfaces 81 (2010), 513-520.
130. Cao Y., Gu Y., Ma H., Bai J., Liu L., Zhao P., He H., "Self-assembled nanoparticle drug delivery systems from galactosylated polysaccharide-doxorubicin conjugate loaded doxorubicin". Int J Biol Macromol 46 (2010), 245-249.
131. Narrainen A. P., Lovell P. A. "Mechanism and kinetics of free-radical degradation of xyloglucan in aqueous solution". Polymer 51 (2010,) 6115-6122.
132. Vodenicarovà M., Drimalovà G., Hromadkovà Z., Malovıkovà A., Ebringerovà A. "Xyloglucan degradation using different radiation sources: a comparative study". Ultrason Sonochem 13 (2006), 157-164.
133. Patel T. R., Morris G. A., Ebringerova A., Vodenicarova M., Velebny V., Ortega A., Garcia de la Torre J., Harding S. E. "Global conformation analysis of irradiated xyloglucans". Carbohyd Polym 74 (2008), 845-851.
134. Brun-Graeppi A. S. A. K, Richard C., Bessodes M., Scherman D., Narita T., Ducouret G., Merten O. "The effect of sterilization methods on the thermo-gelation properties of xyloglucan hydrogels. Polym Degr Stab 95 (2010), 254-259.
135. Nisbet D. R., Crompton K. E., Hamilton S. D., Shirakawa S., Prankerd R. J., Finkelstein D. I., Horne M. K., Forsythe J. S. "Morphology and gelation

of thermosensitive xyloglucan hydrogels". Biophys Chem 121 (2006), 14-20.

136. Edwards, M., Bowman, Y. J. L., Dea, I. C. M., Reid, J. S. G. "A β-D-Galactosidase from Nasturtium (Tropaeolum-Majus L) Cotyledons - Purification, Properties, and Demonstration That Xyloglucan Is the Natural Substrate". J Biol Chem 263 (1988), 4333-4337.
137. de Alcântara P. H. N., Martim L., Silva C. O., Dietrich S. M. C., Buckeridge, M.S. "Purification of a β-galactosidase from cotyledons of Hymenaea courbaril L. (Leguminosae). Enzyme properties and biological function". Plant Physiol Bioch 44 (2006), 619-627.
138. Fanutti C., Gidley M. J., Reid J. S. G. A. "Xyloglucan Oligosaccharide-Specific α-D-Xylosidase or Exo-Oligoxyloglucan-αXylohydrolase from Germinated Nasturtium (Tropaeolum-majus) Seeds - Purification, Properties and Its Interaction with a Xyloglucan-Specific endo-(1-4)-β-D-Glucanase and Other Hydrolases During StorageXyloglucan Mobilization". Planta 184 (1991), 137-147.
139. Trincone A., Cobucci-Ponzano B., Di Lauro B., Rossi M., Mitsuishi Y., Moracci, M. "Enzymatic synthesis and hydrolysis of xylogluco-oligosaccharides using the first archaeal α-xylosidase from Sulfolobus solfataricus". Extremophiles 5 (2001), 277-282.
140. Schülein, M. "Protein engineering of cellulases". BBA - Protein Struct M 1543 (2000), 239-252.
141. Fanutti C., Gidley M. J., Reid J. S. G. A. "Action of a pure xyloglucan endo-transglycosylase (formerly called xyloglucan-specific endo-(1-->4)-beta-D-glucanase) from the cotyledons of germinated nasturtium seeds". Plant J 3, 5 (1993), 691-700.
142. Mkedder I., Travelet C., Durand-Terrasson A., Halila S., Dubreuil F., Borsali R. "Preparation and enzymatic hydrolysis of nanoparticles made from single xyloglucan polysaccharide chain" Carbohyd Polym 94 (2013), 934-939.

143. Chandroth K. S., Tholath E. A. “Biodegradable biocompatible xyloglucan films for various applications”. Colloid Polym Sci 288 (2010), 297-306.
144. Avachat A. M., Gujar K. N., Wagh K. V. “Development and evaluation of tamarind seed xyloglucan-based mucoadhesive buccal films of rizatriptan benzoate”. Carbohyd Pol 91 (2013), 537-542.
145. Jo T. A., Petri D. F. S., Beltramini L. M., Lucyszyn N., Sierakowski M. R., “Xyloglucan nano-aggregates: physico-chemical characterisation in buffer solution and potential application as a carrier for camptothecin, an anti-cancer drug”. Carbohyd Polym 82 (2010), 355-362.
146. Chandramouli Y., Firoz S., Vikram A., Mahitha B., Rubia yasmeen B., Hemanthpavankumar K. “Tamarind seed polysaccharide (TSP) - an adaptable excipient for novel drug delivery systems”. Intern J Pharm Pract Drug Res 2 (2012), 57-63.
147. Miyazaki S., Kawasaki N., Kubo W., Endo K., Attwood D.. “Comparison of in situ gelling formulations for the oral delivery of cimetidine”. Int J Pharm 220 (2001) 161-168.
148. Miyazaki S., Suisha F., Kawasaki N., Shirakawa M., Yamatoya D., Attwood D. “Thermally reversible xyloglucan gels as vehicles for rectal drug delivery”. J Control Release 56 (1998) 75-83.
149. Kawasaki N., Ohkura R., Miyazaki S., Uno Y., Sugimoto S., Attwood D. “Thermally reversible xyloglucan gels as vehicles for oral drug delivery”. Int J Pharm 181 (1999), 227-234.
150. Yoo M. K, Choi H. K., Kim T. H., Choi Y. J., Akaike T., Shirakawa M., Cho C. S. “Drug release from xyloglucan beads coated with Eudragit for oral drug delivery”. Arch Pharm Res 28 (2005), 736-742.
151. Chen D., Guo P., Chen S., Cao Y., Ji W., Lei X., Liu L., Zhao P., Wang R., Qi C., Liu Y., He H. “Properties of xyloglucan hydrogels as the biomedical sustained release carriers”. J Mater Sci: Mater Med 23 (2012), 955-962.
152. Suisha F., Kawasaki N., Miyazaki S., Shirakawa M., Yamatoya K., Sasaki M., Attwood D. “Xyloglucan gels as sustained release vehicles for the

intraperitoneal administration of mitomycin C". Int J Pharm 172 (1998), 27-32.

153. Miyazaki S., Suzuki S., Kawasaki N., Endo K., Takahashi A., Attwood D. "In situ gelling xyloglucan formulations for sustained release ocular delivery of pilocarpine hydrochloride". Int J Pharm 229 (2001), 29-36.
154. Burgalassi S., Chetoni P., Panichi L., Boldrini E., Saettone M. F. "Xyloglucan as a novel vehicle for timolol: pharmacokinetics and pressure lowering activity in rabbits". J. Ocular Pharmacol Ther 16 (2000), 497-509.
155. Takahashi A., Suzuki S., Kawasaki N., Kubo W., Miyazaki S., Loebenberg R., Bachynsky J., Attwood D. "Percutaneous absorption of non-steroidal anti-inflammatory drugs from in situ gelling xyloglucan formulations in rats". Int J Pharm 246 (2002), 179-186.
156. Nisbet D. R., Moses D., Gengenbach T. R., Forsythe J. S., Finkelstein D. I., Horne M. K., "Enhancing neurite outgrowth from primary neurons and neural stem cells using thermoresponsive hydrogel scaffolds for the repair of spinal cord injury". J Biomed Mater Res A, 89(A), 1 (2008), 24-35.
157. Price L. S. "Morphological control of cell growth and viability". Bioessays 19 (1997), 941-943.
158. Weigel P. H. "Rat hepatocytes bind to synthetic galactoside surface via a patch of asialoglycoprotein receptors". J Cell Biol 87 (1980), 855-861.
159. Kobayashi A., Akaike T., Kobayashi K., Sumitomo H. "Enhanced adhesion and survival efficacy of liver cells in culture dishes coated with a lactose-carrying styrene homopolymer". Macromol Chem Rapid Commun 7 (1986), 645-50.
160. Gutsche A. T., Parsons-Wingerter P., Chand D., Saltzman W. M., Leong K. W. "N-acetylglucosamine and adenosine derivatized surfaces for cell culture: 3T3 fibroblast and chicken hepatocyte response". Biotechnol Bioeng 43 (1994), 801-809.
161. Seo S-J., Akaike T., Choi Y-J., Shirakawa M., Kang I-K., Cho C. S. "Alginate microcapsules prepared with xyloglucan as a synthetic

extracellular matrix for hepatocyte attachment". Biomaterials 26 (2005), 3607-3615.

162. Nisbet D. R., Horne M. "Implantation of functionalized thermally gelling xyloglucan hydrogel within the brain: associated neurite infiltration and inflammatory response". Tissue Eng A: Tissue Eng 16, 9, (2010), 2833-2842.
163. Potmesil M., Pinedo H. M., "Camptothecins: new anticancer agents". USA: CRC Press.
164. Koppel D. E. "Analysis of macromolecular polydispersity in intensity correlation spectroscopy: the method of cumulants," J Chem Phys 57, (1972), 4814-4820.
165. Lang P., Burchard W. "Structure and aggregation behavior of tamarind seed polysaccharide in aqueous-solution" Die Makromoleculare Chemie 194 (1993), 3157-3166.
166. Burchard W "Light Scattering from polysaccharides as soft matter" in Soft-Matter characterization . R. Borsali & R. Pecora Eds, Springer, 2008, Vol. 1, chap 9.
167. Todaro S., Sabatino M.A., Mangione M.R., Bulone D., Dispenza C., "Influence of gamma-irradiation on thermally-induced mesoscopic gelation of degalactosylated xyloglucans". Rad Phys Chem (2014), 94, 245-248.
168. Schmitz K. S. "An introduction to Dynamic Light Scattering by Macromolecules", Academic Press, Inc, 1990.
169. Gözte, W.; Sjögren. "Relaxation processes in supercooled liquids". L Rep Prog Phys 55 (1992), 241-376.
170. Schaefer, D. W.; Han, C. C. In Dynamic Light Scattering; Pecora, R., Ed.; Plenum Press: New York, 1985; Chapter 5, p 181.
171. Sciortino F., Gallo P., Tartaglia P., Chen S. H. "Supercooled water and the kinetic glass transition". Phys Rev E 54 (1996), 6331-6343.
172. Ngai, K. L. "Dynamics of semidilute solutions of polymers and associating polymers" Adv Coll Inter Sci (1996) 64, 1-43.

173. Burchard W. “Particle Scattering Factors of Some Branched Polymers” Macromolecules 10 (1977), 919-927.

174. Rahier, N. J., Eisenhauer B.M., Gao R., Jones S. H., Hecht S. M. “Water-soluble camptothecin derivatives that are intrinsic topoisomerase I poisons”. Org Lett 6 (2004), 321-324.

175. Gottlieb J. A., Guarino A. M., Call J. B., Oliverio V. T., Block J. B. “Preliminary pharmacologic and clinical evaluation of camptothecin sodium (NSC-100880)”. Cancer Chemoter Rep 54 (1970), 461-470.

176. Moertel C. G., Schutt A. J., Reitemeier R. J., Hahn R. G. “Phase II study of camptothecin (NSC-100880) in the treatment of advanced gastrointestinal cancer”. Cancer chemother Rep 56 (1972), 95-101.

177. Muggia F.M., Creaven P.J., Hansen H. H., Cohen M. H., Selawry O. S. “Phase I clinical trial of weekly and daily treatment with camptothecin (NSC-100880): correlation with preclinical studies”. Cancer Chemother Rep 56 (1972), 515-521.

178. Rivory L. P., Robert J. “Molecular, cellular and clinical aspects of the pharmacology of 20(S)camptothecin and its derivatives”. Pharmacol Therapeut 68 (1995), 269-296.

179. Martins S., Tho I., Reimold I., Fricker G., Souto E., Ferreira D., Brandl M. “Brain delivery of camptothecin by means of solid lipid nanoparticles: formulation design, *in vitro* and *in vivo* studies”. Int J Pharm 439 (2012), 49-62.

180. Ostwald W. “Uber die Geschwindigkeitsfunktion der ¨Viskosit¨at disperser Systeme”. I Colloid Polym Sci 36 (1925), 99-117.

181. de Waele A. “Viscometry and plastometry”. J Oil Colour Chem Assoc 6 (1923), 33-69.

182. Launay, B., Doublier, J. L., Cuvelier, G. “Flow properties of aqueous solutions and dispersions of polysaccharides”. In: J. R. Mitchell and D. A. Ledward, eds. Functional Properties of Food Macromolecules. New York: Elsevier Applied Science Publishers (1986), 1-78.

183. Kew S. J., Gwynee J. H., Abu-Rub M., Pandit A., Zeugolis D., Brooks R. A., Rushton N., Best S. M., Cameron R. E. "Regeneration and repair of tendon and ligament tissue using collagen fibre biomaterials". Acta Biomater 7 (2011), 3237-3247.
184. Muzzarelli R. A. A., Muzzarelli C., Cosani A., Terbojevich M. "6-Oxychitins, novel hyaluronan-like polysaccharides obtained by regioselective oxidation of chitins". Carbohyd Polym 39 (1999), 361-367.
185. de Nooy A. E. J, Besemer A. C.,van Bekkum, H. "Highly TEMPO mediated oxidation of primary alcohol groups in polysaccharides". Recl Trav Chim Pays-Bas, 113 (1994), 165-166.
186. de Nooy A. E. J., Besemer A. C., van Bekkum H. "Highly selective nitroxyl radical-mediated oxidation of primary alcohol groups in water soluble glucans". Carbohyd Res 269 (1995), 89-98.
187. de Nooy A. E. J., Besemer A. C., van Bekkum H., van Dijk, J. A. P. P., Smit, J. A. M. "TEMPO-mediated oxidation of pullulan and influence of ionic strength and linear charge density on the dimensions of the obtained polyelectrolyte chains". Macromolecules 29 (1996), 6541-6547.
188. Roure, I., Rinaudo, M., Milas, M., & Frollini, E. "Viscometric behaviour of polyelectrolytes in the presence of low salt concentration". Polymer 39 (1998), 5441-5445.
189. Howell J., Stuck J. "Kinetics of Solka Floc, Cellulose Hydrolysis by *Trichoderma viride* Cellulase". Biotechnol Bioeng 17 (1975), 873.